Design of controllers based on Active Disturbance Rejection Control (ADRC) and its integration with Model Predictive Control (MPC)

Doctoral thesis

Author: Blanca Viviana Martínez Carvajal

Advisors: Dr. Javier Sanchis Sáez
            Dr. Sergio García-Nieto Rodríguez

April 2023

A mis seres queridos, gracias por desear que mis decisiones llenen mi vida de experiencias satisfactorias, por su cariño genuino y reconfortante. Es mi esperanza el poder retribuir su comprensión. Por quienes han partido y nos esperan. Por quienes permanecemos.

Abstract

Active disturbance rejection control was initially seen as a paradigm shift because it is rooted in the challenging idea that controlling a process does not require a detailed model of its dynamics. The key is to reformulate the control problem in the disturbance estimation and rejection framework so that the discrepancy between the controlled process and a desired disturbance-free plant is compensated in the loop without elaborately describing the process or the disturbances. The research in this area has provided a solid theoretical foundation and a compilation of successful applications that have established ADRC among the Disturbance Observer-Based Control (DOBC) techniques and have increased interest in designing control loops using this technology.

Numerous and varied contributions based on the ADRC are currently available. On the one hand, some works address the ADRC methodology. Still, only some offer a comprehensive explanation of its design and application aimed at those researchers who are starting to explore this control strategy. On the other hand, the ADRC tuning and the ADRC-based composite control are open research areas. One of the discussions that remain active in the literature is related to how to select the LADRC main parameters so that closed-loop stability is achieved with appropriate disturbance rejection and robustness, mainly when the ADRC is used to control processes approximated by more straightforward representations such as the first-order plus delay (FOPDT) model. Likewise, the active estimation of uncertainty and disturbances has made integrating the ADRC topology with advanced control techniques, like Model-Based Predictive Control (MPC), attractive. The major challenge in realising this combination lies in how to formulate the control loop so that

the ADRC disturbance rejection mechanism transforms the behaviour of the controlled system into that of a simplified desired plant, thus relaxing the requirement for a detailed model while directly considering the constraints on the loop variables.

This thesis presents three contributions to ADRC knowledge to address the challenges mentioned above. The first is a guide for designing and applying linear controllers using conventional active disturbance rejection control. This guide offers a review of the theoretical foundation of the ADRC. It condenses in an algorithm the steps for designing these control loops to facilitate their implementation according to the problem formulation in the disturbance estimation and rejection framework and the empirical selection of their gains.

The second contribution of this dissertation is a set of tuning rules for computing the three distinctive parameters of the ADRC with which the state observer and control law gains are designed. These rules allow tuning the ADRC to control an approximate process using a first-order plus delay model and offer different sets of parameters according to a desired level of robustness. This contribution is based on developing multi-objective optimisation design procedures focused on controlling a group of nominal FOPDT plants. The results of these procedures were fitted to the tuning formulae provided.

The third contribution is a new control architecture that combines the disturbance rejection mechanism of the ADRC and the receding horizon strategy of the MPC. In this loop, a predictive control law governs a first-order plus integrator plant enforced on the real process subject to constraints. The above is possible by compensating for the mismatch between the real and desired plants and incorporating the ADRC compensation term in the constraints formulation of the predictive controller. The loop is intended to provide a solution to control constrained systems for which no nominal model has been identified.

This dissertation addresses researchers interested in exploring active disturbance rejection control and those considering this technology as one of their main lines of research. The contributions of this dissertation serve those new to the study of ADRC, controller designers seeking to implement linear ADRC by considering the disturbance rejection response of processes approximated using first-order plus delay models, and researchers open to discussing the potential benefits of combining ADRC with advanced techniques such as MPC.

Resumen

El control por rechazo activo de perturbaciones (ADRC, del inglés Active Disturbance Rejection Control) fue visto inicialmente como un cambio de paradigma porque se sustenta en la idea desafiante de que para controlar un proceso no es necesario un modelo detallado del mismo. La clave está en reformular el problema de control en el marco de la estimación y el rechazo de perturbaciones de modo que la discrepancia existente entre el proceso controlado y una planta deseada libre de perturbaciones se compense en el lazo sin describir detalladamente el proceso o las perturbaciones. La investigación en esta área ha proporcionado una fundamentación teórica sólida y una recopilación de aplicaciones exitosas que han consolidado al ADRC entre las técnicas de control basadas en observadores de perturbaciones (DOBC, del inglés Disturbance-Observer-Based Control) y han hecho crecer el interés por el diseño de lazos de control empleando esta tecnología.

Actualmente existen numerosas y variadas contribuciones basadas en el ADRC. Por un lado, algunos trabajos abordan la metodología ADRC. Sin embargo, son pocos los que ofrecen una explicación exhaustiva de su diseño y aplicación, dirigida a aquellos investigadores que están empezando a explorar esta estrategia de control. Por otro lado, la sintonización del ADRC y el control compuesto basado en ADRC son áreas de investigación abiertas. Una de las discusiones que se mantiene activa en la literatura está relacionada con la forma de seleccionar los parámetros principales del ADRC de modo que se alcance la estabilidad de lazo cerrado con un rechazo de perturbaciones y robustez apropiadas, especialmente cuando el ADRC se emplea para controlar procesos aproximados mediante representaciones más sencillas como el modelo de

primer orden más retardo (FOPDT, del inglés First-Order Plus Dead Time). Asimismo, la estimación activa de la incertidumbre y las perturbaciones ha hecho atractiva la idea de integrar la topología ADRC con técnicas de control avanzado, por ejemplo, con el control predictivo basado en modelo (MPC, del inglés Model Predictive Control). El mayor desafío que surge al realizar esta combinación radica en cómo formular el lazo de control para que el mecanismo de rechazo de perturbaciones del ADRC transforme el comportamiento del sistema controlado en el de una planta deseada simplificada, relajando así el requisito de un modelo detallado y considerando directamente las restricciones en las variables del lazo.

Esta tesis presenta tres contribuciones al conocimiento del ADRC para abordar los desafíos expuestos anteriormente. La primera de ellas es una guía para el diseño y aplicación de controladores lineales mediante el control convencional por rechazo activo de perturbaciones. Esta guía ofrece, a modo de tutorial, una revisión de la fundamentación teórica del ADRC y condensa en un algoritmo los pasos para el diseño de estos controladores con el propósito de facilitar su implementación de acuerdo con la formulación del problema en el marco de la estimación y rechazo de perturbaciones y la selección empírica de sus ganancias.

La segunda contribución de esta disertación es un conjunto de reglas de sintonía para el cálculo de los tres parámetros distintivos del ADRC con los que se diseñan las ganancias del observador de estados y de la ley de control. Estas reglas permiten sintonizar el ADRC para el control de un proceso aproximado mediante un modelo de primer orden más retardo y ofrecen al diseñador diferentes conjuntos de parámetros de acuerdo con un nivel de robustez deseado. Esta contribución se basa en el desarrollo de procedimientos de diseño de optimización multiobjetivo enfocados al control de un grupo de plantas FOPDT nominales. Los resultados de dichos procedimientos se ajustaron a las fórmulas de sintonía proporcionadas.

La tercera contribución es una nueva arquitectura de control que combina el mecanismo de rechazo de perturbaciones del ADRC y la estrategia de horizonte deslizante del MPC. En este lazo, una ley de control predictivo gobierna una planta de primer orden más integrador que se induce sobre proceso real sujeto a restricciones. Lo anterior es posible compensando el desajuste entre las plantas real y deseada e incorporando el término de compensación del ADRC en la formulación de las restricciones del controlador predictivo. El bucle pretende proporcionar una solución para controlar sistemas con restricciones para los que no se ha identificado un modelo nominal.

Esta disertación está dirigida tanto a los investigadores interesados en explorar el control por rechazo activo de perturbaciones como a aquellos que consideran a esta tecnología como una de sus líneas de investigación principales. Las contribuciones de esta tesis sirven a quienes se inician en el estudio del ADRC, a los diseñadores de controladores que buscan implementar el ADRC lineal considerando la respuesta al rechazo de perturbaciones de procesos aproximados mediante modelos de primer orden más retardo, y a los investigadores abiertos a la discusión de los beneficios potenciales de combinar el ADRC con técnicas avanzadas como el MPC.

Resum

El control per rebuig actiu de pertorbacions (ADRC, de l'anglès Active Distur-
bance Rejection Control) va ser vist inicialment com un canvi de paradigma
perquè se sustenta en la idea desafiadora que per a controlar un procés no és
necessari un model detallat d'aquest. La clau està a reformular el problema de
control en el marc de l'estimació i el rebuig de pertorbacions de manera que
la discrepància existent entre el procés controlat i una planta desitjada lliure
de pertorbacions es compense en el llaç sense descriure detalladament el pro-
cés o les pertorbacions. La investigació en aquesta àrea ha proporcionat una
fonamentació teòrica sòlida i una recopilació d'aplicacions reeixides que han
consolidat al ADRC entre les tècniques de control basades en observadors de
pertorbacions (DOBC, de l'anglès Disturbance-Observer-Based Control) i han
fet créixer l'interès pel disseny de llaços de control emprant aquesta tecnologia.

Actualment existeixen nombroses i variades contribucions basades en el ADRC.
D'una banda, alguns treballs aborden la metodologia ADRC. No obstant això,
són pocs els que ofereixen una explicació exhaustiva del seu disseny i aplica-
ció, dirigida a aquells investigadors que estan començant a explorar aquesta
estratègia de control. D'altra banda, la sintonització del ADRC i el control
compost basat en ADRC són àrees d'investigació obertes. Una de les discus-
sions que es manté activa en la literatura està relacionada amb la manera de
seleccionar els paràmetres principals del ADRC de manera que s'aconseguisca
l'estabilitat de llaç tancat amb un rebuig de pertorbacions i robustesa apro-
piades, especialment quan el ADRC s'empra per a controlar processos aproxi-
mats mitjançant representacions més senzilles com el model de primer ordre
més retard (FOPDT, de l'anglès First-Order Plus Dead Time). Així mateix,

l'estimació activa de la incertesa i les pertorbacions ha fet atractiva la idea d'integrar la topologia ADRC amb tècniques de control avançat, per exemple, amb el control predictiu basat en model (MPC, de l'anglès Model Predictive Control). El major desafiament que sorgeix en realitzar aquesta combinació radica en com formular el llaç de control perquè el mecanisme de rebuig de pertorbacions del ADRC transforme el comportament del sistema controlat en el d'una planta desitjada simplificada, relaxant així el requisit d'un model detallat i considerant directament les restriccions en les variables del llaç.

Aquesta tesi presenta tres contribucions al coneixement del ADRC per a abordar els desafiaments exposats anteriorment. La primera d'elles és una guia per al disseny i aplicació de controladors lineals mitjançant el control convencional per rebuig actiu de pertorbacions. Aquesta guia ofereix, a manera de tutorial, una revisió de la fonamentació teòrica del ADRC i condensa en un algorisme els passos per al disseny d'aquests controladors amb el propòsit de facilitar la seua implementació d'acord amb la formulació del problema en el marc de l'estimació i rebuig de pertorbacions i la selecció empírica dels seus guanys.

La segona contribució d'aquesta dissertació és un conjunt de regles de sintonia per al càlcul dels tres paràmetres distintius del ADRC amb els quals es dissenyen els guanys de l'observador d'estats i de la llei de control. Aquestes regles permeten sintonitzar el ADRC per al control d'un procés aproximat mitjançant un model de primer ordre més retard i ofereixen al dissenyador diferents conjunts de paràmetres d'acord amb un nivell de robustesa desitjat. Aquesta contribució es basa en el desenvolupament de procediments de disseny d'optimització multiobjectiu enfocats al control d'un grup de plantes FOPDT nominals. Els resultats d'aquests procediments es van ajustar a les fórmules de sintonia proporcionades.

La tercera contribució és una nova arquitectura de control que combina el mecanisme de rebuig de pertorbacions del ADRC i l'estratègia d'horitzó lliscant del MPC. En aquest llaç, una llei de control predictiu governa una planta de primer ordre més integrador que s'indueix sobre procés real subjecte a restriccions. L'anterior és possible compensant el desajustament entre les plantes real i desitjada i incorporar el terme de compensació del ADRC en la formulació de les restriccions del controlador predictiu. El bucle pretén proporcionar una solució per a controlar sistemes amb restriccions per als quals no s'ha identificat un model nominal.

Aquesta dissertació està dirigida tant als investigadors interessats a explorar el control per rebuig actiu de pertorbacions com a aquells que consideren a aquesta tecnologia com una de les seues línies d'investigació principals.

Les contribucions d'aquesta tesi serveixen als qui s'inicien en l'estudi del ADRC, als dissenyadors de controladors que cerquen implementar el ADRC lineal considerant la resposta al rebuig de pertorbacions de processos aproximats mitjançant models de primer ordre més retard, i als investigadors oberts a la discussió dels beneficis potencials de combinar el ADRC amb tècniques avançades com el MPC.

Glossary

Acronyms

ADRC	Active Disturbance Rejection Control
AMIGO	Approximate M-constrained Integral Gain Optimisation
AOF	Aggregate Objective Function
CESO	Cascade Extended State Observer
CRHPC	Constrained Receding-Horizon Predictive Control
CSTR	Stirred Tank Reactor
DDC	Disturbance Decoupling Control
DMC	Dynamic Matrix Control
DOBC	Disturbance Observer-Based Control
ESO	Extended State Observer
FOPDT	First Order Plus Dead Time
GESO	General Extended State Observer
GFCL	Generate First Choose Later
GPC	Generalised Predictive Control
GPIO	Generalised Proportional Integral Observer
HGC	High Gain Control
IAE	Integral of Absolute Error
IMC	Internal Model Control
IMP	Internal Model Principle
ISE	Integral of Squared Error
ITSE	Integral of Time Weighted Squared Error

LADRC	Linear Active Disturbance Rejection Control
LESO	Linear Extended State Observer
LTI	Linear Time Invariant
MADRPC	Modified Active Disturbance Rejection Predictive Control
MCDM	Multi-Criteria Decision Making
MD	Maximum Deviation
MIMO	Multiple Input Multiple Output
MOOD	Multi-Objective Optimisation Design
MOP	Multi-Objective Problem
MPC	Model Predictive Control
NADRC	Non-linear Active Disturbance Rejection Control
OF-MPC	Offset-Free Model Predictive Control
OP	Optimisation Problem
OS	Overshoot
QDMC	Quadratic Dynamic Matrix Control
PID	Proportional Integral Derivative
SISO	Single Input Single Output
SMC	Sliding Model Control
TV	Total Variation of control action
US	Undershoot

Nomenclature

A, Γ	upper-case denotes matrices
$\mathbf{x}$, $\boldsymbol{\ell}$	boldface lower-case denotes vectors
$\mathcal{Z}$	calligraphic letters denote Laplace transforms
s	complex variable for frequency domain formulations
$\dot{x}$, $\ddot{x}$	dot notation indicates first and second order derivatives
$y^{(n)}$	superscripts in brackets indicate higher order derivatives
$\hat{x}$	circumflex accent represents estimation of states
x_k	subscript k indicates discrete instant k
$x_{i|k}$	future value at instant $i + k$ based on conditions at instant k
$G(s)$	dependence on s denotes transfer functions
$\exp(\cdot)$	Euler constant to the power of $(\cdot)$
$\text{diag}(\cdot)$	diagonal matrix with equal diagonal elements $(\cdot)$
$\min\{\cdot\}$	minimisation of given cost function $\{\cdot\}$
$\|\cdot\|_\gamma^2$	quadratic form with scaling factor γ
$[\,\cdot\,]^\top$	transpose

I_L	all-ones lower triangular matrix of appropriate dimensions
1	all-ones vector of appropriate length
0	zero vector of appropriate length

For models formulations

$\tilde{r}$, y_r	desired reference
y	system output
n	system order
b	critical gain
b_0	nominal value of critical gain
K	static gain
T	apparent time constant
l	apparent delay or dead time
Θ	nominal delay or nominal dead time
τ	normalised delay or normalised dead time
d	load disturbances acting on the system
k	gain scaling of a given plant
ω_p	frequency scaling of a given plant

For observers formulations

f, f_i	lumped total perturbation, i-th total perturbation
e	estimation error
β_i	i-th gain of the Extended State Observer
$\gamma_i(e)$	i-th non-linear function of the estimation error
ω_o	observer bandwidth
ℓ_i	i-th gain of the continuous-time Linear Extended State Observer
ℓ_{di}	i-th gain of the discrete-time Linear Extended State Observer
ℓ_{oi}	i-th gain of the discrete-time LESO from the MADRPC

For controllers formulations

u	control law governing the actual plant (system input)
Δu	rate of manipulated variable
u_0	control law governing the modified plant
Δu_0	rate of the control law u_0
α_i, $\overline{\alpha}_i$, δ, $\overline{\delta}$	constants for evaluation of the NADRC non-linear functions
ω_c	controller bandwidth
k_i	i-th gain for computation of u_0 from the LADRC
k_b, n_b, a_b, b_b, c_b	coefficients of the tuning rule for computation of b_0
k_ω, n_ω	coefficients of the tuning rule for computation of ω_c and ω_o
K_c	proportional gain for PID controllers
T_i	integral time for PID controllers
T_d	derivative time for PID controllers
$\overline{y}$	maximum allowed value for the output
$\overline{u}$	maximum allowed value for the input
$\overline{\Delta u}$	maximum allowed value for the rate of input
$\underline{y}$	minimum allowed value for the output
$\underline{u}$	minimum allowed value for the input
$\underline{\Delta u}$	minimum allowed value for the rate of input
t_s	sampling time
p	prediction horizon
c	control horizon
γ	weighting factor for the prediction error
λ	weighting factor for the rate of input
ε_1, ε_2	weighting factors for the slack variables

For performance definitions

$t_{98\%}$	settling time within the $2\,\%$ error band
M_S	maximum peak of the sensitivity function
M_T	maximum peak of the complementary sensitivity function
ε	mixed robustness
$\lvert G(j\omega)\rvert$	magnitude of the frequency response

Contents

Chapter 1

Introduction

This chapter gives an overview of the research developed for the elaboration of this dissertation. The first section tells how aiming at a theoretical and practical understanding of Active Disturbance Rejection Control (ADRC) led to synthesising the ADRC knowledge into a tutorial and identifying the two research areas addressed in this thesis. The second section exposes the main contributions putting them into context through the literature reviewed, the research challenges identified, and the significance of the results presented in this dissertation.

1.1   Motivation

The term Active Disturbance Rejection Control (ADRC) is described in [1] as a new control paradigm alternative to the Proportional-Integral-Derivative (PID) control that inherits from the PID controller its independence from the plant model and seeks to compensate for its weaknesses through the concept of disturbance estimation and rejection.

The disturbance estimation and rejection is understood as estimating the influence of the disturbance in the system from measurable variables to compensate for it, and the group of control strategies integrating this observation mechanism with a controller in a composite loop are denoted as Disturbance Observer-based controllers (DOBC) [2].

Within the DOBC set, the ADRC stands out because its estimator, the Extended State Observer (ESO), was conceived to estimate the system states and the combined non-modelled dynamics and external signals affecting the system. This is, the possible neglected dynamics, uncertainty and non-manipulable external forces are lumped and estimated based on the plant input-output information to compensate for them with the control action. As a result, the ADRC induces the real plant to behave like an assumed modified plant, conventionally adopted as a cascade integrator chain.

In summary, three outstanding characteristics of the ADRC can be listed [3].

1. It does not require a nominal model of the process to be controlled. Initially, only the system order and a factor relating the influence of the control action to the output evolution are sufficient. The latter is referred to in the literature as the *critical gain*.

2. It estimates as a single state the uncertainty and disturbances to avoid their impact on the desired output. On the one hand, this reflects the robustness of the ADRC since, typically, the robust controllers are denoted as those who keep the loop insensitive to the differences between the actual system and its nominal model. This model mismatch is referred to in the control literature as uncertainty [4]. On the other hand, the disturbances are regarded as external signals that can affect the normal or steady state of the controlled variable. The ADRC makes no distinction between uncertainty and disturbances. Instead, they are merged and labelled under the name *total perturbation* to be estimated by the ESO.

3. It induces the process to behave like an assumed disturbance-free modified plant that facilitates the controller design.

The above constitutes the most notable difference between ADRC and other types of DOBC strategies because the ADRC actively allows state estimation and disturbance rejection even when the available plant information is minimal, highlighting its attractiveness in engineering. Besides, the ADRC can be used in single-input, single-output (SISO) and multiple-input multiple-output (MIMO)processes.

When the ESO and the control law are designed by evaluating non-linear functions, the algorithm is named NADRC (Non-linear ADRC). On the contrary, if a linear observer and a linear control law are used, the control strategy is denoted as LADRC (Linear ADRC). The latter has gained popularity due to its simple structure and reduced amount of parameters to be tuned compared to the NADRC. This, together with the increasing emergence of innovative LADRC solutions, motivated the study of this technology as the main topic in this research. Therefore, the contributions presented within this dissertation are framed in the control of processes using LADRC, conceived as described previously.

Although the ADRC seeks to alleviate the model dependence for the loop design, the canonical form adopted for the observer design, the selection of the loop gains and other aspects, such as its integration with advanced control methodologies, are active discussion topics in the literature. Consequently, a review related to the design and application of active disturbance rejection controllers was conducted at the beginning of this research. This led to the elaboration of a tutorial about ADRC, and, what is more, two promising research areas were identified. The first is linked to the LADRC tuning when the modified plant is a first-order plus dead time system, and the second involves merging the LADRC with an advanced control technique such as the Model Predictive Control (MPC).

Given the challenging idea that the ADRC is an alternative for designing control loops for systems of different nature and complexity and that the design is possible by approximating the behaviour of the process to a simplified representation, this thesis researches how the conventional ADRC is straightforwardly implemented, how multi-objective optimisation can be used to derive rules for the computation of the main LADRC parameters, and how the LADRC and the state-space MPC can be integrated into a control algorithm that enhances the unique advantages of these techniques while addressing their weaknesses.

1.2 Main contributions

The search for answers to the research questions introduced in section 1.1 and the others that emerged from them during the development of this dissertation was always aimed at offering alternative solutions for the control-engineering field. Solutions such as a concise guide to the design and application of ADRC, which is considered of value for researchers exploring the ADRC subject; a set of tuning rules for the control engineers interested in the LADRC implementation applied to first-order plus dead time approximations; and a control loop for constrained systems with a relaxed requirement in the process modelling.

A guide for the design and application of active disturbance rejection controllers.

As mentioned, the ADRC was initially presented as a non-linear control strategy (NADRC). However, the number of parameters of the NADRC and the difficulty of their tuning are commonly pointed out as its main disadvantage. On the contrary, the linear structure of the LADRC has allowed its validation in different applications, and it continues to impulse the use of the LADRC as a control technology because the concepts of control theory related to stability, convergence and performance in the time and frequency domains can be applied.

A qualitative and quantitative comparison between NADRC and LADRC is presented in [5]. In this work, a ball-beam system is adopted as a case study to show that the NADRC performs an adequate estimation of the states, even when the initial conditions of the observer are varied. However, the NADRC performance is limited as the magnitude of the load perturbation increases; in the latter case, the performance of LADRC is better. A more detailed theoretical approach to ADRC and its relationship to other control techniques such as Internal Model Principle (IMP) control, High-Gain Control (HGC) and Sliding Mode Control (SMC) can be found in [6].

One of the first contributions to the theoretical justification of the LADRC was the study of the linear ESO (LESO) convergence and the closed-loop stability since the observer must adequately perform the task of estimating the total disturbance for it to be rejected and the process to be enforced to behave like the assumed modified plant. In [7], it is concluded that when the derivative of the total perturbation is known and can be included in the LESO, the estimation error and the tracking error are asymptotically stable. Conversely, if the total perturbation is not known, but its first derivative is known to be bounded, the estimation and tracking errors are also bounded, and their upper

bounds depend on the LESO gains adjustment. These results are validated numerically and experimentally in [8] by simulating a non-linear system and testing on a motion control platform.

The relevance of including the available model information to improve the observer performance is also studied in [9]. Here, the performance of the LESO is analysed when measurements of all states are available, or a reduced-order observer is implemented by assuming that the first state is accessible.

The incorporation of process information into the LESO increased the researchers interest due to the limitations of the conventional LADRC exposed in [10] for non-minimum phase linear systems, especially those with inverse response to a step input which evidences the dynamics of zeros in the right half-plane. For instance, in [11], the conditions for the control of second-order linear systems with non-minimum phase zeros are revealed, suggesting a controllable canonical form for the modified plant that includes information about the position of the poles and zeros. The numerical results of this work show that the robustness of the loop is increased and that the selection of the LESO gains significantly influences the stability. Other LADRC formulations mainly designed for systems with non-minimum phase behaviour have been proposed under model-assisted ADRC [12], generalised ADRC [13], and modified ADRC [14].

As can be deduced from the above, several works have contributed to the theoretical justification of the ADRC and the study of its performance in the time and frequency domain. The advances in the research of this technology have been presented either as a compendium of successful applications or from a methodological approach. For example, [15] summarises the results obtained when the ADRC was applied to the vibration rejection in motion control, angular position control of a manipulator used in rehabilitation exercises, flow and pressure control in power generation systems, temperature control in extrusion lines, and design of new technology for motor control. The transition from PID to ADRC in thermal power plants is studied in [16], and reviews of the ADRC applications in other ambitious areas, such as robotics and aerospace, are presented in [17] and [18], correspondingly. On the other hand, [19] addresses the ADRC formulation for systems described by ordinary differential equations and [20] and [21] expand the analysis to uncertain systems represented through partial differential equations.

Although the summarised literature exposes the ADRC theory deeply, these works may seem like advanced texts for the control practitioners exploring the ADRC subject. This concern is addressed in [22] through a comprehensive

simulation analysis of LADRC for linear systems. However, this study does not cover the ADRC implementation for multi-variable systems, limiting the study to control first and second-order transfer functions.

The above lead to research questions on how to formulate a control problem in the disturbance estimation and rejection framework to implement the LADRC, how to tune the gains of the LADRC loop according to the available system information, and what can be expected when controlling highly non-linear systems with LADRC. Therefore, the first contribution of this thesis is a guide for the design and application of active disturbance rejection controllers developed in a tutorial fashion. It offers the researchers a route for implementing control loops with LADRC and a summary of the main characteristics and differences among some of the LADRC formulations available in the literature. During the development of this phase of the research, it was concluded that the proposal of new tuning methodologies and the formulation of composite control loops based on ADRC are promising research areas.

A set of tuning rules for active disturbance rejection controllers.

When the LADRC loop is implemented, it is necessary to choose the LESO and the linear control law gains. The bandwidth parameterization introduced in [23] simplifies the tuning by formulating the observer and controller gains as functions of two main parameters: *the observer bandwidth* and *the controller bandwidth*. Their selection can be based on the closed-loop desired behaviour, but in most cases, the values need to be readjusted, turning the tuning problem into an empirical process.

The literature approaches that take bandwidth parameterization as a foundation include those that compute the gains by using pre-existing controllers from the loop or employing optimisation techniques that evaluate performance indices of interest.

Since the ADRC was proposed as an improved alternative to the PID control, some authors have researched the LADRC tuning starting from the existing PID controllers in the loop. This is the case of [24] or [25]. These works provide a starting point and require empirical tuning according to performance requirements, similar to the bandwidth parameterization approach.

On the other hand, [26] proposes the calculation of the LADRC gains from a known strictly proper controller with an integrator, similar to the one described in [27], by converting the LADRC loop into a two-degree-of-freedom system under the IMC approach. The methodology in [26] guarantees the same dis-

turbance rejection as the reference controller. However, different performance levels regarding trajectory tracking can be obtained if multiple solutions exist.

The similarity of the PID structure with the LADRC or its analysis as a two-degree-of-freedom system offers the advantage that the control engineer knowledge can facilitate the empirical process of gain tuning in a transition from PID to LADRC. For this reason, the tuning approaches mentioned so far do not discuss the selection of the critical gain and assume that its approximate value is known. Some of the first proposals that included this parameter within the design gains estimated its value online.

In [28], the values of the critical gain and observer bandwidth are obtained by minimising the tracking squared error and the estimation squared error, and the controller bandwidth is computed according to the closed-loop requirements. Likewise, [29] formulates an optimisation problem to minimise the integral of time-weighted absolute error. The only decision variable is the nominal value of the critical gain because the controller bandwidth is adjusted according to the performance requirements, and the observer bandwidth scales that value. Both contributions offer improvements compared to the cases when the critical gain value is assumed constant.

More recently, the research on LADRC tuning has turned towards strategies to determine a set of rules for the computation of the three primary parameters (the nominal value of the critical gain and the two bandwidths). As expected, this new line has brought awareness about interdependence among the parameters and the closed-loop stability regions resulting from the selection of the parameters bounds.

It is well known that the derivation of tuning rules for a particular controller usually is linked to a type of process. A model is chosen such that the synthesised controller tuned by the proposed rules is suitable for controlling systems whose dynamics is approximated by the selected model. This approach is adopted in [30], where rules for the LADRC tuning are provided assuming that the controlled process is a high-order system modelled as n cascaded first-order plants. The rules are obtained based on the interpretation of the maximum sensitivity (M_S) in the Nyquist diagram of the loop transfer function.

High-order plants can be used as approximations for some industrial processes. Nevertheless, the First Order Plus Dead Time (FOPDT) model is a widely accepted approximation that considers delays due to mass or energy transport or limitations related to measuring and energy conversion devices as argued in [31]. This work studies the LADRC stability region when controlling FOPDT

processes and shows how this information can contribute to the LADRC tuning of the controller bandwidth.

The interest in controlling the FOPDT systems using LADRC has inspired the tuning rules proposed in [32], which were obtained through formulating an optimisation problem following the Aggregate Objective Function (AOF) approach. The two performance indices of settling time and the Integral of Squared Error (ISE) were merged into the Integral of Time Weighted Squared Error (ITSE) for minimisation subject to a fixed constraint related to a robustness measure.

The methodological approach used in [32] to derive the rules points out the importance of balancing the disturbance rejection performance with the closed-loop robustness. However, including the robustness as a constraint for the optimisation problem could result in solutions offering an optimised performance (in terms of the index selected) but with a robustness measure that tends to be in the upper limit allowed. This may be enough for some designers, but for others, given the complexity of the process, robustness also becomes a design objective and a balance among all performance indices is required.

An alternative to the AOF method is to use the Generate-First Choose-Later (GFCL) multi-objective approach in which the design objectives are optimised simultaneously, providing a set of solutions with different trade-offs to be examined by the designer who makes the final decision. Few works in the literature have been developed for the LADRC tuning in the GFCL context, and those contributions use this multi-objective approach to select some of the LADRC parameters to control a particular system or the optimisation process needs to be performed for each design.

On the one hand, in [33], the Integral of Absolute Error (IAE) and the maximum sensitivity (M_S) are simultaneously minimised to select the LADRC bandwidths to control a power plant. On the other hand, in [34], a tuning scheme for the model-assisted ADRC [12] for time delay systems is formulated as a multi-objective optimisation problem regarding the setpoint following and the disturbance rejection. However, this methodology is intended to adapt the problem according to the system to be controlled. It means that the proper ADRC order should be selected, and the optimisation plus decision-making stages need to be carried out for each study case to obtain the control law and observer gains.

In summary, the LADRC tuning focused on using different methodological approaches for calculating the main parameters or the deduction of rules for

their computation are considered growing research areas. In this dissertation, the general challenge of how the GFCL multi-objective optimisation can be designed to obtain a set of solutions from which it is possible to deduce tuning rules for the LADRC applied to FOPDT systems is tackled. Questions like what are conflicting design objectives regarding the LADRC performance, how to define the search space for the parameters acting as decision variables according to the possible stability regions, why the bandwidth parameterization is needed to obtain some sort of tendency in the decision variables solutions when a multi-objective optimisation procedure is applied for a set of nominal FOPDT plants, how to fit the selected solutions with suitable functions, how to define tuning rules to offer the designer bounded intervals for computation of the parameters, and to what extend the derived rules can cover or improve the performance obtained with other controllers designed for FOPDT systems are also addressed.

Consequently, the second contribution of this thesis is a set of tuning rules for the LADRC design suitable for the control of systems whose dynamics can be approximated to a FOPDT plant. These rules differ from other proposals in the literature mainly because they were derived through a multi-objective optimisation design procedure to obtain a trade-off between the disturbance rejection performance and the closed-loop robustness. Even though the LADRC has a certain level of robustness because it addresses the differences between the actual system and the assumed plant in the total perturbation, its tuning considering the robustness as an objective design balances this feature with the closed-loop performance and this is reflected in the tuning rules. Besides, a range of values for each LADRC parameter can be computed, or three different sets of parameters can be calculated if a particular robustness measure is preferred.

The Modified Active Disturbance Rejection Predictive Control.

Throughout this chapter, emphasis has been placed on one of the essential characteristics of the LADRC: its ability to induce the controlled process to behave like a desired modified plant. This is achieved thanks to the manipulated variable on the real system being proportional to adding the total perturbation provided by the LESO to a control signal designed to govern the modified plant. The mechanism comprised of the LESO and the internal addition operation where the manipulated variable is computed is referred to as the *disturbance rejector*, and its presence in the LADRC loop makes it possible to estimate and reject the total effect of the multiple disturbances that produce a difference between the real and modified plants.

The research community positive acceptance of the ADRC has inspired works intended to integrate it with other control methods, such as MPC. The latter is a set of advanced control techniques whose main feature is its ability to predict the process behaviour while operating within active constraints. To compute future outputs over a prediction horizon, an assumed trajectory of current and unknown future inputs is applied to an explicit internal model considered as a proper representation of the real system; the goal is then to choose the input trajectory such that the output reaches the desired value at the end of that prediction horizon. The proper inputs are selected by solving an optimisation problem dependent on predictions, the measured output, and subject to desired constraints. Once the input trajectory is obtained, only the first of its elements is applied to the actual plant, and the whole procedure is repeated at the next instant when a new output measurement is available. This is what is known as the receding horizon strategy.

It has been argued that MPC is a satisfactory approach for a variety of problems [35], which has led it to establish itself as an impactful technology in the process industry [36] and gain interest in other applications such as power electronics [37], [38], building climate [39], [40], and networked systems [41], [42]. However, the need for a precise prediction model is still considered its main shortcoming [43].

The integration of the ADRC and the MPC is an open area of research where two approaches can be identified. On the one hand, there is the ESO-based control in which a nominal state-space model of the process to be controlled is used to design a General ESO (GESO) [44],[45]. In [46] the discretised GESO is used to update the dynamics of a prediction model to control the system states trajectories. More recently, in [47] the stability of the predictive ESO-based control is studied when the discrete GESO is employed as part of a predictive control problem that penalises the deviations of states predictions from zero. The above contributions have exploited the ESO structure by augmenting the state vector with states corresponding to disturbances. However, these implementations still require an identified nominal model of the process for the state and output observer equations which turns into the standard approach of the disturbance observer-based control. Some recent practical applications of MPC integration with disturbance observers include power electronics [48], [49], motor control [50], [51], [52], autonomous vehicles [53], [54] and process control [55].

On the other hand, there are works where the modified plant concept has been used in combination with the prediction strategy. For instance, in [56] the output voltage of a DC-DC buck converter is rearranged as a function of total

perturbation and input voltage and the Taylor series expansion of this function is used to implement an unconstrained continuous-time predictive control. As the prediction model requires output and total perturbation derivatives, a reduced-order Generalized Proportional Integral Observer (GPIO) [57] is implemented. Even though this continuous configuration is analogous to the discrete-time MPC, some simplification should be made for its practical implementation to truncate the number of higher-order derivatives of the Taylor series expansion and a discretisation of the control algorithm is needed to apply the input to the real plant.

In [58], the ESO is used to estimate the external disturbances and modelling errors that arise from obtaining a lateral vehicle model for the steering control of a two-wheel vehicle. In this work, a constrained predictive control law is computed and further modified with the compensation term to calculate the manipulated variable. However, the upper limit of the control action constraint in the optimisation problem is set as the upper limit of the real manipulated variable. With this definition, the control action computed during the optimisation process is likely to be within the constraint band, but the manipulated variable applied to the real system could evolve to a value outside the allowed limits due to the compensation term.

From another point of view, in [59], [60], the discrete transfer function of an nth-order integrator is assumed as the modified plant and then employed as the prediction model of a Generalized Predictive Controller (GPC). As expected, the ESO is in charge of estimating the total perturbation further compensated. Although these proposals resemble a combination of the ADRC with an MPC method, none of them addresses the definition of constraints and the possible influence of the compensation term in their handling.

According to the findings presented in the previous literature, the integration of ADRC with MPC methods offers potential benefits in terms of performance and disturbance rejection. Still, the following challenges are identified: how to tap the disturbance estimation-rejection mechanism of ADRC to reject the ignored dynamics actively and thus avoid the modelling effort imposed on MPC, how to incorporate the disturbance compensation term in the MPC optimisation problem definition to ensure that the manipulated variable satisfies the real operating limits in servo-regulatory operation, and to what extent the integration of MPC and ADRC frameworks allows obtaining the desired performance for different types of systems.

In the above context, the third significant contribution of this thesis is a new control architecture that merges the disturbance rejection capability of ADRC

with the receding horizon strategy of the state-state MPC suitable for single-input single-output systems with no nominal model available and subject to constraints in output and the increment and absolute value of the manipulated variable. The proposal has been named after Modified Active Disturbance Rejection Predictive Control (MADRPC). As a significant advantage, it relaxes the modelling requirement to an assumed discrete-time second-order state-space formulation of a first-order plus integrator. It offers proper disturbance rejection for linear and non-linear systems.

The development of this dissertation led to the following products.

Journal articles

[61] Martínez, B. V., Sanchis, J., García-Nieto, S., Martínez, M. 2021. Active disturbance rejection control: a guide for design and application. Revista Iberoamericana de Automática e Informática Industrial 18, 201-217. https://doi.org/10.4995/riai.2021.14058.

[62] Martínez, B. V.; Sanchis, J.; García-Nieto, S.; Martínez, M. Tuning Rules for Active Disturbance Rejection Controllers via Multiobjective Optimization: A Guide for Parameters Computation based on Robustness. *Mathematics* 2021, *9*, 517. https://doi.org/10.3390/math9050517.

- Martínez, B. V.; Sanchis, J.; García-Nieto, S.; Martínez, M. Modified Active Disturbance Rejection Predictive Control: a fixed-order state-space formulation for SISO systems. Under review in ISA Transactions journal.

Complementary software

[63] B. V. Martínez, Active Disturbance Rejection Control. Implementation examples. Version 1.0.0, Computer Software, 2020.
url: https://www.mathworks.com/matlabcentral/fileexchange/78459.

[64] B. V. Martínez, LADRC automatic parameters computation based on robustness. Version 1.0.0, Computer Software, 2021.
url: https://es.mathworks.com/matlabcentral/fileexchange/86403.

Chapter 2

Design and application of Active Disturbance Rejection Controllers

This chapter addresses the design of controllers by active disturbance rejection control reuniting the conventional methods in a straightforward design guide. The first section briefly presents the scope of this chapter. The second section describes the ADRC block diagram according to its non-linear or linear nature. The third section addresses the control problem formulation under the disturbance rejection framework, and the corresponding loop gains tuning is introduced in the fourth section. The fifth section brings together the previous sections into a controller design guide. Finally, the guide is applied to thermal control and multi-variable control of a chemical process in the sixth section.

2.1   Introduction

The design of an active disturbance rejection controller can be understood as a three-phase procedure.

1. Formulation of the control problem in the disturbance rejection framework, where the total perturbation should be identified.

2. Tuning of the loop gains set.

3. Implementation of the control loop and validation of the closed-loop performance.

This chapter addresses the above phases in a tutorial fashion to provide the reader with the theoretical background that serves as the foundation for the contributions of the oncoming chapters. What is presented in this chapter constitutes the conventional design methods for the linear ADRC. Therefore, a five-step algorithm is provided, allowing the LADRC design to be straightforward.

2.2   Active disturbance rejection control

The active disturbance rejection control loop contains three main blocks, as shown in Figure 2.1.

- Tracking differentiator: takes as input the desired reference $\tilde{r}$ and generates a transient profile r and its n derivatives $\dot{r}$, $\ddot{r}$, ..., $r^{(n)}$.

- Extended State Observer: provides the estimated system states $\hat{x}_1, \ldots, \hat{x}_n$ and the estimated additional state $\hat{x}_{n+1}$, which merges the non-modelled dynamics and perturbations.

- Controller: computes a state feedback control law u_0 assuming the real plant has been modified such that its behaviour resembles a disturbance-free nominal system. This is, the control action u_0 governs the *modified plant* and the manipulated variable acting on the real plant is given by $u = (u_0 - \hat{x}_{n+1})/b_0$.

The non-linear or linear nature of the three comprising blocks determines the ADRC formulation. Notice that the loop implementation requires the knowledge of the system order n and the approximate value of the critical gain b_0.

14
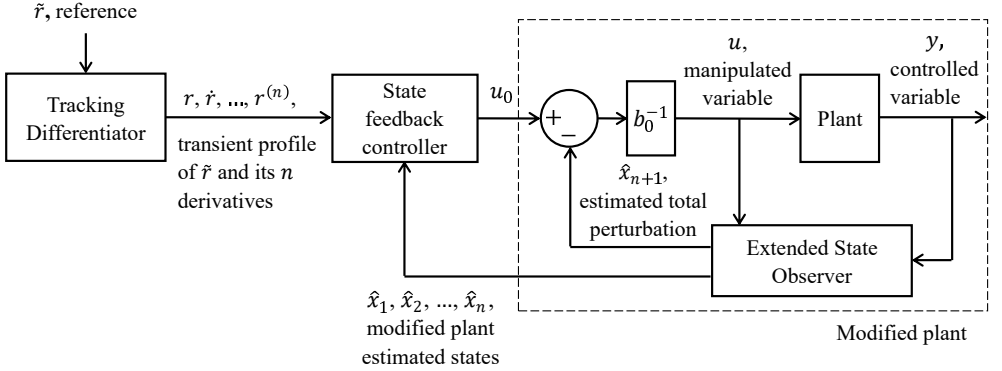
Figure 2.1: Active disturbance rejection control loop.

2.2.1 Non-linear active disturbance rejection control

The active disturbance rejection control applies to single-input single-output (SISO) systems and multiple-input multiple-output (MIMO) systems. To simplify the mathematical notation, let the non-linear ADRC (NADRC) algorithm be introduced for the SISO system

$$\ddot{y} = -a_1\dot{y} - a_0y + bu. \tag{2.1}$$

Equation 2.1 is the input-output model of a second-order system with y as the controlled output, u is the manipulated variable, a_0 and a_1 are constants determining the location of the system poles and b is known as critical gain.

The state space representation of (2.1) is given by (2.2), where d has been included to indicate the load disturbances acting on the system.

$$\begin{cases} \dot{x}_1 = x_2 \\ \dot{x}_2 = -a_0x_1 - a_1x_2 + bu + d \\ y = x_1 \end{cases} \tag{2.2}$$

In the case that a_0 and a_1 are unknown, the first two terms on the right side of the expression for $\dot{x}_2$ in (2.2) can be lumped in a function called total perturbation, which also includes load disturbances and the difference between the actual value of b and its known nominal value denoted by b_0. Thus,

$$f = -a_0x_1 - a_1x_2 + (b - b_0)u + d. \tag{2.3}$$

15

The model (2.4) is obtained by substituting (2.3) in (2.2).

$$\begin{cases} \dot{x}_1 = x_2 \\ \dot{x}_2 = f + b_0 u \\ y = x_1 \end{cases} \tag{2.4}$$

As the total perturbation is an unknown function, f is treated as an additional state that must be estimated and compensated by the control loop. The resulting extended state space model with $x_3 \triangleq f$ and $h = \dot{f}$ unknown is

$$\begin{cases} \dot{x}_1 = x_2 \\ \dot{x}_2 = x_3 + b_0 u \\ \dot{x}_3 = h \\ y = x_1. \end{cases} \tag{2.5}$$

The estimation of states in (2.5) is achieved through the Extended State Observer (ESO) (2.6), whose inputs are the measured output y and the control action u.

$$\begin{cases} \dot{\hat{x}}_1 = \hat{x}_2 - \beta_1 \gamma_1(e) \\ \dot{\hat{x}}_2 = \hat{x}_3 + b_0 u - \beta_2 \gamma_2(e) \\ \dot{\hat{x}}_3 = -\beta_3 \gamma_3(e) \\ e = \hat{x}_1 - y \end{cases} \tag{2.6}$$

In Equation 2.6, $\hat{x}_i$ represents the estimation of the ith-state x_i, the β_i are the gains, and the $\gamma_i(e)$ corresponds to non-linear functions of the estimation error e, which constitutes the correction terms of the observer.

The active disturbance rejection is achieved by subtracting the total perturbation information, contained in $\hat{x}_3$, from the control law u_0, according to

$$u = \frac{u_0 - \hat{x}_3}{b_0}. \tag{2.7}$$

By substituting (2.7) in (2.4) and assuming that $\hat{x}_3 \approx f$, the system is *transformed* into

$$\begin{cases} \dot{x}_1 = x_2 \\ \dot{x}_2 = u_0 \\ y = x_1. \end{cases} \tag{2.8}$$

The state-space model (2.8) represents a disturbance-free and pure-integrating *modified plant* on which acts the control law

$$u_0 = k_1 \text{fal}(r - \hat{x}_1, \alpha_1, \delta) + k_2 \text{fal}(\dot{r} - \hat{x}_2, \alpha_2, \delta) \qquad (2.9)$$

$$\text{fal}(\tilde{e}, \alpha_i, \delta) = \begin{cases} \dfrac{\tilde{e}}{\delta^{1-\alpha_i}}, & |\tilde{e}| \leq \delta \\ |\tilde{e}|^{\alpha_i} \text{sign}(\tilde{e}), & |\tilde{e}| > \delta \end{cases} \qquad (2.10)$$

The non-linear function (2.10) was proposed by [1] and, with a different combination of its arguments, it allows the evaluation of the non-linear expressions related to the ESO following that $\gamma_i(e) = \text{fal}(e, \bar{\alpha}_i, \bar{\delta})$.

According to this subsection, the control of the system (2.2) by NADRC requires the selection of six types of parameters: the observer gains β_i, the constants $\bar{\alpha}_i$ and $\bar{\delta}$ for the evaluation of the observer non-linear functions, and the gains k_i together with the constants α_i and δ for the control law design. Following a similar approach, the NADRC algorithm can be used to control non-linear systems of order n. In this case, the total perturbation would also include the terms related to the non-modelled and non-linear dynamics.

2.2.2 Linear active disturbance rejection control

Now, that the system (2.2) is controlled by linear active disturbance rejection control (LADRC). The extended model is equivalent to (2.5). However, the states are estimated through a linear version of the ESO, in which $\gamma_i(e) = e$ as a result of evaluating (2.10) with $\bar{\alpha}_i = 1$ [65]. In this sense, the linear extended state observer (LESO) is defined as

$$\begin{cases} \dot{\hat{x}}_1 = \hat{x}_2 + \ell_1 e \\ \dot{\hat{x}}_2 = \hat{x}_3 + b_0 u + \ell_2 e \\ \dot{\hat{x}}_3 = \ell_3 e \\ e = y - \hat{x}_1. \end{cases} \qquad (2.11)$$

In equation (2.11) the variables β_i have been replaced by the ℓ_i to refer to the linear gains of the LESO.

The manipulated variable is as (2.7), but the control action governing the modified plant is the linear state feedback control law (2.12). Notice that $\tilde{r}$ has

been set as the reference in (2.12). This can be done in practice if the tracking differentiator is omitted or the setpoint derivatives are unbounded [66].

$$u_0 = k_1(\tilde{r} - \hat{x}_1) - k_2\hat{x}_2 \tag{2.12}$$

Compared to the NADRC, the LADRC only requires tuning two types of parameters: the observer gains ℓ_i and the controller gains k_i. Nevertheless, the number of design variables in both formulations is directly related to the assumed order n. The approach described in this section is also referred to in the literature as conventional LADRC. Its version of order n is presented in Table 2.1.

The linear formulation of ADRC has allowed its study in the frequency domain. Let the block diagram of Figure 2.1 be transformed into the two-degree-of-freedom configuration of Figure 2.2. The direct loop transfer function $G_c(s)$ and the feedback transfer function $G_F(s)$ are derived as follows.

The linear extended state observer (2.11) in frequency domain is given by

$$\begin{cases} s\mathcal{Z}_1 = \mathcal{Z}_2 + \ell_1(\mathcal{Y} - \mathcal{Z}_1) \\ s\mathcal{Z}_2 = \mathcal{Z}_3 + b_0\mathcal{U} + \ell_2(\mathcal{Y} - \mathcal{Z}_1) \\ s\mathcal{Z}_3 = \ell_3(\mathcal{Y} - \mathcal{Z}_1), \end{cases} \tag{2.13}$$

with s as the complex variable, $\mathcal{Y}$ the Laplace transform of the output, $\mathcal{U}$ the Laplace transform of the control action, and the $\mathcal{Z}_i$ as the Laplace transforms of the estimated states. The expressions (2.14)–(2.16) are obtained by solving the system of equations (2.13).
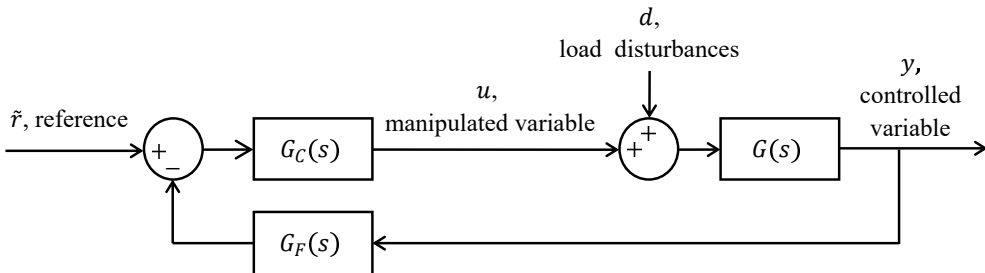
Figure 2.2: Two-degree-of-freedom configuration of LADRC.

$$\mathcal{Z}_1 = \frac{b_0 s}{s^3 + \ell_1 s^2 + \ell_2 s + \ell_3}\mathcal{U} + \frac{(\ell_1 s^2 + \ell_2 s + \ell_3)}{s^3 + \ell_1 s^2 + \ell_2 s + \ell_3}\mathcal{Y} \qquad (2.14)$$

$$\mathcal{Z}_2 = \frac{b_0(s^2 + s\ell_1)}{s^3 + \ell_1 s^2 + \ell_2 s + \ell_3}\mathcal{U} + \frac{(\ell_2 s^2 + \ell_3 s)}{s^3 + \ell_1 s^2 + \ell_2 s + \ell_3}\mathcal{Y} \qquad (2.15)$$

$$\mathcal{Z}_3 = \frac{-\ell_3 b_0}{s^3 + \ell_1 s^2 + \ell_2 s + \ell_3}\mathcal{U} + \frac{\ell_3 s^2}{s^3 + \ell_1 s^2 + \ell_2 s + \ell_3}\mathcal{Y} \qquad (2.16)$$

On the other hand, the control action (2.17) is deduced by combining the frequency domain expressions of (2.7) and (2.12), with $\mathcal{R}$ being the Laplace transform of the reference.

$$\mathcal{U} = \frac{1}{b_0}\left(k_1\mathcal{R} - k_1\mathcal{Z}_1 - k_2\mathcal{Z}_2 - \mathcal{Z}_3\right) \qquad (2.17)$$

Therefore, substituting (2.14)–(2.16) in (2.17) and reorganising terms, $\mathcal{U}$ is rewritten as

$$\begin{aligned} \mathcal{U} = \frac{k_1}{b_0}&\left[\frac{s^3 + \ell_1 s^2 + \ell_2 s + \ell_3}{s^3 + (\ell_1 + k_2)s^2 + (k_2\ell_1 + \ell_2 + k_1)s}\right]\mathcal{R} \\ &- \left[\frac{(k_1\ell_1 + k_2\ell_2 + \ell_3)s^2 + (k_1\ell_2 + k_2\ell_3)s + k_1\ell_3}{b_0(s^3 + (\ell_1 + k_2)s^2 + (k_2\ell_1 + \ell_2 + k_1)s)}\right]\mathcal{Y}. \end{aligned} \qquad (2.18)$$

From Figure 2.2 and in the absence of load disturbance ($d = 0$),

$$\mathcal{U} = G_C(s)\mathcal{R} - G_C(s)G_F(s)\mathcal{Y}. \qquad (2.19)$$

Hence, the resulting direct loop transfer function (2.20) and the feedback transfer function (2.21) are obtained by comparing the factors of $\mathcal{R}$ and $\mathcal{Y}$ in (2.18) with those in (2.19).

$$G_C(s) = \frac{k_1}{b_0}\left(\frac{s^3 + \ell_1 s^2 + \ell_2 s + \ell_3}{s^3 + (\ell_1 + k_2)s^2 + (k_2\ell_1 + \ell_2 + k_1)s}\right) \qquad (2.20)$$

$$G_F(s) = \frac{(k_1\ell_1 + k_2\ell_2 + \ell_3)s^2 + (k_2\ell_3 + k_1\ell_2)s + k_1\ell_3}{k_1(s^3 + \ell_1 s^2 + \ell_2 s + \ell_3)} \qquad (2.21)$$

Finally, the transfer function from output to load disturbance is

$$G_D(s) = \frac{G(s)}{1 + G(s)G_C(s)G_F(s)}, \tag{2.22}$$

and the transfer function from control action to output is

$$G_U(s) = -G_C(s)G_F(s). \tag{2.23}$$

Equation (2.22) describes the system response to a load disturbance and (2.23) represents the LADRC transfer function for disturbance rejection.

2.3 Control problem formulation under the LADRC framework

Although the ADRC starts from the idea that through the design of the control law, a linear or non-linear system can be transformed into a linear decoupled system similar to (2.8), the success in the application of this strategy lies in the formulation of the control problem, such that the unknown quantities (modelling uncertainty and disturbances) are combined in the total perturbation [19]. This formulation begins with selecting the controlled and manipulated variables, involves understanding the system through mathematical representations or signals available for analysis, and leads to choosing the LADRC *canonical form* for the observer design.

2.3.1 *Identification of controlled and manipulated variables*

The identification of the outputs of the system to be controlled and the inputs through which control can be carried out is the first step in the design of controllers regardless of the strategy employed. The ADRC was initially formulated for single-input, single-output systems, as discussed in 2.2, but was quickly adapted to multi-variable systems under the name Disturbance Decoupling Control (DCC) [67].

Consider the $m \times m$ MIMO system (2.24), where the rate of change in each output (represented by the derivative of order n_i, $y^{(n_i)}$) is modelled as the sum of the total perturbation of each channel $f_i(\nu_i, p_i, d)$ and the product of the nominal value of the critical gain b_{0ii} and its dominant input u_i.

$$\begin{cases} y_1^{(n_1)} = f_1(\nu_1, ..., \nu_m, p_1, ...p_m, d) + b_{011}u_1 \\ y_2^{(n_2)} = f_2(\nu_1, ..., \nu_m, p_1, ...p_m, d) + b_{022}u_2 \\ \vdots \\ y_m^{(n_m)} = f_m(\nu_1, ..., \nu_m, p_1, ...p_m, d) + b_{0mm}u_m \\ \nu_i = (y_i, \dot{y}_i, ..., y_i^{(n_i-1)}) \\ p_i = (u_i, \dot{u}_i, ..., u_i^{(n_i-1)}) \end{cases} \quad (2.24)$$

The total perturbation functions in (2.24) combines the non-modelled internal dynamics and coupling between channels, represented by ν_i, p_i, and the load perturbations, denoted by d. Therefore, to achieve decoupling, a SISO LADRC is designed in each loop. This way, the multi-variable system is transformed into a set of m outputs whose behaviour in each channel resembles that of an integrator of order n_i.

The main advantage of DDC is that a proper observer design allows real-time active cancellation of the total disturbance of each channel. However, the proposal requires prior selection of the dominant output-input pairs and tuning of $(2n_i + 1)$ parameters in each loop.

2.3.2 System characterisation and LADRC order selection

After the first publications [68], [69] in which some of the studies that demonstrated the viability of ADRC as a new control paradigm were reviewed, the need to deepen the theoretical justification of the strategy became evident. In particular, in the definition of conditions that would allow deciding whether a process can be controlled by ADRC and the influence of the design parameters on the closed-loop performance.

Next, the applicability of ADRC is discussed from two perspectives. In the first one, it is assumed that there is some mathematical representation or model of the process that, when reformulated, allows identifying the unknown quantities that make up the total disturbance, as well as the real or relative order and an approximation of the critical gain. On the other hand, the characteristics that have guided the study of ADRC (mainly in linear systems) and constitute the necessary understanding of the problem for the following design phases are mentioned.

When the control objective is output regulation, the input-output model of the process, such as (2.1), allows the unknown terms that make up the total disturbance to be identified. However, when complete control of the state vector is desired, the reformulation of the problem must ensure that both the control signal and the external disturbances only affect the rate of change of the last state [70]. This condition is known as the *matching condition* in English literature [2]. An example clarifies the above.

Given the second-order SISO system

$$\begin{cases} \dot{x}_1 = x_2 + w \\ \dot{x}_2 = -c_1 x_1 - c_2 x_2 + u \\ y = x_1, \end{cases} \tag{2.25}$$

where c_1 and c_2 are unknown positive constants and w is a perturbation affecting the first state evolution. Defining $\overline{x}_1 = x_1$ and $\overline{x}_2 = x_2 + w$ leads to

$$\dot{\overline{x}}_2 = \frac{d}{dt}(x_2 + w) \tag{2.26}$$

$$\dot{\overline{x}}_2 = \dot{x}_2 + \dot{w} \tag{2.27}$$

$$\dot{\overline{x}}_2 = -c_1 x_1 - c_2 x_2 + u + \dot{w} \tag{2.28}$$

$$\dot{\overline{x}}_2 = -c_1 \overline{x}_1 - c_2(\overline{x}_2 - w) + u + \dot{w} \tag{2.29}$$

Therefore, the system (2.25) is equivalent to

$$\begin{cases} \dot{\overline{x}}_1 = \overline{x}_2 \\ \dot{\overline{x}}_2 = -c_1 \overline{x}_1 - c_2(\overline{x}_2 - w) + \dot{w} + u \\ y = \overline{x}_1, \end{cases} \tag{2.30}$$

from which it follows that $f = -c_1 \overline{x}_1 - c_2(\overline{x}_2 - w) + \dot{w}$ is the total disturbance and $\overline{x}_3 \triangleq f$ is the additional state. Thus, under the ADRC approach, the control problem is solved by estimating and cancelling the effect of f rather than the individual action of the external disturbance w.

Active disturbance rejection control was conceived as a control technology that seeks to eliminate the dependence on a precise process model, understanding that all controller designs are based on some interpretation of the system, mathematical or otherwise [71]. Consequently, ADRC is considered appropriate for systems with little knowledge of the dynamics, and its characterisation is performed by analysing the manipulated and controlled signals. Features of interest include the identification of relative order or dominant dynamics and the presence of inverse response (*undershoot*), such as that caused by non-minimum phase zeros, dead time and instability.

Regarding the ADRC order, it was initially proposed that it should coincide with the relative order of the system [1]. However, most works are developed with first-order or second-order ADRC implementations assuming that the processes or practical applications have such dominant dynamics. In the case of SISO systems, two theorems have been put forward that guide LADRC design when the process order is unknown. Their main conclusions are summarised below [24].

- For a process whose behaviour resembles that of a minimum-phase Linear Time-Invariant (LTI) system, there is a set of LADRC gains that achieve closed-loop stability, provided that the estimated critical gain b_0 maintains the sign of the actual critical gain and the order of implementation is equal to or greater than the relative order of the system.

- For a process with behaviour similar to a stable open-loop LTI model, there is a set of first-order or higher LADRC gains that achieve closed-loop stability. In addition to the design of the controller and observer gains, it is suggested to increase the absolute value of b_0 until the desired performance is achieved.

The LADRC implementation in minimum-phase LTI systems has greater robustness concerning variations in nominal critical gain when the system order is low. However, the selection of b_0 below the actual value $(b_0 < b)$ reduces the level of uncertainty allowed in systems with delay [72]. That is, the value of b_0 can be set over a broader range of values when n is small, which is convenient if first-order or second-order dominant dynamics are considered, but this advantage is limited in systems with dead time.

2.3.3   Selection of the LADRC canonical form

The canonical form ADRC refers to the desired behaviour of the modified plant (see Figure 2.1). In the conventional ADRC discussed in section 2.2.2, the observer and the manipulated variable (2.7) combined action is assumed to induce the system to behave like the set of disturbance-free cascaded integrators (2.8). Consequently, the ADRC *transforms* an unknown and uncertain system into a more straightforward and less uncertain linear version that reduces the complexity in the design of the control law u_0 [3].

If information about the system model is available, it can be incorporated into the extended state observer to improve its estimation capability. According to the type of information used to design the LESO, the modified plant is no longer assumed to be the cascaded integrators characterising the conventional LADRC version. These new proposals are considered alternative canonical forms in the ADRC approach and have been referred to by their authors in different ways. Table 2.1 reunites the formulations of the model-assisted ADRC [12], the generalised ADRC [13] and the modified ADRC [14]. In those proposals where a nominal model is assumed, it is considered that the system is represented by the input-output equation (2.31), where the notation $y^{(n)}$ or $u^{(n)}$ indicates a derivative of order n. Table 2.1 also includes the LESO formulations associated to each LADRC implementation. In all cases, $\hat{\mathbf{x}} = [\hat{x}_1, \ldots, \hat{x}_n, \hat{x}_{n+1}]^\top$ represents the estimated states vector and $\boldsymbol{\ell} = [\ell_1, \ldots, \ell_n, \ell_{n+1}]^\top$ the gains vector.

$$y^{(n)} + \cdots + a_1\dot{y} + a_0 y = b_n u^{(n)} + \cdots + b_1\dot{u} + b_0 u \tag{2.31}$$

Likewise, some comments are included in Table 2.2 to highlight the main differences among the above and to guide the reader on the selection and implementation of one of them according to the application of interest.

Finally, it is worth mentioning that the expected behaviour of the modified plant depends significantly on the selection of the observer gains and the critical gain. Previously it was noted that the knowledge of the estimated value of this parameter is necessary for implementing the LADRC, and its tuning, at first, was proposed based on the experience of the control engineer and the characterisation of the process. The following subsection discusses the tuning of the LADRC gain set.

Canonical form	Extended State Observer

Conventional LADRC [23]

$$
\begin{bmatrix} \dot{x}_1 \\ \vdots \\ \dot{x}_{n-1} \\ \dot{x}_n \end{bmatrix} = \underbrace{\begin{bmatrix} 0 & 1 & \cdots & 0 \\ \vdots & \vdots & \ddots & \vdots \\ 0 & 0 & 0 & 1 \\ 0 & 0 & 0 & 0 \end{bmatrix}}_{A} \begin{bmatrix} x_1 \\ \vdots \\ x_{n-1} \\ x_n \end{bmatrix} + \underbrace{\begin{bmatrix} 0 \\ \vdots \\ 0 \\ 1 \end{bmatrix}}_{B} u
$$

$$
y = \underbrace{\begin{bmatrix} 1 & \cdots & 0 & 0 \end{bmatrix}}_{C} \begin{bmatrix} x_1 \\ \vdots \\ x_{n-1} \\ x_n \end{bmatrix}
$$

$$
A_o = \begin{bmatrix} A & \begin{bmatrix} 0_{(n-1)\times 1} \\ 1 \\ 0 \end{bmatrix} \\ 0_{1\times n} & 0 \end{bmatrix} \quad B_o = b_0 \begin{bmatrix} B \\ 0 \end{bmatrix}
$$

$$
C_o = \begin{bmatrix} C & 0 \end{bmatrix}
$$

$$
\dot{\hat{\mathbf{x}}} = A_o \hat{\mathbf{x}} + B_o u + \boldsymbol{\ell}(y - C_o \hat{\mathbf{x}})
$$

Model assisted LADRC[12]

$$
\begin{bmatrix} \dot{x}_1 \\ \vdots \\ \dot{x}_{n-1} \\ \dot{x}_n \end{bmatrix} = \underbrace{\begin{bmatrix} 0 & 1 & \cdots & 0 \\ \vdots & \vdots & \ddots & \vdots \\ 0 & 0 & 0 & 1 \\ -a_0 & -a_1 & \cdots & -a_{n-1} \end{bmatrix}}_{A} \begin{bmatrix} x_1 \\ \vdots \\ x_{n-1} \\ x_n \end{bmatrix} + \underbrace{\begin{bmatrix} \beta_1 \\ \vdots \\ \beta_{n-1} \\ \beta_n \end{bmatrix}}_{B} u
$$

$$
y = \underbrace{\begin{bmatrix} 1 & \cdots & 0 & 0 \end{bmatrix}}_{C} \begin{bmatrix} x_1 \\ \vdots \\ x_{n-1} \\ x_n \end{bmatrix}
$$

$$
A_o = \begin{bmatrix} A & B \\ 0_{1\times n} & 0 \end{bmatrix} \quad B_o = \begin{bmatrix} B \\ 0 \end{bmatrix}
$$

$$
C_o = \begin{bmatrix} C & 0 \end{bmatrix}
$$

$$
\dot{\hat{\mathbf{x}}} = A_o \hat{\mathbf{x}} + B_o u + \boldsymbol{\ell}(y - C_o \hat{\mathbf{x}})
$$

To be continued

Table 2.1 (continued)

Canonical form	Extended State Observer

Generalised LADRC [13]

$$\begin{bmatrix} \dot{x}_1 \\ \vdots \\ \dot{x}_{n-1} \\ \dot{x}_n \end{bmatrix} = \underbrace{\begin{bmatrix} 0 & 1 & \cdots & 0 \\ \vdots & \vdots & \ddots & \vdots \\ 0 & 0 & 0 & 1 \\ -a_0 & -a_1 & \cdots & -a_{n-1} \end{bmatrix}}_{A} \begin{bmatrix} x_1 \\ \vdots \\ x_{n-1} \\ x_n \end{bmatrix} + \underbrace{\begin{bmatrix} 0 \\ \vdots \\ 0 \\ b_0 \end{bmatrix}}_{B} u$$

$$y = \underbrace{\begin{bmatrix} 1 & \cdots & b_{n-2}/b_0 & b_{n-1}/b_0 \end{bmatrix}}_{C} \begin{bmatrix} x_1 \\ \vdots \\ x_{n-1} \\ x_n \end{bmatrix}$$

$$A_o = \begin{bmatrix} A & \begin{bmatrix} 0_{(n-1)\times 1} \\ 1 \\ 0 \end{bmatrix} \\ 0_{1\times n} \end{bmatrix} \quad B_o = \begin{bmatrix} B \\ 0 \end{bmatrix}$$

$$C_o = \begin{bmatrix} C & 0 \end{bmatrix}$$

$$\dot{\hat{\mathbf{x}}} = A_o \hat{\mathbf{x}} + B_o u + \boldsymbol{\ell}(y - C_o \hat{\mathbf{x}})$$

Modified conventional LADRC [14]

$$\begin{bmatrix} \dot{x}_1 \\ \vdots \\ \dot{x}_{n-1} \\ \dot{x}_n \end{bmatrix} = \underbrace{\begin{bmatrix} 0 & 1 & \cdots & 0 \\ \vdots & \vdots & \ddots & \vdots \\ 0 & 0 & 0 & 1 \\ 0 & 0 & 0 & 0 \end{bmatrix}}_{A} \begin{bmatrix} x_1 \\ \vdots \\ x_{n-1} \\ x_n \end{bmatrix} + \underbrace{\begin{bmatrix} 0 \\ \vdots \\ 0 \\ 1 \end{bmatrix}}_{B} u$$

$$y = \underbrace{\begin{bmatrix} 1 & \cdots & 0 & 0 \end{bmatrix}}_{C} \begin{bmatrix} x_1 \\ \vdots \\ x_{n-1} \\ x_n \end{bmatrix}$$

$$A_o = \begin{bmatrix} 0_{n\times 1} & I_{n\times n} \\ 0 & \mathbf{a} \end{bmatrix} \quad B_o = b_0 \begin{bmatrix} B \\ -a_{n-1} \end{bmatrix}$$

$$C_o = \begin{bmatrix} C & 0 \end{bmatrix}$$

$$\dot{\hat{\mathbf{x}}} = A_o \hat{\mathbf{x}} + B_o u + \boldsymbol{\ell}(y - C_o \hat{\mathbf{x}})$$

Table 2.2: Differentiating characteristics of the LADRC formulations from the literature.

LADRC	Characteristics
Conventional [23]	- The modified or nominal plant is assumed to be a set of cascaded integrators or an integrator of order n. - The control action on the plant is $u = \dfrac{1}{b_0} \left[k_1(\tilde{r} - \hat{x}_1) - \sum_{i=2}^{n} (k_i \hat{x}_i) - \hat{x}_{n+1} \right]$.
Model assisted [12]	- The modified plant is assumed to be a non-minimum phase system of order n. - The first state coincides with the controlled output and its measurement is accessible. - The β_i $(i = 1, ..., n)$ values are computed from the coefficients representing the nominal process. - The first state coincides with the controlled output and its measurement is accessible. - Through bandwidth parameterization, the observer gains in the $\boldsymbol{\ell}$ vector are computed by comparing the coefficients in the characteristic equation $|sI - (A_o - \boldsymbol{\ell} C_o)|$ with those in the polynomial $(s + \omega_o)^{n+1}$. As the matrix A_o contains process model information, the elements in $\boldsymbol{\ell}$ are dependent on this information. - The control action on the plant is $u = u_0 - \hat{x}_{n+1}$. - The control action u_0 is the output from a feedforward controller comprising a signal generator and a compensator. This proposal seeks that the system response reaches the steady state in a required settling time and under a constraint on the inverse response (*undershoot*). The feedforward controller design is addressed in detail in [73].

To be continued

<div align="center">Table 2.2 (continued)</div>

LADRC	Characteristics
Generalised [13]	- The modified plant is assumed to be a system of order n with the known nominal location of poles and zeros. - The controlled output is a linear combination of the states. - Through bandwidth parameterization, the observer gains in the $\boldsymbol{\ell}$ vector are computed by comparing the coefficients in the characteristic equation $\lvert sI - (A_o - \boldsymbol{\ell}C_o) \rvert$ with those in the polynomial $(s + \omega_o)^{n+1}$. As the matrix A_o contains process model information, the elements in $\boldsymbol{\ell}$ are dependent on this information. - The control law on the plant is $u = r - \dfrac{1}{b_0}\left[\sum_{i=1}^{n}\left(k_i \hat{x}_i\right) - \hat{x}_{n+1}\right]$. - The k_i values are computed following that $k_i = \binom{n}{i-1}\omega_c^{n+1-i} - a_{i-1}$. - To improve the trajectory tracking, it is necessary to filter the reference signal according to $r = F\tilde{r}$, where $F = 1/\left[-C(A - BK)^{-1}B\right]$ and $K = [k_1 \; \cdots \; k_n \; 1]/b_0$.
Modified conventional [14]	- The modified or nominal plant is assumed to be a set of cascaded integrators or an integrator of order n. - The first state coincides with the controlled output and its measurement is accessible. - It is assumed that the total perturbation is the sum of a known component f_k, which models the dynamics of the poles, and an unknown component f_u, which includes the non-modelled dynamics of the zeros and the unwanted external forces. - As the model of f_k is known, the information of $\dot{f}_k$ is included in the extended state observer through the elements of the vector $\mathbf{a} = [-a_0 \; \cdots \; -a_{n-1}]$. Therefore, the observer gains in the $\boldsymbol{\ell}$ vector are computed by comparing the coefficients in the characteristic equation $\lvert sI - (A_o - \boldsymbol{\ell}C_o) \rvert$ with those in the polynomial $(s + \omega_o)^{n+1}$.

2.4   LADRC gains tuning

The design of the LADRC parameters has gained attention as the study of this technology has progressed. A common feature among the contributions is that most are based on the bandwidth parameterization proposed in [23], which expresses the observer and controller gains as a function of two quantities named observer bandwidth ω_o and controller bandwidth ω_c, respectively.

In line with the formulation presented in section 2.2 for a second-order SISO system, consider the state space representation of its extended model (2.5)

$$
\begin{bmatrix} \dot{x}_1 \\ \dot{x}_2 \\ \dot{x}_3 \end{bmatrix} = \underbrace{\begin{bmatrix} 0 & 1 & 0 \\ 0 & 0 & 1 \\ 0 & 0 & 0 \end{bmatrix}}_{A} \begin{bmatrix} x_1 \\ x_2 \\ x_3 \end{bmatrix} + \underbrace{\begin{bmatrix} 0 \\ b_0 \\ 0 \end{bmatrix}}_{B} u + \underbrace{\begin{bmatrix} 0 \\ 0 \\ 1 \end{bmatrix}}_{E} h \tag{2.32}
$$

$$
y = \underbrace{\begin{bmatrix} 1 & 0 & 0 \end{bmatrix}}_{C} \begin{bmatrix} x_1 \\ x_2 \\ x_3 \end{bmatrix},
$$

whose matrix form is

$$
\dot{\mathbf{x}} = A\mathbf{x} + Bu + Eh \tag{2.33}
$$
$$
y = C\mathbf{x},
$$

with $\mathbf{x} = [x_1, x_2, x_3]^\top$. Similarly, the matrix form of the LESO (2.11), defining $\hat{\mathbf{x}} = [\hat{x}_1, \hat{x}_2, \hat{x}_3]^\top$ and $\boldsymbol{\ell} = [\ell_1, \ell_2, \ell_3]^\top$, is

$$
\dot{\hat{\mathbf{x}}} = A\hat{\mathbf{x}} + Bu + \boldsymbol{\ell}(C\mathbf{x} - C\hat{\mathbf{x}}). \tag{2.34}
$$

Let $\mathbf{e} = \mathbf{x} - \hat{\mathbf{x}}$ be the estimation error. Its dynamic behaviour is given by (2.35) and it is obtained after subtracting (2.34) from (2.33).

$$
\dot{\mathbf{e}} = (A - \boldsymbol{\ell}C)\mathbf{e} + Eh \tag{2.35}
$$

Assuming that h, even if it is unknown, is also differentiable and bounded, the observer gains can be calculated through pole placement. In [23], it is proposed that the three poles be located at position $-\omega_o$ in the left semi-plane such as

$$
sI - (A - \boldsymbol{\ell}C) = (s + \omega_o)^3. \tag{2.36}
$$

Consequently, the parameterization of the observer gains (2.37) is obtained as a function of ω_o by solving for both sides of (2.36) and comparing factors. The convergence analysis of the LESO, when designed using the above approach, is addressed in [7]. Likewise, [74] discusses the pertinence of assuming h bounded.

$$\ell_1 = 3\omega_o \quad \ell_2 = 3\omega_o^2 \quad \ell_3 = \omega_o^3 \tag{2.37}$$

The bandwidth parameterization can be generalised for an observer of order $n+1$ with characteristic equation (2.38). In this case, the gains ℓ_i are computed as (2.39).

$$s^{n+1} + \ell_1 s^n + ... + \ell_n s + \ell_{n+1} = (s + \omega_o)^{n+1} \tag{2.38}$$

$$\ell_i = \binom{n+1}{i} \omega_o^i \; ; \; i = 1, 2, ..., n+1 \tag{2.39}$$

On the other hand, the controller gains design takes into account the frequency representations of the modified plant (2.8) and the control action (2.12) to obtain the closed-loop transfer function

$$G_Y(s) = \frac{k_1}{s^2 + k_2 s + k_1}. \tag{2.40}$$

According to the characteristic equation of (2.40), the closed-loop poles depend on the selection of the gains k_1 and k_2. Then, following the approach from [23], the poles are located at $-\omega_c$ as in (2.41) and the controller gains parameterization of (2.42) is derived.

$$s^2 + k_2 s + k_1 = (s + \omega_c)^2 \tag{2.41}$$

$$k_1 = \omega_c^2 \quad k_2 = 2\omega_c \tag{2.42}$$

Extending the analysis to a system of order n, the gains of the control law u_0 are calculated according to

$$k_i = \binom{n}{i-1} \omega_c^{n+1-i} \; ; \; i = 1, 2, ..., n \tag{2.43}$$

The selection of ω_o and ω_c results in a trial-and-error process in which the controller bandwidth is often set to the desired closed-loop performance, and the observer bandwidth corresponds to a scaled ω_c value ($\omega_o = k_o\omega_c$, $k_o \geq 1$). An increase in the values of both parameters can improve the estimation error and the system response speed but cause oscillations along with an increase in the control action magnitude and rate of change. The main disadvantage of this strategy is its empirical nature, as it does not always provide satisfactory results and retuning supported by other techniques may be necessary.

In the case where a canonical form other than the conventional one is adopted, (2.39) and (2.43) include information from the nominal model of the system according to the modifications presented in Table 2.1.

2.5 A guide for the LADRC implementation

This section combines the concepts and ideas presented in the previous sections into a guide for designing control loops using LADRC.

A five-step algorithm is presented in Guide 2.5.1. Reference is made to the section of this chapter where the corresponding theory was discussed. Some hints for the computation of the LADRC gains are also included. For example, suppose the open-loop step response of a stable system with first-order dominant dynamics is accessible. In that case, the approximate value of the critical gain b_0 can be computed as the ratio of the static gain K to the time constant T. On the other hand, if second-order dominant dynamics is assumed, the nominal value b_0 is approximated as the ratio of the static gain to the square of the time constant T [22].

The desired closed-loop settling time $t_{98\%}$ can be used to calculate the controller bandwidth and subsequently scale the result to obtain the observer bandwidth. In each case, the computation suggestions represent initial values for the gains and may need to be adjusted according to performance requirements, as indicated in the final step.

Guide 2.5.1: Algorithm for the Linear Active Disturbance Rejection Control (LADRC) design

1. Define the type of system (plant) to be controlled.

   Single-Input Single-Output   Multiple-Input Multiple-Output
   (SISO)   (MIMO)
   ↓   ↓
   LADRC (section 2.2.2)   DDC (section 2.3.1)
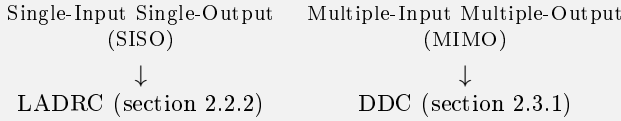
2. Identify the system characteristics of interest.

   Is the system
   open-loop stable?   →   Yes   →   Obtain the step response to determine n and b_0.

   If $n = 1$, then

   $$\dot{y} = -\frac{1}{T}y + \frac{K}{T}u,\ b_0 \approx K/T$$

   No

   If $n = 2$, then

   $$\ddot{y} = -2\frac{D}{T}\dot{y} - \frac{1}{T^2}y + \frac{K}{T^2}u,\ b_0 \approx K/T^2$$

   Use a mathematical representation (e.g., a input-output model as (2.1)) to determine n and b_0.
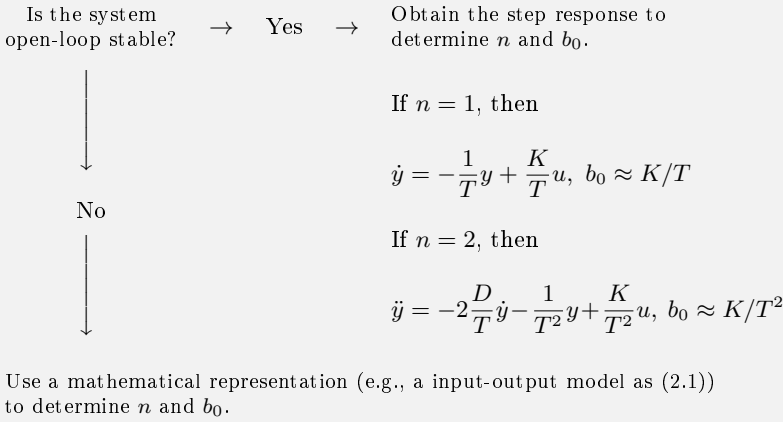
3. Choose a canonical form, for example, the conventional LADRC (section 2.2.2 and Table 2.1).

4. Compute the LADRC gains by bandwidth parameterization (section 2.4).

   If the canonical LADRC is chosen

   First-order LADRC ($n = 1$)   Second-order LADRC ($n = 2$)
   ↓   ↓
   $\omega_c = 5/t_{98\%},\ \omega_o = k_o\omega_c$ $\omega_c = 8/t_{98\%},\ \omega_o = k_o\omega_c$

   $k_1 = \omega_c$ $k_1 = \omega_c^2, k_2 = 2\omega_c$

   $\ell_1 = 2\omega_o,\ \ell_2 = \omega_o^2$ $\ell_1 = 3\omega_o,\ \ell_2 = 3\omega_o^2,\ \ell_3 = \omega_o^3$
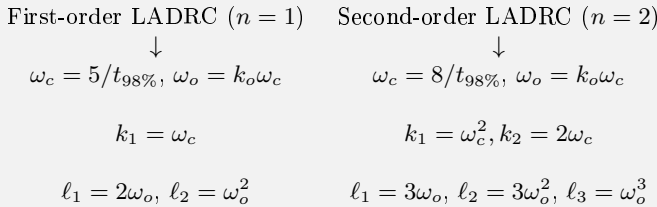
   Otherwise, see Table 2.1.

5. Evaluate the closed-loop performance and retune the gains if necessary.

2.6 LADRC implementation examples

This section presents two examples to illustrate the design of the LADRC loop according to Guide 2.5.1. In the first one, the temperature of a thermoelectric module is controlled. In the second one, the LADRC is used to control the concentration of a product and the temperature inside a reactor. Both examples were developed in MATLAB-Simulink. These implementations are available in MATLAB Central [63], so the reader can reproduce the results of this section or use the codes to apply the LADRC design guide to other control problems.

EXAMPLE 2.6.1 The temperature control of a thermoelectric module operating according to the Peltier principle and whose dynamics is non-linear around its operating zones of *cooling* ($\approx 4\,^\circ\mathrm{C}$) and *freezing* ($\approx -8\,^\circ\mathrm{C}$) is considered.

A thermoelectric module is an array of thermocouples connected electrically in series and thermally in parallel, as depicted in Figure 2.3. When current is driven through the thermocouples, it produces heating or cooling depending on the current direction. The energy transported by the electrons changes as the current passes from one type of material to the other, leading to a difference in energy which is transformed into heating or cooling. The above is known as the *Peltier effect* [75]. In the refrigeration mode, the positive current produces that heat flows from the heat source to the heat sink, causing a decrease in temperature in the former with respect to the heat sink thermal conductor. Consequently, the heat source turns out to be the cooling face of the Peltier cell.

The thermoelectric module behaviour is described by the thermal balance equations presented next and whose variables are listed in Table 2.3.
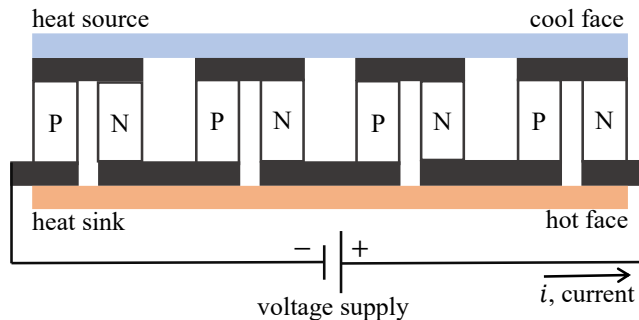
Figure 2.3: Simple sketch of the Peltier thermoelectric module in refrigeration mode.

Table 2.3: Description of variables of the Peltier thermoelectric module model.

Variable	Units	Description
T_c	K	Temperature on the cold face
T_h	K	Temperature on the hot face
T_r	K	Temperature in the radiator
V_{in}	%	Voltage applied to the Peltier thermoelectric module
I_p	A	Current flow in the Peltier thermoelectric module
Q_{cf}	W	Net heat flow on the cold face
Q_{acf}	W	Heat flow transmitted by convection between the environment and the cold face
Q_{pcf}	W	Heat flow absorbed by the cold face due to the Peltier effect
Q_j	W	Heat flow generated by Peltier cell due to Joule effect
Q_{cond}	W	Heat flow transferred by conduction from the hot face to the cold face
Q_{hf}	W	Net heat flow on the hot face
Q_{rhf}	W	Heat flow transmitted by radiation between the hot face and radiator
Q_{phf}	W	Heat flow dissipated by the hot face due to Peltier effect
Q_{rf}	W	Net heat flow into the radiator
Q_{acc}	W	Heat flow transmitted by convection between the environment and the radiator

The parameters of the non-linear model were taken from [76], where an evolutionary multi-objective optimisation methodology and experimental data were used to identify the first principle model of a Peltier cell laboratory set-up. The corresponding values are reported in Table 2.4.

The thermal balance in the cold face is described as

$$Q_{cf} = m_c \dot{T}_c \tag{2.44}$$

$$Q_{cf} = Q_{acf} - Q_{pcf} - Q_j + Q_{cond} \tag{2.45}$$

$$Q_{acf} = (T_a - T_c) K_e \tag{2.46}$$

$$Q_{pcf} = \alpha_s T_c I_p \tag{2.47}$$

$$Q_j = \frac{1}{2} I_p^2 R_p \tag{2.48}$$

$$I_p = \frac{1}{R_p} \left[V_{in} - \alpha_s \left(T_h - T_c \right) \right] \tag{2.49}$$

$$Q_{cond} = 0.2 \left(T_h - T_c \right). \tag{2.50}$$

The thermal balance in the hot face is

$$Q_{hf} = m_c \dot{T}_h \tag{2.51}$$

$$Q_{hf} = Q_{rhf} + Q_{phf} + Q_j - Q_{cond} \tag{2.52}$$

$$Q_{rhf} = K_r \left(T_r - T_h \right) \tag{2.53}$$

$$Q_{phf} = \alpha_s T_h I_p. \tag{2.54}$$

And finally, the radiator equilibrium corresponds to

$$Q_{rf} = m_r \dot{T}_r \tag{2.55}$$

$$Q_{rf} = Q_{acc} - Q_{rhf} \tag{2.56}$$

$$Q_{acc} = K_f \left(T_a - T_r \right). \tag{2.57}$$

Table 2.4: Parameters of the Peltier thermoelectric module model [76].

Variable	Value	Units	Description
m_c	9.2	$\mathrm{J\,K^{-1}}$	Thermal capacity in the cold face
m_h	13	$\mathrm{J\,K^{-1}}$	Thermal capacity in the hot face
m_r	722.55	$\mathrm{J\,K^{-1}}$	Thermal capacity in the radiator
K_e	0.5	$\mathrm{W\,K^{-1}}$	Coefficient of thermal convection between the hot face and the environment
K_p	0.2	$\mathrm{W\,K^{-1}}$	Coefficient of thermal convection of the Peltier thermoelectric module
K_r	9.59	$\mathrm{W\,K^{-1}}$	Coefficient of thermal convection between the hot face and the radiator
K_f	7.11	$\mathrm{W\,K^{-1}}$	Amplification factor of convection between the environment and the radiator due to the action of a fan coupled to the thermoelectric module
α_s	0.041	$\mathrm{V\,K^{-1}}$	Seebeck coefficient
R_p	0.82	Ω	Thermoelectric module resistance
T_a	23.5	K	Ambient temperature

Following the steps from Guide 2.5.1

1. *Type of system.* The main objective is to control the thermoelectrical module temperature through the voltage supply. Therefore, in this single-input single-output loop, the controlled variable is the temperature on the cold face T_c, and the manipulated variable is the input voltage V_{in}.

2. *System characteristics.* The system is open-loop stable. With a voltage level of 26 %, the temperature on the cold face evolves from the initial temperature of 23.5 °C to an operating temperature of 4 °C in approximately 40 s. Figure 2.4 shows this behaviour. A dominant first-order dynamics is assumed.

   Since the temperature change experienced by the Peltier thermoelectric module to the increase in voltage is negative, i.e., an increase in voltage causes a decrease in temperature, it follows that the critical gain is negative, and its approximated value is computed as

$$b_0 = \frac{K}{T} = \frac{\Delta T_c}{V_{in} T} = \frac{4 - 23.5}{(26)(8)} = -0.094 \, \frac{°C}{\% \, s} \tag{2.58}$$
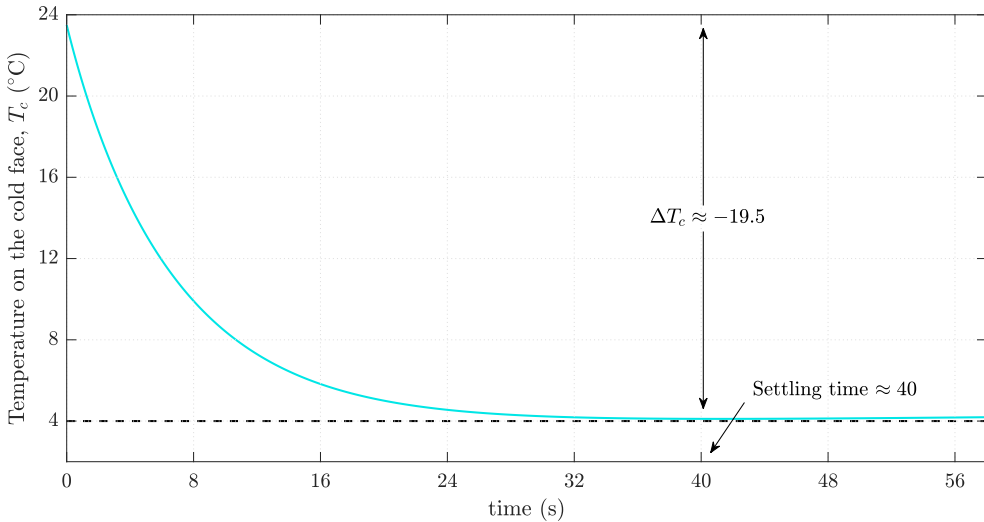
Figure 2.4: Open-loop response of the thermoelectric module when the input voltage is increased to $V_{in} = 26\,\%$. The temperature on the cold face decreases from $T_a = 23.5\,°C$ to $T_c = 4\,°C$ in approximately 40 s.

Notice that the static gain in (2.58) is assumed to be the ratio of the temperature change to the voltage change, and the time constant is approximated as one-fifth of the settling time.

3. *Canonical form.* Conventional LADRC is chosen such that the modified plant is assumed to be a first-order integrator. The corresponding LESO, with initial states $\hat{x}_1(0) = T_a$ and $\hat{x}_2(0) = 0$, is

$$\begin{bmatrix} \dot{\hat{x}}_1 \\ \dot{\hat{x}}_2 \end{bmatrix} = \begin{bmatrix} -\ell_1 & 1 \\ -\ell_2 & 0 \end{bmatrix} \begin{bmatrix} \hat{x}_1 \\ \hat{x}_2 \end{bmatrix} + \begin{bmatrix} b_0 \\ 0 \end{bmatrix} V_{in} + \begin{bmatrix} \ell_1 \\ \ell_2 \end{bmatrix} T_c \qquad (2.59)$$

and the control action on the thermoelectric module is

$$V_{in} = \frac{u_0 - \hat{x}_2}{b_0} = \frac{k_1 \left(\tilde{r} - \hat{x}_1 \right) - \hat{x}_2}{b_0} \qquad (2.60)$$

4. *LADRC tuning.* Using bandwidth parameterization, the controller bandwidth is designed to reach the desired temperature on the cold face in approximately $10\,\mathrm{s}$. According to (2.43)

$$k_1 = \omega_c = \frac{5}{t_{98\%}} = \frac{5}{10} = 0.5\,\frac{\mathrm{rad}}{\mathrm{s}} \qquad (2.61)$$

The observer bandwidth is chosen as $\omega_o = 2\omega_c$. Thus, following (2.39)

$$\ell_1 = 2\omega_o = 2\left(2\omega_c\right) = (4)(0.5) = 2\,\frac{\mathrm{rad}}{\mathrm{s}} \qquad (2.62)$$

$$\ell_2 = \omega_o^2 = [2(0.5)]^2 = 1\,\frac{\mathrm{rad}^2}{\mathrm{s}^2} \qquad (2.63)$$

5. *Performance evaluation.* The closed-loop response of the thermoelectric module around its cooling zone for different temperature setpoints is shown in Figure 2.5.The performance achieved with the PI controller (2.64), which was designed in [77] by multi-objective optimisation, is also included for qualitative comparison. Random noise with variance $\sigma^2 = 0.005$ and sampling frequency of $100\,\mathrm{Hz}$ is added to the output.

$$C_{PI}(s) = 0.86 \left(1 + \frac{1}{0.89s} \right) \qquad (2.64)$$
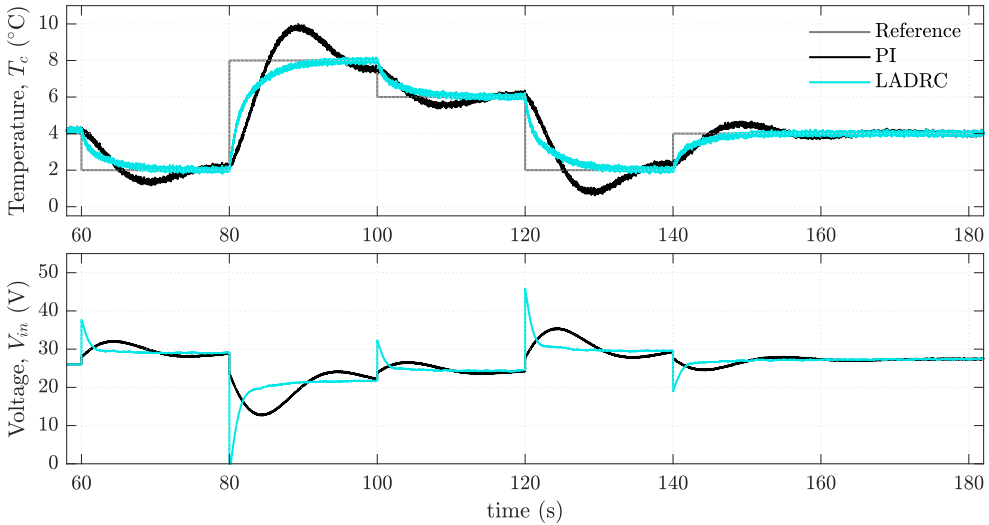
Figure 2.5: Closed-loop response of the thermoelectric module in its cooling zone when controlled by first-order LADRC. Comparison with a PI controller.
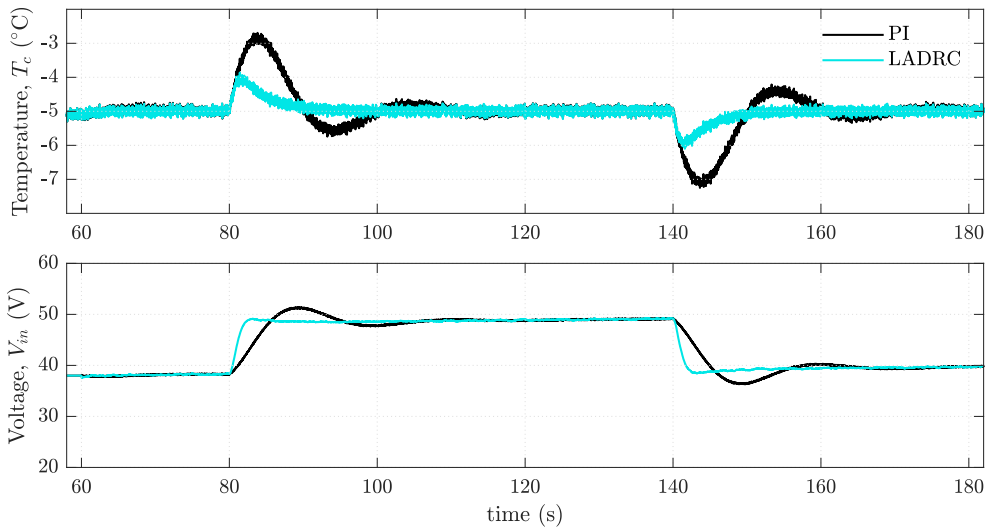
Figure 2.6: Closed-loop response of the thermoelectric module in its freezing zone when controlled by first-order LADRC and the voltage supply is reduced at $t = 80\,\text{s}$ by $10\,\%$ during one minute. Comparison with a PI controller.

The results show that the LADRC can control the non-linear system with a settling time that meets the design requirement and has no overshoot compared to the PI controller. With a higher LADRC controller bandwidth, the loop is still stable, and the settling time decreases at the cost of significant changes in the voltage when the setpoint changes. On the other hand, a larger observer bandwidth does not bring improvements in the system response; on the contrary, it generates more oscillation in the control action due to the noise.

Finally, we consider the case where the thermoelectric module operates in the freezing zone. With the same gains set, the LADRC maintains the cold face temperature at the desired value of $-5\,^\circ$C, as seen in Figure 2.6. At $t = 80\,$s, a power supply failure was simulated, which decreased the module voltage by $10\,\%$ for one minute. The LADRC rejects the disturbance effect on the output, with a maximum deviation of $1\,^\circ$C, and returns the system to its desired operating point faster than the PI controller.

EXAMPLE 2.6.2 The LADRC is now designed to control a Continuous Stirred Tank Reactor (CSTR).

In a CSTR (Figure 2.7), an irreversible first-order chemical reaction $A \rightarrow B$ takes place in the liquid generating heat. Therefore, a cooling liquid at temperature T_j circulates through a jacket covering the tank that contributes to regulating the temperature T_s inside. Moreover, controlling the concentration C_a of product A inside the tank is also of interest.
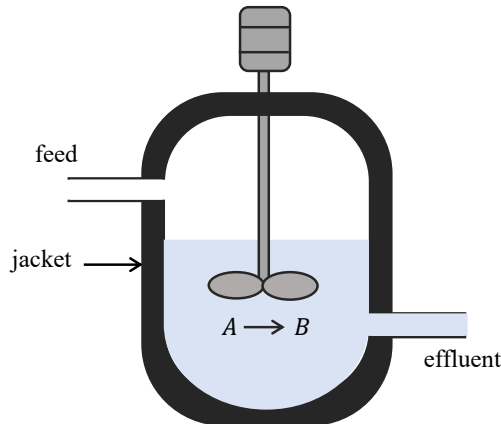
Figure 2.7: Continuous Stirred Tank Reactor (CSTR).

The CSTR behaviour is described by a set of highly non-linear equations resulting from the mass and energy balance of the reactor [78]. The solution of these equations when the accumulation terms are zero allows the calculation of the equilibrium points $P_i = [C_{as} \ T_{ss} \ T_{js}]$ which, depending on the reactor design, can be multiple. That is, the system can operate at different concentration and temperature values when the flow rates and other parameters are kept constant [79]. Let the CSTR presented in [80] be the system to be controlled and whose dynamics is given by

$$\dot{C}_a = \frac{F}{V}\left(C_{a0} - C_a\right) - k_0 C_a \exp\left(-\frac{E}{RT_s}\right) \tag{2.65}$$

$$\dot{T}_s = \frac{F}{V}\left(T_0 - T_s\right) + \frac{\Delta H}{\rho c_p}k_0 C_a \exp\left(-\frac{E}{RT_s}\right) - \frac{UA}{\rho c_p V}\left(T_s - T_j\right) \tag{2.66}$$

$$\dot{T}_j = \frac{F_j}{V_j}(T_{j0} - T_j) + \frac{UA}{\rho_j c_j V_j}(T_s - T_j) \tag{2.67}$$

The parameters from (2.65)-(2.67) are listed in Table 2.5. If the inlet flow rate, F, and coolant flow rate, F_j, are set at, for example, $F = 1.13\,\mathrm{m^3\,h^{-1}}$ and $F_j = 1.41\,\mathrm{m^3\,h^{-1}}$, the reactor exhibits the three equilibrium points listed in Table 2.6. At each of these temperatures, the heat generated by the reaction equals the heat removed with the aid of the coolant, as shown in Figure 2.8.

Table 2.5: Parameters of the CSTR (Example 2.6.2) [80].

Variable	Value	Units	Description
V	1.3592	$\mathrm{m^3}$	Reactor volume
V_j	0.0849	$\mathrm{m^3}$	Jacket volume
k_0	7.08×10^{10}	$\mathrm{h^{-1}}$	Reaction rate constant
E/R	8375.2	K	Activation energy term
ΔH	69 828	kJ/kmol	Heat of reaction
UA	7.136×10^4	$\mathrm{kJ/(h\,{}^{\circ}C)}$	Heat transfer term
ρ	800	$\mathrm{kg/m^3}$	Feed density
ρ_j	1000	$\mathrm{kg/m^3}$	Coolant density
c_p	3.142	$\mathrm{kJ/(kg\,K)}$	Feed heat capacity
c_j	4.189	$\mathrm{kJ/(kg\,K)}$	Cooling heat capacity
C_{a0}	8	$\mathrm{kmol\,A/m^2}$	Feed concentration
T_0	294.4	K	Feed temperature
T_{j0}	294.4	K	Coolant temperature

Table 2.6: CSTR equilibrium points (Example 2.6.2).

Point	C_{as} (kmol/m^3)	T_{ss} (K)	T_{js} (K)	Type
P_1	7.503	300.378	299.944	Stable
P_2	4.316	330.693	327.941	Unstable
P_3	0.839	363.766	358.486	Stable
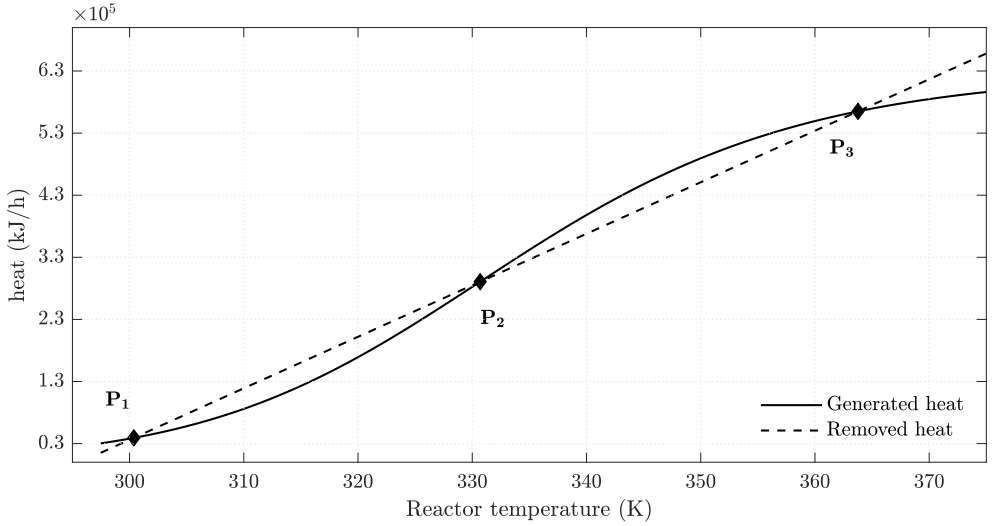
Figure 2.8: CSTR equilibrium points (Example 2.6.2). At the points P_1 (stable), P_2 (unstable), and P_3 (stable) the heat generated by the reaction equals the heat removed by the coolant.

The Guide 2.5.1 is used next to control the CSTR at points P_1 and P_2.

1. *Type of system.* It is desired to control the temperature T_s and the concentration C_a inside the reactor by manipulating the feed flow rate F and the coolant flow rate F_j. Consequently, the system is multi-variable.

   Under the DDC approach, the control of the CSTR requires the implementation of two SISO LADRC loops. The inlet flow rate controls the concentration, and the temperature inside the reactor is controlled by the flow rate of the coolant circulating through the jacket.
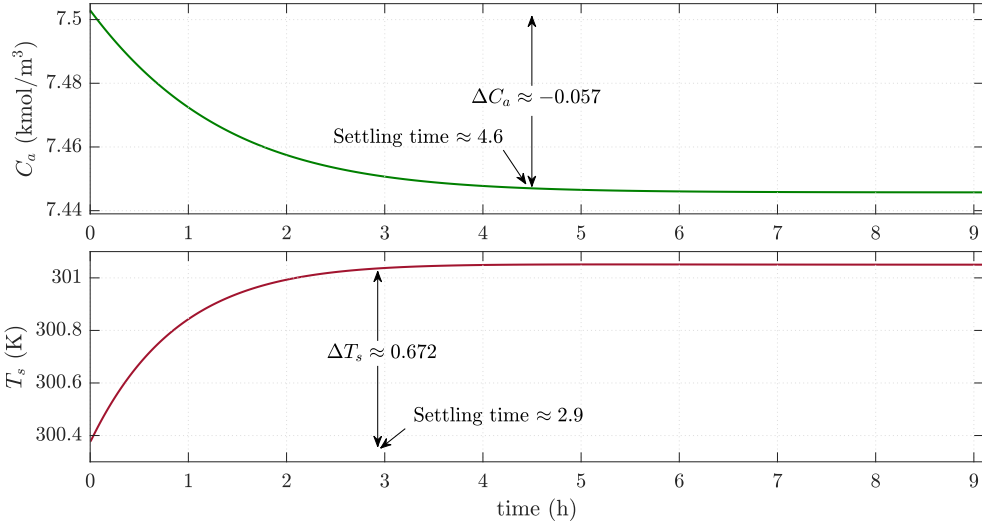
Figure 2.9: Open-loop response of the CSTR from Example 2.6.2 to a change in one of the manipulated variables at a time. Upper graph: C_a variation when F decreases from $1.130\,\mathrm{m}^3/\mathrm{h}$ to $1.017\,\mathrm{m}^3/\mathrm{h}$. Lower graph: T_s variation when F_j decreases from $1.410\,\mathrm{m}^3/\mathrm{h}$ to $1.269\,\mathrm{m}^3/\mathrm{h}$.

2. *System characteristics.* The upper graph in Figure 2.9 shows the evolution of the concentration with a decrease in the inlet volumetric flow rate of $10\,\%$ of its nominal value when the system operates in the equilibrium point P_1. Likewise, the lower graph shows the change in the reactor temperature when there is a decrease in the coolant flow rate of $10\,\%$ of its equilibrium value.

First-order LADRC is chosen for each controlled channel such that the system described by (2.65)-(2.67) is reformulated as

$$\dot{C}_a = f_1 + b_{011}F \tag{2.68}$$

$$\dot{T}_s = f_2 + b_{022}F_j \tag{2.69}$$

where f_1 and f_2 represent the unknown dynamics and perturbations of each loop.

The approximate values for b_{011} (2.70) and b_{022} (2.71) are computed according to the data from Figure 2.9, assuming that t_{ca} and t_r are the time constants of the concentration and temperature responses, respectively.

$$b_{011} = \frac{\Delta C_a}{\Delta F t_{ca}} = \frac{7.446 - 7.503}{(1.017 - 1.130)(0.923)} = 0.547 \; \frac{\text{kmol}}{\text{m}^6} \tag{2.70}$$

$$b_{022} = \frac{\Delta T}{\Delta F_j t_r} = \frac{301.050 - 300.378}{(1.269 - 1.410)(0.590)} = -8.078 \; \frac{\text{K}}{\text{m}^3} \tag{2.71}$$

3. *Canonical form.* The DDC assumes the conventional canonical form in each loop, so the LESO must estimate four states: $\hat{x}_{11}$ and $\hat{x}_{12}$ correspond to the estimated concentration and total disturbance of the first loop, and $\hat{x}_{21}$ and $\hat{x}_{22}$ represent the temperature and total disturbance of the second loop, respectively.

The LESO structure is

$$\dot{\hat{\mathbf{x}}} = A\hat{\mathbf{x}} + B\mathbf{u} + \boldsymbol{\ell}\,(\mathbf{y} - C\hat{\mathbf{x}}) \tag{2.72}$$

$$A = \begin{bmatrix} 0 & 0 & 1 & 0 \\ 0 & 0 & 0 & 1 \\ 0 & 0 & 0 & 0 \\ 0 & 0 & 0 & 0 \end{bmatrix} \quad B = \begin{bmatrix} b_{011} & 0 \\ 0 & b_{022} \\ 0 & 0 \\ 0 & 0 \end{bmatrix} \quad C = \begin{bmatrix} 1 & 0 & 0 & 0 \\ 0 & 1 & 0 & 0 \end{bmatrix} \tag{2.73}$$

$$\boldsymbol{\ell} = \begin{bmatrix} 2\omega_{o1} & 0 \\ 0 & 2\omega_{o2} \\ \omega_{o1}^2 & 0 \\ 0 & \omega_{o2}^2 \end{bmatrix} \quad \hat{\mathbf{x}} = \begin{bmatrix} \hat{x}_{11} \\ \hat{x}_{21} \\ \hat{x}_{12} \\ \hat{x}_{22} \end{bmatrix} \quad \mathbf{y} = \begin{bmatrix} C_a \\ T_s \end{bmatrix} \tag{2.74}$$

$$\mathbf{u} = \begin{bmatrix} \dfrac{\omega_{c1}(\tilde{r}_1 - \hat{x}_{11}) - \hat{x}_{12}}{b_{011}} \\[3mm] \dfrac{\omega_{c2}(\tilde{r}_2 \hat{x}_{21}) - \hat{x}_{22}}{b_{022}} \end{bmatrix} \tag{2.75}$$

It should be clarified that the LESO can be implemented as two independent state observers, one for each loop. Also, the matrices can be rearranged as long as the canonical LADRC form is respected. For this example, the last two states of $\hat{\mathbf{x}}$ are the estimated values of the total disturbances of each loop. Finally, the gains as a function of the bandwidths (ω_{c1}, ω_{o1} for the first loop and ω_{c2}, ω_{o2} for the second loop) are included in $\boldsymbol{\ell}$ and $\mathbf{u}$ since their values are defined in the next step.

(a)

(b)
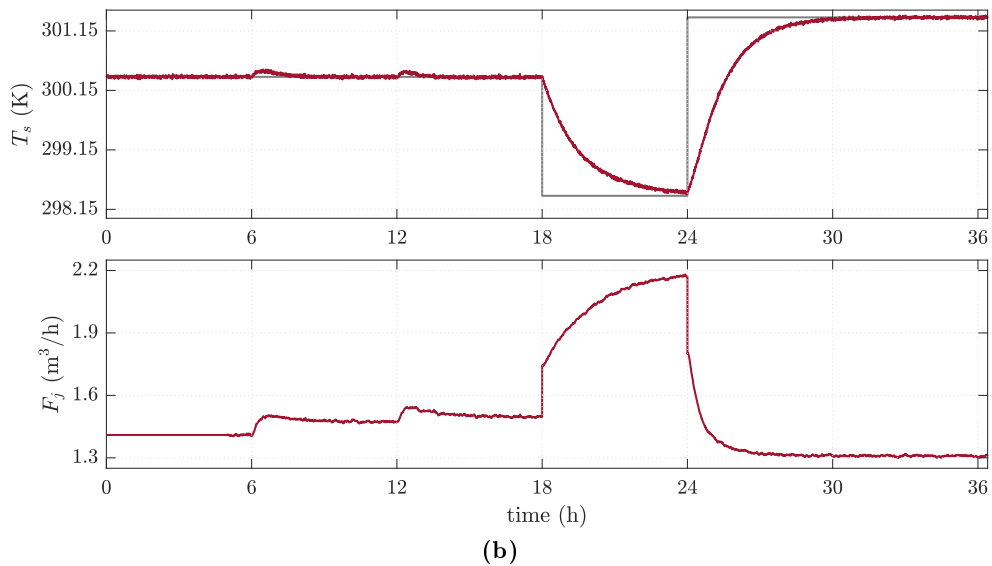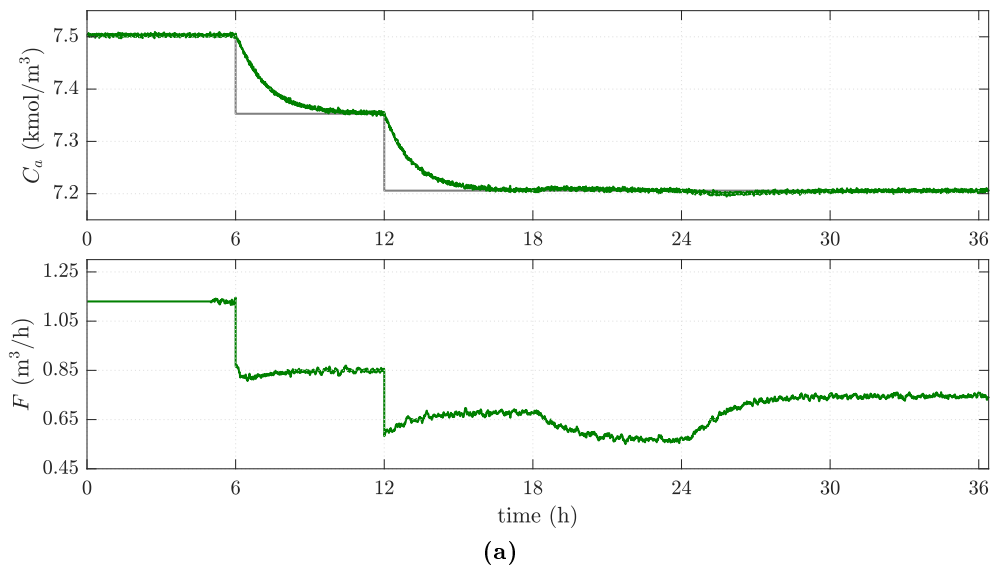
Figure 2.10: Closed-loop time response of the CSTR (Example 2.6.2) when controlled by DDC around the stable equilibrium point P_1. **(a)** Concentration of product A. **(b)** Reactor temperature.

4. *LADRC tuning.* The controller bandwidth of each loop is designed so that both outputs reach the steady state in approximately 5 h after a step change in reference. That is, $\omega_{c1} = \omega_{c2} = 1\,\mathrm{rad/h}$. The observers bandwidths are computed by scaling by ten the values of the controller bandwidths according to $\omega_{o1} = \omega_{o2} = 10\,\mathrm{rad/h}$.

5. *Performance evaluation.* Figure 2.10 shows the evolution of the concentration of product A and the reactor temperature for different reference values starting from the equilibrium point P_1. The outputs follow the references with the DDC by varying the two flow rates and reducing the channel coupling. Random noise was included with variance $\sigma^2 = 4{\times}10^{-6}$ for the measured concentration and $\sigma^2 = 2 \times 10^{-4}$ for the measured temperature.

The operation at unstable point P_2 is now considered. In this state, feedback control is necessary to maintain the process since any variation in the initial conditions leads the reactor to evolve towards one of the other two equilibrium points [78]. Figure 2.11 shows the system response when the disturbance decoupling controller designed for point P_1 is used. The DDC, in this case, maintains the reactor in its desired state and additionally rejects two types of disturbances: a 10 % decrease in the feed flow rate from instant $t = 8\,\mathrm{h}$ to instant $t = 16\,\mathrm{h}$ and a 10 % increase in the concentration of product A entering the reactor from instant $t = 16\,\mathrm{h}$ to instant $t = 24\,\mathrm{h}$. The first is viewed as a loading perturbation, and the second is a parametric uncertainty. In both cases, the volumetric flows evolve to return the reactor to a steady state in the required time.

Finally, for comparison, Figure 2.11 also includes the performance achieved with a DDC in which a second-order LADRC was implemented in each loop. The noise was removed to better visualisation of the controllers performance. The parameters were adjusted following Guide 2.5.1, keeping $t_{98\%} = 5\,\mathrm{h}$. Consequently, $b_{011} = 0.593\,\mathrm{kmol/m^6}$, $b_{022} = -13.701\,\mathrm{K/m^3}$, $\omega_{c1} = \omega_{c2} = 1.6\,\mathrm{rad/h}$, $\omega_{o1} = 16\,\mathrm{rad/h}$, and $\omega_{o2} = 8\,\mathrm{rad/h}$.

As can be seen in Figure 2.11, increasing the controller order reduces the maximum deviation occurring at the outputs with a slightly more considerable total variation in the control signals than in the first-order DDC. The above is reflected in the integral of absolute value of error reported in Table 2.7 for the two said cases; case 1: variation of the feed flow rate and case 2: variation of the concentration of product A entering the tank.

(a)

(b)
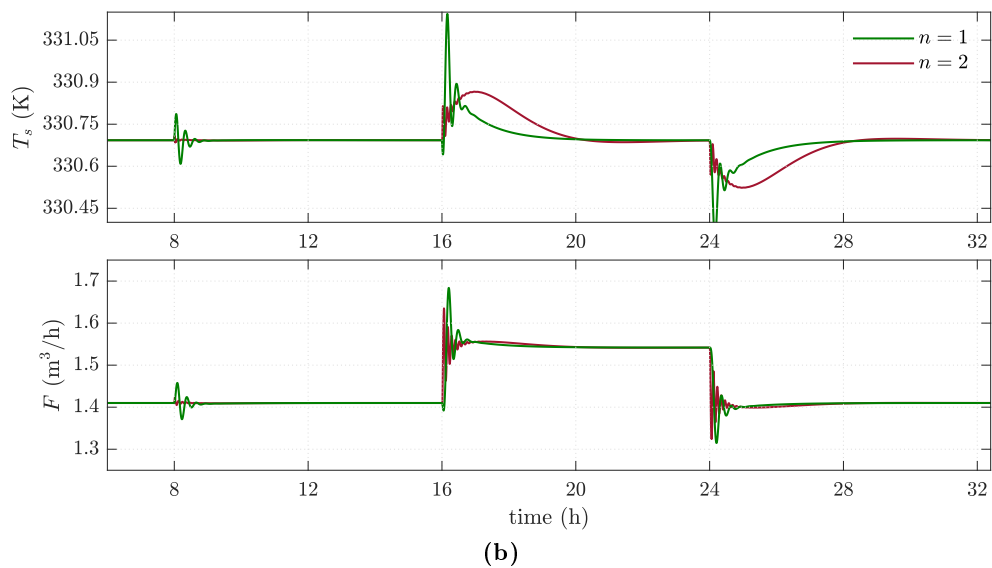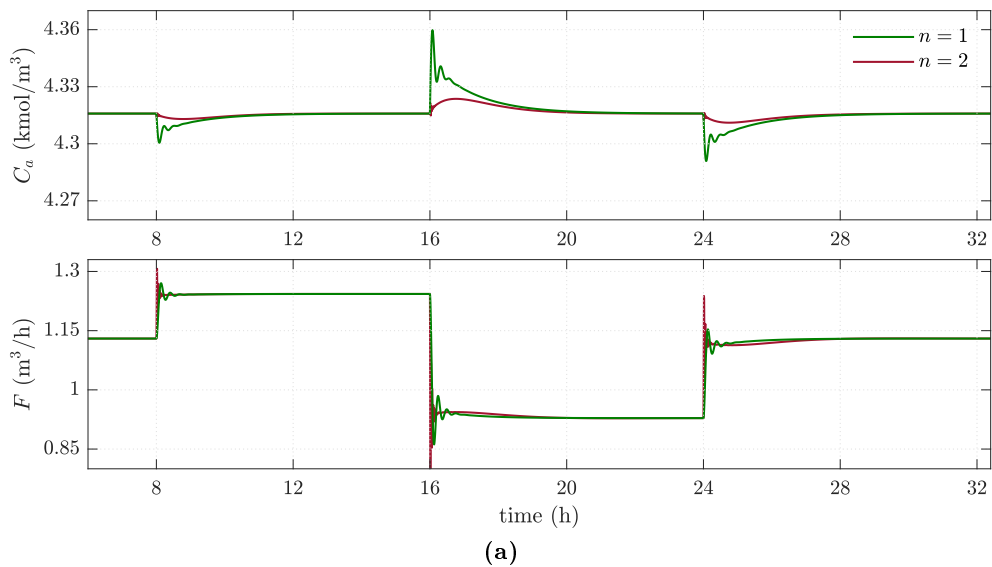
Figure 2.11: Closed-loop time response of the CSTR (Example 2.6.2) when controlled by DDC around the unstable equilibrium point P_2. Feed flow rate is decreased by $10\,\%$ from $t = 8\,\mathrm{h}$ to $t = 16\,\mathrm{h}$ and feed concentration is increased by $10\,\%$ from $t = 16\,\mathrm{h}$ to $t = 24\,\mathrm{h}$ **(a)** Concentration of product A. **(b)** Reactor temperature.

Table 2.7: Integral of absolute value of error IAE $= \int_0^{t_s} |e(t)|dt$ for the disturbance rejection performance of DDC when controlling a CSTR (Example 2.6.2).

	Case 1		Case 2	
	IAE_{C_a}	IAE_{T_s}	IAE_{C_a}	IAE_{T_s}
$n = 1$	0.014	0.034	0.038	0.228
$n = 2$	0.007	0.014	0.019	0.405

End of example 2.6.2 ■

As this chapter exposed, ADRC is a control algorithm that estimates and cancels unknown differences between the controlled plant and its assumed nominal model in real-time. These differences may include non-modelled dynamics, uncertainty and other perturbations. In concluding remarks

Conventional ADRC does not require a precise model to control a linear or non-linear system. Only the dominant dynamics order and the critical gain are necessary; specifications that may be approximated from the input and output signals analysis. The ADRC algorithm generally induces the system to behave as a cascaded integrator of order n governed by the designed control law.

ADRC is an alternative technology for the control of processes with challenging dynamics. The bandwidth parameterization is a starting point for tuning its gains, and new methodologies for parameter selection can be developed from here. Moreover, if ADRC is combined with advanced control techniques, new questions related to the loop structure arise, becoming new research challenges.

Chapter 3

Tuning Rules for Active Disturbance Rejection Controllers via Multi-objective Optimisation

This chapter introduces a set of tuning rules for the design of linear active disturbance rejection controllers, which offer three different levels of compromise between disturbance rejection and robustness. These tuning rules are the result of a curve fitting performed on the data obtained from a Multi-objective Optimisation Design (MOOD) procedure applied to the control of batch processes, and they are intended as a tool for designers who seek to implement LADRC by considering the load disturbance response of plants whose behaviour is approximated by a general first-order system with delay. The first section presents the main highlights of the proposed tuning method. The second section recalls the closed-loop parameterization employed in the tuning process. The third section shows the pertinence of the MOOD procedure for the LADRC tuning task. The fourth section describes the MOOD procedure performed to collect the data. The fifth section presents the data fitting and the resulting LADRC tuning rules. Finally, the sixth and seventh sections close the chapter by validating the proposed tuning method on illustrative examples and the control of a thermal process, respectively.

3.1   Introduction

This chapter provides a set of tuning rules for the second-order LADRC parameters computation applicable to the control of linear or non-linear systems whose dynamics can be approximated by a First-Order Plus Dead Time (FOPDT) model. The methodology used to derive the rules consisted of three phases. First, a MOOD procedure was applied to control a group of parametrised nominal plants to obtain a set of Pareto optimal solutions representing controllers with a compromise between the load disturbance response and the closed-loop robustness. Next, the LADRC parameters were fitted to functions of the normalised delay, and finally, these functions were scaled to make them suitable for the control of a general first-order system with delay.

The tuning rules presented here have the following advantages:

- They can be used to control systems approximated by a FOPDT model because only the static gain, apparent time constant and apparent delay are required as prior information. The FOPDT model is also known as the three-parameter model and is widely accepted in the control of industrial processes.

- The LADRC main parameters, this is, the nominal value of control gain, the controller bandwidth, and the observer bandwidth, are automatically computed through the substitution of the model parameters in the given formulae.

- The designers can select a robustness quality (low, medium or high) for the computation of the parameters, which allows their involvement as a decision-maker but eliminates the time and complexity of performing an entire optimisation process for the controller design. This is possible because robustness was included as a design objective in the optimisation process formulation, in contrast with other approaches from literature where robustness is imposed just as a constraint. Different Pareto optimal solutions were also used for the derivation of the rules.

- The parameters computed through the proposed rules ensure closed-loop stability and a reasonable compromise between disturbance rejection and loop robustness.

- The designer could use the rules to obtain intervals for each LADRC parameter and adjust the selection according to the preferred performance.

3.2 Control loop parameterization

The control loop parameterization seeks a set of parameters that allows the computation of the complete set of LADRC gains. In addition, if a LADRC is designed to control a nominal system (e.g., a nominal FOPDT system), the loop parameterization also allows the parameters scaling to make the controller suitable for other systems of the same nature.

Consider the following theorem related to the scaling and bandwidth parameterization of the LADRC loop.

Theorem 3.2.1 *[23] Assuming $G_a(s)$ is a stabilising controller for plant $G_n(s)$ and the loop gain crossover frequency is ω_c, then the controller*

$$\overline{G}_a(s) = \frac{1}{k}G_a\left(\frac{s}{\omega_p}\right) \tag{3.1}$$

will stabilise the plant $\overline{G}_n(s) = kG_n(s/\omega_p)$.

The new loop gain $\overline{\mathcal{L}}(s) = \overline{G}_n(s)\overline{G}_a(s)$ will have a crossover frequency $\omega_c\omega_p$ and the same stability margins of $\mathcal{L}(s) = G_n(s)G_a(s)$.

In equation (3.1), k represents the gain scaling of plant $kG_n(s)$ respect to $G_n(s)$ and ω_p is the frequency scaling of plant $G_n(s/\omega_p)$ respect to $G_n(s)$.

Let $G_A(s)$ be the transfer function obtained by multiplying the direct loop transfer function $G_C(s)$ (2.20) and the feedback transfer function $G_F(s)$ (2.21). This is,

$$G_A(s) = \frac{(k_1\ell_1 + k_2\ell_2 + \ell_3)s^2 + (k_2\ell_3 + k_1\ell_2)s + k_1\ell_3}{b_0(s^3 + (\ell_1 + k_2)s^2 + (\ell_2 + k_2\ell_1 + k_1)s)}. \tag{3.2}$$

Equation (3.2) is a function of b_0, the observer gains L_i, and the controller gains k_i. With the bandwidth parameterization from (2.37) and (2.42), (3.2) becomes

$$G_A(s) = \frac{\left(3\omega_c^2\omega_o + 6\omega_c\omega_o^2 + \omega_o^3\right)s^2 + \left(2\omega_c\omega_o^3 + 3\omega_c^2\omega_o^2\right)s + \omega_c^2\omega_o^3}{b_0\left[s^3 + (3\omega_o + 2\omega_c)s^2 + (3\omega_o^2 + 6\omega_c\omega_o + \omega_c^2)s\right]}. \tag{3.3}$$

Therefore, by proper selection of b_0, ω_c and ω_o, the second-order LADRC estimates and rejects the load disturbances acting on the loop.

Consider now that the process to be controlled is the FOPDT system

$$G(s) = \frac{K}{Ts+1}e^{-ls}, \tag{3.4}$$

where K is the static gain, T is the apparent time constant and l is the apparent delay or dead time [81].

If $G_n(s)$ is considered as a nominal FOPDT plant, then, following the scaling and bandwidth parameterization theorem [see (3.1)], the model (3.4) can be treated as a scaled version of (3.5) in which $k = K$, $\omega_p = 1/T$ and $\Theta = l/T$, as shown in (3.6).

$$G_n(s) = \frac{1}{s+1}e^{-\Theta s} \tag{3.5}$$

$$G(s) = K \left(\frac{1}{\frac{s}{1/T}+1} \right) e^{-\frac{l}{T}\frac{s}{1/T}}. \tag{3.6}$$

Hence, if $G_A(s)$ from (3.3) is a stabilising controller for (3.5), a stabilising controller $\overline{G}_A(s)$ exists for the general FOPDT system (3.4).

According to (3.1),

$$\overline{G}_A(s) = \frac{1}{k} \times \tag{3.7}$$

$$\frac{(3\omega_c^2\omega_o + 6\omega_c\omega_o^2 + \omega_o^3)\left(\frac{s}{\omega_p}\right)^2 + (2\omega_c\omega_o^3 + 3\omega_c^2\omega_o^2)\left(\frac{s}{\omega_p}\right) + \omega_c^2\omega_o^3}{b_0\left[\left(\frac{s}{\omega_p}\right)^3 + (3\omega_o + 2\omega_c)\left(\frac{s}{\omega_p}\right)^2 + (3\omega_o^2 + 6\omega_c\omega_o + \omega_c^2)\left(\frac{s}{\omega_p}\right)\right]}.$$

Substituting $k = K$ and $\omega_p = 1/T$ in (3.7) leads to

$$\overline{G}_A(s) = \frac{1}{K} \times \tag{3.8}$$

$$\frac{T^2 \left(3\omega_c^2\omega_o + 6\omega_c\omega_o^2 + \omega_o^3\right)s^2 + T\left(2\omega_c\omega_o^3 + 3\omega_c^2\omega_o^2\right)s + \omega_c^2\omega_o^3}{b_0\left[T^3 s^3 + T^2\left(3\omega_o + 2\omega_c\right)s^2 + T\left(3\omega_o^2 + 6\omega_c\omega_o + \omega_c^2\right)s\right]},$$

which after some mathematical manipulation can be rewritten as

$$\overline{G}_A(s) = \frac{T^2}{Kb_0} \times \tag{3.9}$$

$$\frac{\left(3\dfrac{\omega_c^2}{T^2}\dfrac{\omega_o}{T} + 6\dfrac{\omega_c}{T}\dfrac{\omega_o^2}{T^2} + \dfrac{\omega_o^3}{T^3}\right)s^2 + \left(2\dfrac{\omega_c}{T}\dfrac{\omega_o^3}{T^3} + 3\dfrac{\omega_c^2}{T^2}\dfrac{\omega_o^2}{T^2}\right)s + \dfrac{\omega_c^2}{T^2}\dfrac{\omega_o^3}{T^3}}{\left[s^3 + \left(3\dfrac{\omega_o}{T} + 2\dfrac{\omega_c}{T}\right)s^2 + \left(3\dfrac{\omega_o^2}{T^2} + 6\dfrac{\omega_c}{T}\dfrac{\omega_o}{T} + \dfrac{\omega_c^2}{T^2}\right)s\right]}.$$

Comparing the terms in (3.3) and (3.9), it is deduced that the scaled controller $\overline{G}_A(s)$ corresponds to a second-order LADRC with the parameter set

$$\bar{b}_0 = \frac{Kb_0}{T^2} \quad \overline{\omega}_c = \frac{\omega_c}{T} \quad \overline{\omega}_o = \frac{\omega_o}{T}. \tag{3.10}$$

In conclusion, if a stable second-order LADRC with parameters b_0, ω_c and ω_o is designed for the nominal system (3.5), then the scaled LADRC with parameters $\bar{b}_0$, $\overline{\omega}_c$ and $\overline{\omega}_o$ is suitable for the control of the general FOPDT plant (3.4).

3.3 Multi-objective optimisation design procedure

When designing a controller, the tuning process or solution obtained is strongly dependent on the desired performance for the closed-loop. The behaviour of the output, control action and any other signals of interest is usually measured through some performance indices or design objectives. If these indices are wanted to be minimised or maximised, then an optimisation statement can be formulated.

For each minimised or maximised index, a particular solution is obtained. Therefore, if different design objectives are optimised simultaneously, multiple solutions can be suitable for tuning the same controller, not implying that one is better than the other but suggesting that a solution can be selected with a particular trade-off among the aforementioned conflicting objectives. In this case, if the designer is interested, for example, in the simultaneous minimisation of two performance indices, a MOOD procedure could aid in the tuning problem.

A MOOD procedure comprises three fundamental steps [77].

1. Multi-objective Problem (MOP) definition: The design objectives of interest are stated as well as the decision variables and the possible constraints.

2. Optimisation Process (OP): An algorithm is selected to search throughout the decision space for the approximations of the optimal solutions (Pareto Set) and their corresponding objective values (Pareto Front). This algorithm should fulfil some desirable characteristics to provide the designer with valuable solutions.

3. Multi-criteria Decision Making (MCDM): Specialized visualisation techniques are employed to analyse the Pareto Front and Pareto Set approximations. The best solution is the one that meets the designer preferences.

As an example, Figure 3.1 illustrates the concepts of Pareto dominance, Pareto Front and Pareto Set for the bi-objective optimisation problem $\min_\theta J(\theta) = [J_1(\theta), J_2(\theta)]$ with decision variables $\theta = [\theta_1, \theta_2]$. The decision vectors $\theta^1, ..., \theta^5$ dominate the vectors θ^6 and θ^7 because the objective vectors $J(\theta^1), ..., J(\theta^5)$ are not worse than $J(\theta^6)$, $J(\theta^7)$ in both objectives and are better in at least one.

To explore the suitability of the multi-objective optimisation approach for the LADRC tuning problem, the responses to a unit step load disturbance ($\tilde{r} = 0, d = 1$) and to a unit step setpoint ($\tilde{r} = 1, d = 0$) of the closed-loop of Figure 2.2, with $G(s)$ as (3.11), were obtained for different combinations of the three LADRC tuning parameters in the search space: $b_0 \in [5, 35]$, $\omega_c \in [1, 25]$ rad/s, $\omega_o \in [1, 25]$ rad/s, and following a grid method with $\Delta b_0 = 1$ and $\Delta\omega_o = \Delta\omega_c = 0.2$ rad/s.

$$G_e(s) = \frac{1}{s+1}e^{-s} \tag{3.11}$$
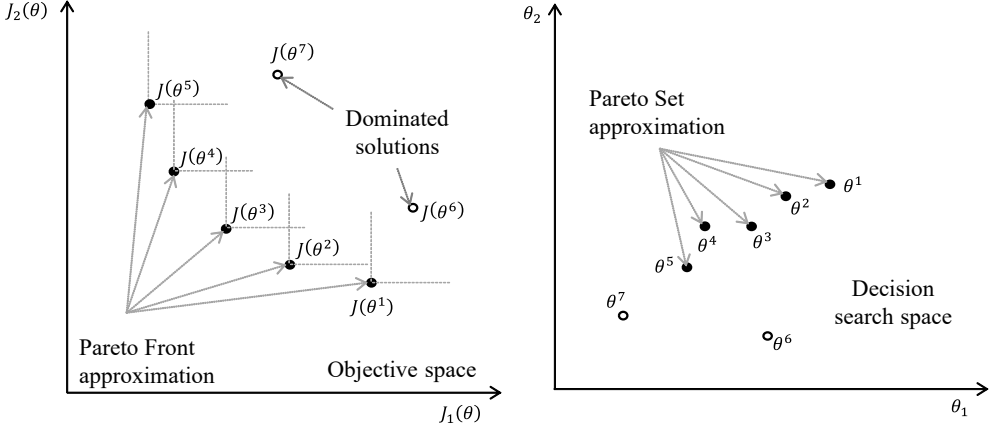
Figure 3.1: Pareto dominance, Pareto Front and Pareto set in a bi-dimensional case. There are no solution vectors dominating $\theta^1, ..., \theta^5$ so these solutions are the approximation of the Pareto Set and their corresponding objective vectors $J(\theta^1), ..., J(\theta^5)$ are the approximation of the Pareto Front.

Initially, the LADRC stability region was analysed. Figure 3.2 shows the pairs (ω_c, ω_o) for the nominal values of the critical gain that produce a stable output in system (3.11). From this figure, it is noted that as the nominal value of the critical gain increases, more pairs appear in the stability region, representing more possible combinations for the LADRC tuning. In other words, a stability bound exists that moves in the increasing direction as a higher value of b_0 is selected. Figure 3.2 also shows the closed-loop response of $G_e(s)$ when the LADRC is tuned with three different sets of parameters for each value of b_0: one of the triads was chosen from the stable area, and the remaining two correspond to LADRC parameters on the stability bound. As can be seen, the triads on the stability bounds produce significant oscillations in the output.

Once the LADRC stability region was obtained, interest was put in the performance computed with those combinations of parameters. Particularly, the integral of time weighted squared error (ITSE) for load disturbance rejection, the robustness, and the total variation of control action (TV) were defined as design objectives as stated in Table 3.1.

Closed-loop robustness is usually measured through the maximum peak M_S of the sensitivity function $S(j\omega)$ and the maximum peak M_T of the complementary sensitivity function $T(j\omega)$, such that $1.3 < M_S < 2$ and $M_T < 1.25$ [4].
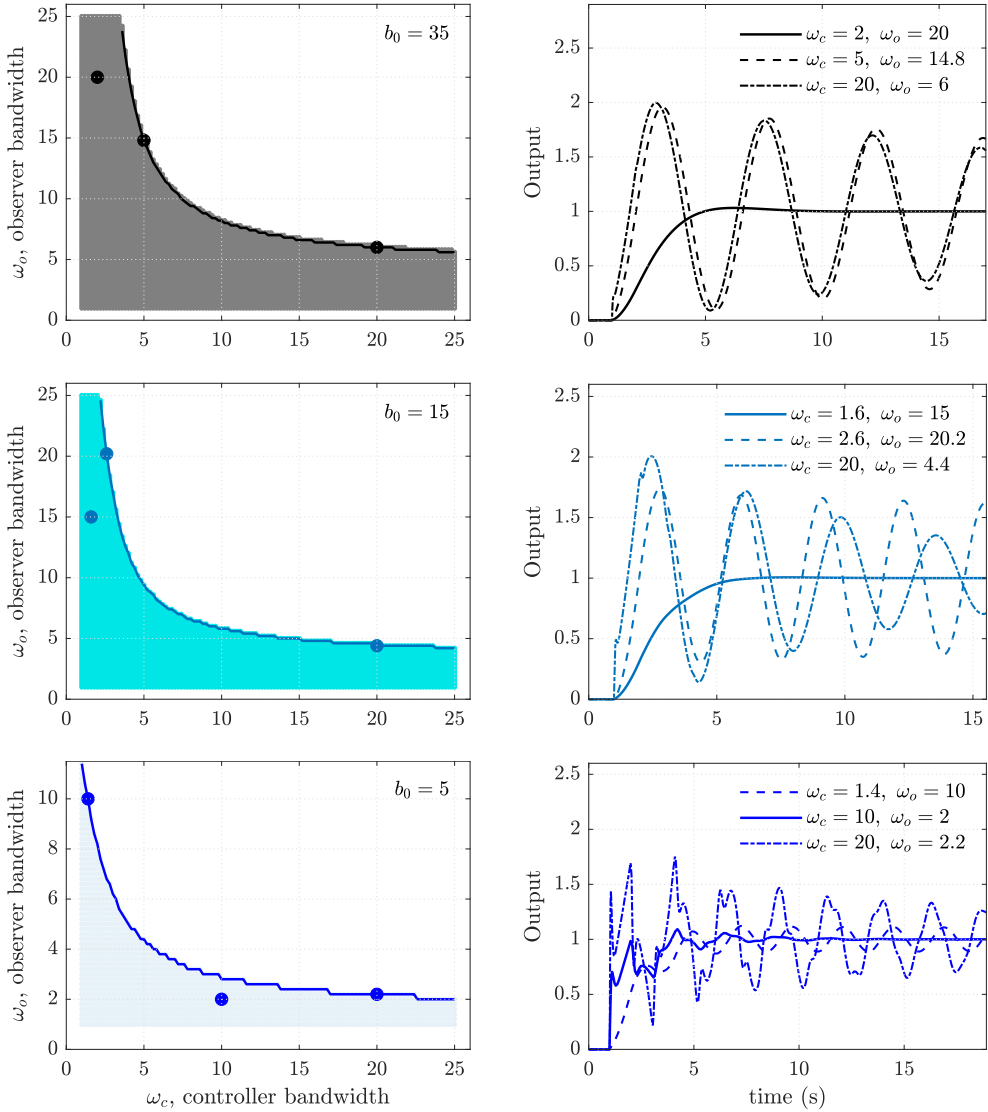
Figure 3.2: Closed-loop stability regions for $G_e(s)$. Each point in the shaded area represents a combination of parameters producing a stable output. For each value of $b_0 \in [5, 35]$ pairs (ω_c, ω_o) exist that produce a stable output. The stable (ω_c, ω_o) for $b_0 = 5, 15, 35$ are plotted as examples to illustrate the shape of the stability regions (left column). Additionally, the closed-loop responses of $G_e(s)$ when controlled with the LADRC tuned with selected triads from the stability region and stability bound are presented (right column).

This thesis adopts a robustness measure denoted by ε as robustness index. It is defined in [82] as the structured singular value of matrix M from an $M - \Delta$ configuration with a diagonal block structure, and it has been previously used in [32] to quantify the robust stability of the closed-loop system with the LADRC. As defined in Table 3.1, the ε index is computed as the maximum peak of the sum of the magnitudes of the frequency responses of the sensitivity function and the complementary sensitivity function. The lower the value of ε, the more robust the closed-loop system.

Table 3.1: Design objectives for the performance evaluation of the LADRC.

Index/Design Objective	Definition
Integral of time weighted squared error	$\text{ITSE} = \displaystyle\int_{t=0}^{t_{98\%}} t \cdot (\tilde{r}(t) - y(t))^2 \, dt$
Total variation of the control action	$\text{TV} = \displaystyle\sum_{i=1}^{t_{98\%}} |u_{i+1} - u_i|$
Mixed robustness	$\varepsilon = \sup_{\omega} \left(|S(j\omega)| + |T(j\omega)| \right)$

A first look at the minimum ITSE value inside the stability region shows that $\text{ITSE}_{\min 1} = 0.82$ for the solution $b_{01} = 17$, $\omega_{c1} = 1.8\,\text{rad/s}$, $\omega_{o1} = 23.6\,\text{rad/s}$. However, the associated robustness of $\varepsilon_1 = 5.93$ is regarded as poor. If the constraint $\varepsilon \leq 3$ is imposed on the robustness index, a new solution $b_{02} = 24$, $\omega_{c2} = 2\,\text{rad/s}$, $\omega_{o2} = 21\,\text{rad/s}$ is found with $\text{ITSE}_{\min 2} = 1.13$ and corresponding robustness $\varepsilon_2 = 2.99$.

On the other hand, a search for the most robust controller results in the parameters $b_{03} = 15$, $\omega_{c3} = 19.8$ rad/s, $\omega_{o3} = 1$ rad/s, which produce $\varepsilon_{\min 3} = 1.38$, but with an extremely high ITSE value of $\text{ITSE}_3 = 113.51$. Also, if the ITSE is constrained, such as $\text{ITSE} \leq 2$, then the new solution is $b_{04} = 19$, $\omega_{c4} = 21$ rad/s, $\omega_{o4} = 2.8$ rad/s with a robustness $\varepsilon_{\min 4} = 2.02$ and a time performance index $\text{ITSE}_4 = 1.99$.

Table 3.2 comprises the solutions and performance comparison discussed above. Some additional indices such as M_S, M_T, total variation of control action for disturbance rejection (TV_d), and total variation of control action for setpoint following (TV_s) are included as complementary information. Notice that each

of the LADRC sets of parameters can be considered as optimal only for the corresponding minimised index. For example, the solution $(b_{02}, \omega_{c2}, \omega_{o2})$ is optimal concerning the ITSE, but the robustness obtained is the maximum allowed according to the constraint.

Table 3.2: Comparison of LADRC performance for control of $G_e(s)$.

Desired performance	LADRC parameters	M_S	M_T	ε	ITSE	TV_d	TV_s
min ITSE	$b_{01} = 17$ $\omega_{c1} = 1.8$ $\omega_{o1} = 23.6$	3.45	2.48	5.93	0.82	3.14	2.50
min ITSE $\varepsilon \leq 3$	$b_{02} = 24$ $\omega_{c2} = 2$ $\omega_{o2} = 21$	1.98	1.16	2.99	1.13	1.40	1.32
min ε	$b_{03} = 15$ $\omega_{c3} = 19.8$ $\omega_{o3} = 1$	1.19	1.00	1.38	113.51	1.02	33.87
min ε ITSE ≤ 2	$b_{04} = 19$ $\omega_{c4} = 21$ $\omega_{o4} = 2.8$	1.50	1.01	2.02	1.99	1.10	29.25

In addition to the solutions reported in Table 3.2, there are other sets of LADRC parameters within the stability region that offer a compromise between disturbance rejection, quantified by ITSE, and robustness. To search for these alternatives, the Pareto dominance definition was applied over the total of parameters combinations, restricting the robustness measure to the range $\varepsilon \in [2,3]$, which represents a maximum sensitivity in the range $M_S \in [1.3, 2]$ and a maximum complementary sensitivity in the interval $M_T \in [1, 1.4]$.

Figure 3.3a shows the Pareto Front approximation for the simultaneous minimisation of ITSE for disturbance rejection and robustness. As expected, the ITSE can not be improved (decreased) without weakening the robustness. Likewise, a more robust closed-loop system is possible as long as the ITSE value is allowed to increase. The solutions $(b_{02}, \omega_{c2}, \omega_{o2})$ and $(b_{04}, \omega_{c4}, \omega_{o4})$ from Table 3.2 would be located around the upper and bottom ends of the Pareto Front approximation, respectively.
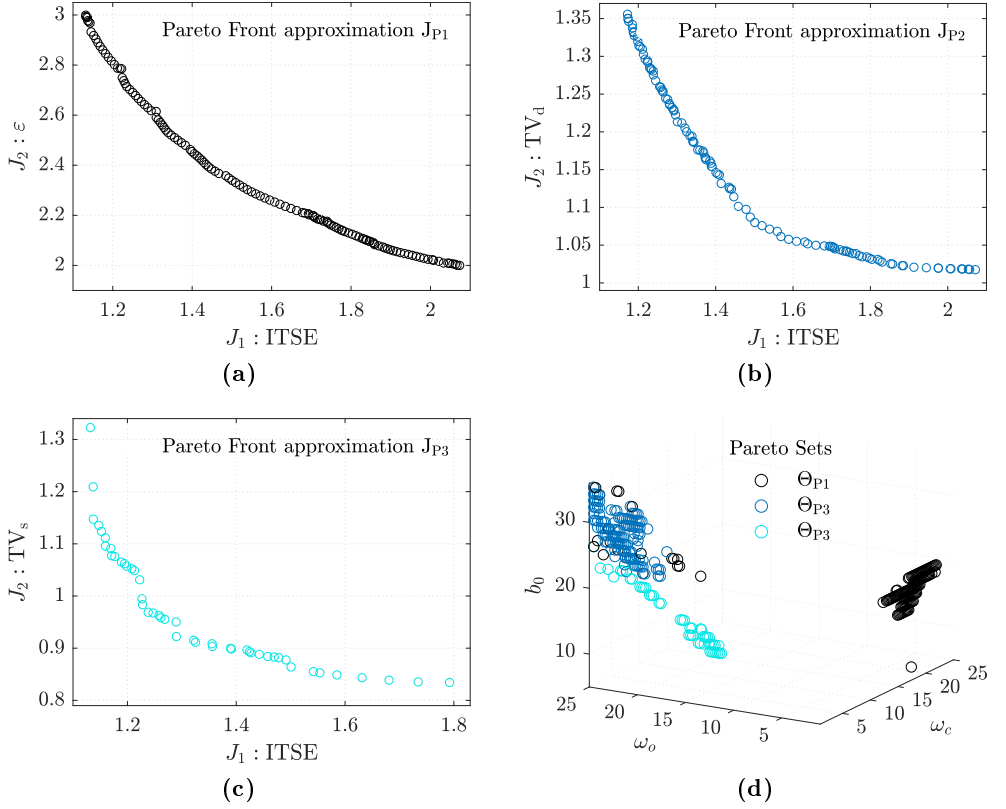
Figure 3.3: Pareto Fronts and Pareto Sets approximations for simultaneous minimisation of two design objectives J_1 and J_2. **(a)** Pareto Front approximation $J_{P1} = \min_\theta [\text{ITSE}, \varepsilon]$. **(b)** Pareto Front approximation $J_{P2} = \min_\theta [\text{ITSE}, \text{TV}_d]$. **(c)** Pareto Front approximation $J_{P3} = \min_\theta [\text{ITSE}, \text{TV}_s]$. **(d)** Pareto Sets approximations Θ_{P1}, Θ_{P2}, Θ_{P3} for the three said cases.

From another point of view, Figure 3.3b is the Pareto Front approximation for minimisation of ITSE and TV for disturbance rejection (TV_d), and Figure 3.3c is the approximation of the Pareto Front when the ITSE for disturbance rejection is minimised simultaneously with the TV of the unit setpoint (TV_s). These figures show that there is also a compromise between the ITSE performance and the control efforts.

Finally, the Pareto Sets approximations for the three said cases are presented in Figure 3.3d. Notice that the optimal values for the nominal critical gain are

higher than $b_0 = 1$, which would be the nominal value ($b_0 = K/T$) computed from the model (3.11), as is commonly suggested in the literature. Moreover, in the solutions with a compromise between ITSE and robustness, the controller bandwidth can be selected to be greater than the observer bandwidth ($\omega_c > \omega_o$) or vice versa ($\omega_c < \omega_o$). Nevertheless, for a compromise between ITSE and the total variation of the control action, a selection of parameters in which $\omega_c < \omega_o$ seems more appropriate.

The case study addressed in this section gave some insight into the LADRC performance in controlling a FOPDT system. In summary, there exists a trade-off between the disturbance rejection performance of the LADRC and its robustness. The LADRC parameters that produce this compromise are Pareto optimal and can be searched through an optimisation process where the objectives related to disturbance rejection and robustness are minimised simultaneously. Besides, the definition of constraints over the objective and search spaces could drive the optimisation process to solutions that meet some desired additional performance. If the aforementioned optimisation procedure is applied over a group of plants of the same kind, then the Pareto optimal alternatives could be used to derive tuning rules reflecting the desired trade-off.

3.4   LADRC tuning by multi-objective optimisation

For the tuning problem of the second-order LADRC related to the control of FOPDT systems, a MOOD procedure was applied to a group of nominal plants in the form of (3.5), which was obtained by varying the nominal delay from $\Theta = 0.5$ to $\Theta = 5$ with a change of $\Delta\Theta = 0.1$.

The FOPDT systems can be characterised based on the normalised dead time $\tau = l/(l + T)$ with $0 \leq \tau \leq 1$ [83]. Particularly, a system is lag-dominated if τ is small, balanced if τ is around 0.5 and delay-dominated if τ is large [84]. In terms of the nominal delay, τ can be written as

$$\tau = \frac{\Theta}{\Theta + 1}. \tag{3.12}$$

Therefore, the MOOD procedure was applied to control plants with τ ranging from 0.09 to 0.83, including lag-dominated, balance, and delay-dominated processes. The MOOD results were used to fit the optimal solutions for the LADRC parameters, and the fitting curves were scaled to obtain the tuning rules as functions of the known FOPDT parameters.

3.4.1   Multi-objective problem definition

The first stage of the MOOD procedure implies defining the decision space, the objective space, and the possible constraints. The decision variables are selected from the parametric controller; the objective space is related to the desired performance, and constraints are the design limitations imposed on the overall concept.

The plant to be controlled corresponds to the FOPDT nominal model (3.5). Note that any controller designed for this plant can be scaled afterwards according to (3.10).

The scaling for observer bandwidth

$$\omega_o = k_o\omega_c, \ \ k_o > 1, \tag{3.13}$$

was also adopted, which indicates that LADRC parameters meeting the relation $\omega_c < \omega_o$ are preferred. This additional scaling is commonly suggested in the literature (e.g., in [23], [30], [31]).

Consider the transfer function (3.14), obtained by substituting (3.13) in (3.3).

$$G_A(s) = \frac{\left(3k_o\omega_c^3 + 6k_o^2\omega_c^3 + k_o^3\omega_c^3\right)s^2 + \left(2k_o^3\omega_c^4 + 3k_o^2\omega_c^4\right)s + k_o^3\omega_c^5}{b_0\left[s^3 + \left(3k_o\omega_c + 2\omega_c\right)s^2 + \left(3k_o^2\omega_c^2 + 6k_o\omega_c^2 + \omega_c^2\right)s\right]}. \tag{3.14}$$

Therefore, choosing a value of $k_o = 10$, the corresponding controller to tune is

$$G_A(s) = \frac{1630\omega_c^3 s^2 + 2300\omega_c^4 s + 1000\omega_c^5}{b_0\left(s^3 + 32\omega_c s^2 + 361\omega_c^2 s\right)}, \tag{3.15}$$

with the decision variables

$$\theta = [b_0, \omega_c]. \tag{3.16}$$

Two design objectives were selected: the ITSE for the response to a unit step load disturbance and the mixed robustness index ε. Thus, the complete multi-objective problem is stated as (3.17).

$$
\begin{aligned}
\min_\theta J(\theta) &= [J_1(\theta), J_2(\theta)] \\
J_1(\theta) &= \text{ITSE}(\theta) \\
J_2(\theta) &= \varepsilon(\theta) \\
\theta &= [b_0, \omega_c]
\end{aligned}
$$

subject to
\hfill (3.17)

$$
\begin{aligned}
J_1(\theta) &\leq \text{ITSE}_{\text{SIMC}} \\
2 \leq J_2(\theta) &\leq 3 \\
1 \leq b_0 &\leq 200 \\
0.1 \leq \omega_c &\leq 20
\end{aligned}
$$

Stable in closed-loop

The constraints on the design objectives were selected considering the performances offered over the group of nominal plants by classical PID tuning rules as IMC [85], SIMC [86], and AMIGO [87], and the LADRC tuning method from [32]. The upper limit of $J_1(\theta)$ was set as the ITSE value obtained with the SIMC approach such that the desired closed-loop time constant was equal to the apparent delay l. The SIMC tuning produced the highest ITSE for each plant compared to the LADRC from [32] and the other PID controllers.

Similarly, the lower limit of $J_2(\theta)$ approximates the robustness obtained with the AMIGO tuning rules, and its upper limit is approximately the robustness computed with the IMC method. The other controllers offer a robustness measure between these limits for all plants. Moreover, the $\varepsilon(\theta)$ limits are related to the commonly adopted limits for maximum sensitivity and maximum complementary sensitivity.

The search space for decision variables was specified following the results from section 3.3, where it was shown that increasing b_0 contributes to a more extensive stability region in terms of the bandwidths and, consequently, lower performance indices can be computed.

The MOOD procedure was implemented in MATLAB®, so the Control System Toolbox function `stepinfo` was used to compute the step response characteristics of the closed-loop, including its stability. However, the stability of the parametrised control loop can be analysed in terms of its frequency response, as it is presented in [88] and [31].

The closed-loop characteristic equation of Figure 2.2 with $G_n(s)$ as the controlled plant is $1 + G_C(s)G_F(s)G_n(s) = 0$, which can be rewritten in the form

$$1 + G_A(s)G_{n0}(s)e^{-\Theta s} = 0, \tag{3.18}$$

where $G_A(s)$ is the parametrised second-order LADRC from (3.15), $G_{n0}(s)$ is the delay-free transfer function of the controlled plant, and $e^{-\Theta s}$ represents the nominal delay. Multiplying (3.18) by $e^{\Theta s}$ and reorganizing terms results in

$$G_A(s)G_{n0}(s) = -e^{\Theta s}. \tag{3.19}$$

Renaming $G_A(s)G_{n0}(s)$ as $H(s)$, the following lemma applies

LEMMA 3.4.1 *[89] Under the condition that $n > m$, being n the denominator degree of $H(s)$ and m the numerator degree of $H(s)$, the closed-loop system is stable if one of the following conditions holds*

(i) *$H(s)$ is stable and the equation $|H(j\omega)| = 1$ has no positive real roots.*

(ii) *There exist a positive real root $\omega = \omega_i$ of equation $|H(j\omega)| = 1$ and the inequality $\varphi\left(H(j\omega_i)\right) > \varphi\left(-e^{j\omega_i\Theta}\right)$ holds, with $\varphi\left(H(j\omega_i)\right)$ and $\varphi\left(-e^{j\omega_i\Theta}\right)$ as the arguments of $H(s)$ and $-e^{\Theta s}$ at $\omega = \omega_i$, respectively. This means that, at the frequency $\omega = \omega_i$, the magnitude of $H(j\omega)$ equals the magnitude of $-e^{j\omega_i\Theta}$ and the phase of $H(j\omega)$ is larger than the phase of $-e^{j\omega_i\Theta}$.*

For the parametrised control loop, $H(s)$ is as (3.20). Therefore, for each plant with nominal delay Θ and given LADRC parameters b_0, ω_c, condition (i) of Lemma 3.4.1 is verified by solving (3.21).

$$H(s) = \frac{1630\omega_c^3 s^2 + 2300\omega_c^4 s + 1000\omega_c^5}{b_0\left(s^3 + 32\omega_c s^2 + 361\omega_c^2 s\right)(s+1)} \tag{3.20}$$

$$\left| \frac{1000\omega_c^5 - 1630\omega_c^3\omega_i^2 + j2300\omega_c^4\omega_i}{b_0\left(\omega_i^4 - 361\omega_c^2\omega_i^2 - 32\omega_c\omega_i^2\right) + jb_0\left(361\omega_c^2\omega_i - 32\omega_c\omega_i^3 - \omega_i^3\right)} \right| = 1 \tag{3.21}$$

If the frequency ω_i exists, the phases $\varphi\left(H(j\omega_i)\right)$ and $\varphi\left(-e^{j\omega_i\Theta}\right)$ can be computed and the condition (ii) of Lemma 3.4.1 can be validated through (3.22).

$$\arctan\left(\frac{2300\omega_c^4\omega_i}{1000\omega_c^5 - 1630\omega_c^3\omega_i^2}\right)$$
$$-\arctan\left(\frac{361\omega_c^2\omega_i - 32\omega_c\omega_i^3 - \omega_i^3}{\omega_i^4 - 361\omega_c^2\omega_i^2 - 32\omega_c\omega_i^2}\right) > \Theta\omega_i - \pi \quad (3.22)$$

3.4.2 Optimisation process

The evolutionary multi-objective algorithm $\not{e}-$MOGA [90] was used to perform the optimisation process. This algorithm uses the epsilon-dominance concept to obtain Pareto Front and Pareto Set approximations with limited memory resources, preserving the Front diversity by adjusting its limits dynamically [91]. The algorithm parameters were set to 200 individuals for the main population, eight individuals for the auxiliary population, 1000 generations and 1000 divisions per dimension.

The Pareto Fronts and Pareto Sets approximations of each of the nominal plants are presented in Figure 3.4 and Figure 3.5. They have been plotted separately for plants with $\tau \leq 0.5$ in Figure 3.4 and for plants with $\tau > 0.5$ in Figure 3.5. The above to better illustrate that the range of the decision variables for plants with $\tau \leq 0.5$ is wider than for plants with $\tau > 0.5$. For instance, a robustness measure between 2 and 3 can be obtained when controlling the plant with $\tau = 0.09$ if the LADRC parameters are selected in the ranges $b_0 \in [86, 115]$ and $\omega_c \in [11.6, 6.6]$ (see Figure 3.4b), whereas the same variation in robustness for the plant with $\tau = 0.833$ is achieved with a controller tuned such that $b_0 \in [6.2, 9.2]$ and $\omega_c = [0.73, 0.71]$ (see Figure 3.5b). Another essential feature is the decreasing trend in the decision variables as the normalised delay increases. However, the rate of change in both parameters tends to be greater for plants with $\tau \leq 0.5$ than for plants with $\tau > 0.5$.

3.4.3 Multi-criteria decision making

Once the Pareto Fronts and Pareto Sets approximations have been obtained, the last step in the MOOD procedure is the selection of the solution or candidate solutions preferred by the designer. A final choice is needed even if most of the preferences were considered in the optimisation process. Depending on the number of design objectives, the visualisation and graphical interpretation of the Pareto Front approximation is crucial. For the bi-objective problem, a two-dimensional scatter plot is sufficient for data visualization.
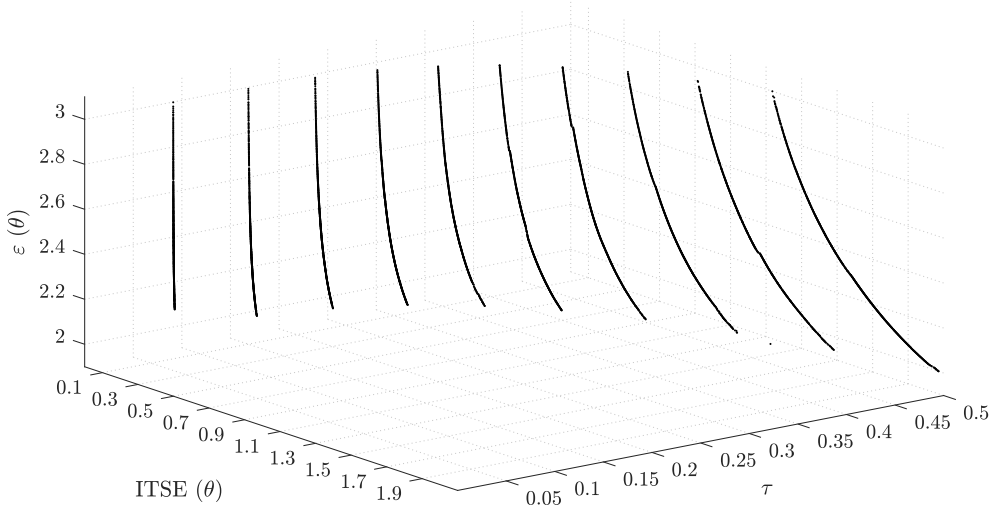
(a) Pareto Fronts approximations
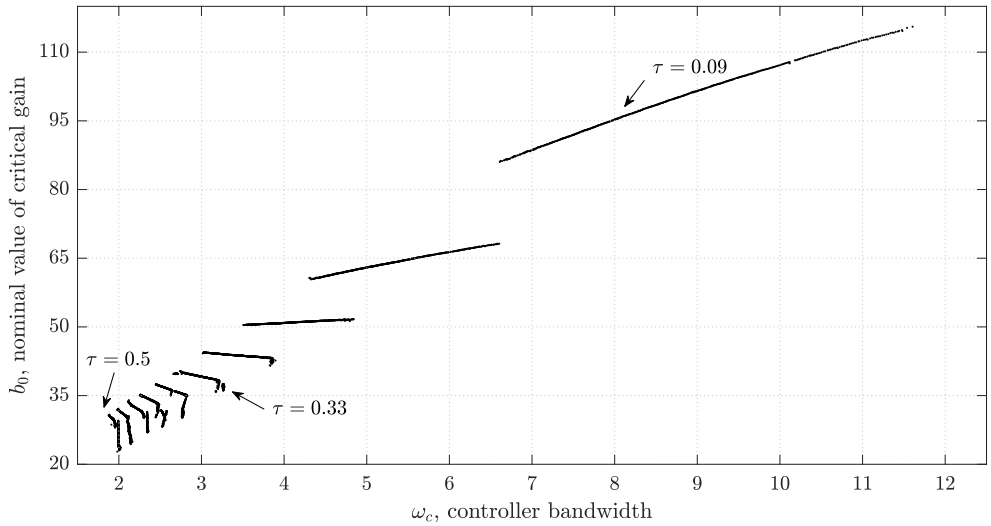
(b) Pareto Sets approximations

Figure 3.4: Results from the optimisation process for the group of nominal plants with $\tau \leq 0.5$. Pareto Sets approximations show a wide range of variation in the LADRC parameters with larger rates of change than those of the LADRC parameters obtained in the Pareto Sets approximations for plants with $\tau > 0.5$ (see Figure 3.5b)
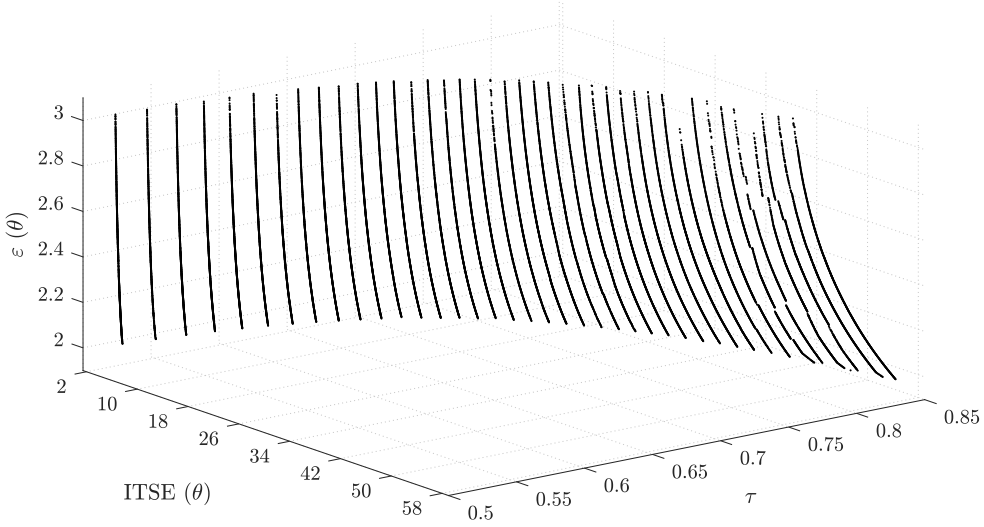
(a) Pareto Fronts approximations
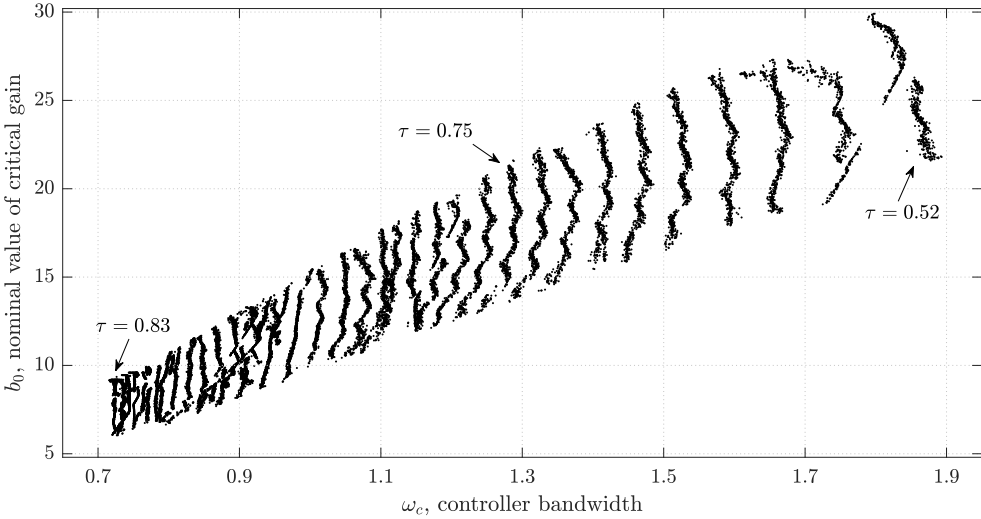
(b) Pareto Sets approximations

Figure 3.5: Results from the optimisation process for the group of nominal plants with $\tau > 0.5$. Pareto Sets approximations show a narrow range of variation in the LADRC parameters with lower rates of change than those of the LADRC parameters obtained in the Pareto Sets approximations for plants with $\tau \leq 0.5$ (see Figure 3.4b)

According to the results from the optimisation process, the following aspects were considered for the decision-making stage.

- For data processing, two main groups were defined: *Group 1* containing data related to plants with a normalised delay $\tau \leq 0.5$ and *Group 2* with data belonging to plants with $\tau > 0.5$.

- Three design alternatives distributed along the front were selected from each Pareto Front approximation.

- For *Group 1*, the selection was made using the entire Pareto Front approximation.

- For *Group 2*, the selection was made by limiting the upper end of the front such that the highest value for $\varepsilon(\theta)$ is 2.5. This criterion is based on the fact that the difficulty in controlling a process increases as its normalised delay increases [83]. Thus, lower values of $\varepsilon(\theta)$ are preferred for this group of plants, which correspond to more robust closed-loop systems.

- Selected solutions are compared in the objective space with other alternatives related to PID and LADRC tuning rules.

Consider the first group of nominal plants (*Group 1*). To select the three desired design alternatives, let the Pareto Fronts to be divided into two regions according to bounds imposed on the mixed robustness measure. The upper region comprises solutions for which $2.5 \leq \varepsilon(\theta) \leq 3$ and the lower region includes those with $2 \leq \varepsilon(\theta) < 2.5$.

On each region, a point corresponding to the Nash solution was calculated by solving the problem [92]

$$\max_{(J_1(\theta), J_2(\theta))} \quad \left(J_1\left(\theta^2\right) - J_1\left(\theta\right) \right) \left(J_2\left(\theta^1\right) - J_2\left(\theta\right) \right), \qquad (3.23)$$

where θ^1 is the optimal vector (minimum) of the first design objective and θ^2 is the vector that minimises the second cost function. The Nash solution $(J_1(\theta), J_2(\theta))$ is considered a *fair* selection because it dominates the larger number of points in the rectangular area $(J_1(\theta^2) - J_1(\theta))(J_2(\theta^1) - J_2(\theta))$ [92].

The third solution for *Group 1* was selected as the midpoint of the Pareto Fronts. This is, the solution meeting the condition $\varepsilon(\theta) = 2.5$.

(a) $\tau = 0.5$

(b) $\tau = 0.75$
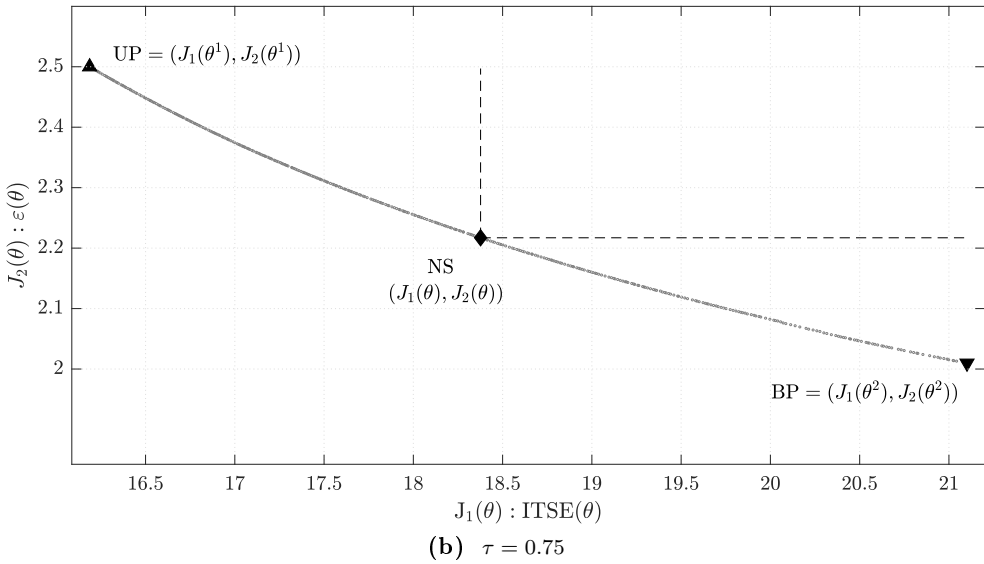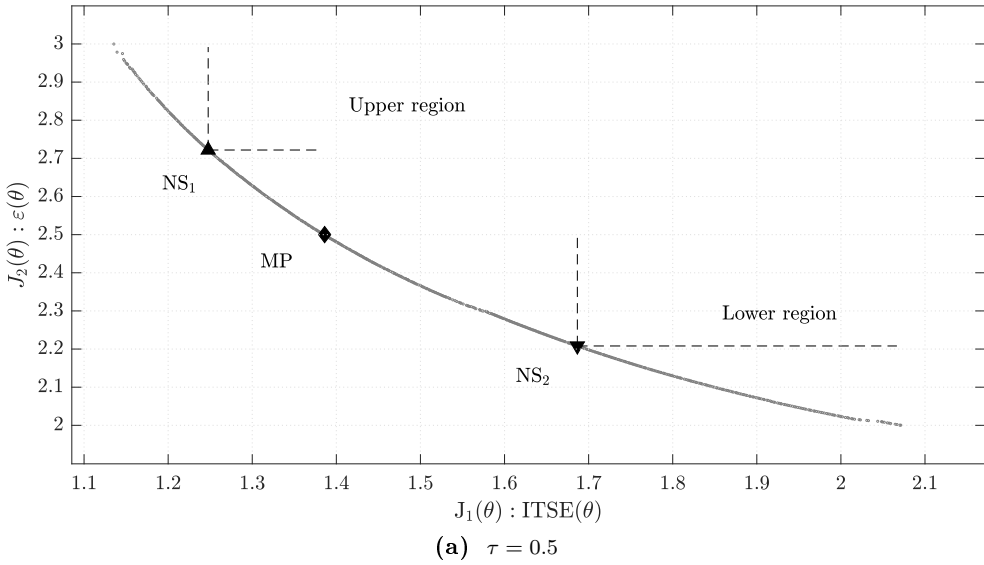
Figure 3.6: Location of the selected solutions into the Pareto Fronts approximations taking as example two nominal plants. (**a**) For plants in *Group 1*, selected solutions are the Nash solution from the upper region NS_1, the midpoint MP, and the Nash solution from the lower region NS_2. (**b**) For plants in *Group 2* the selected solutions are the upper end UP, the Nash solution NS, and the bottom end BP.

For the second group of plants (*Group 2*), the three selected solutions correspond to the two ends of the front and the Nash solution.

Figure 3.6 illustrates the concepts explained above and solutions selected, taking as an example the Pareto Fronts approximations of the nominal plants with $\tau = 0.5$ (*Group 1*) and $\tau = 0.75$ (*Group 2*).

The Pareto Fronts approximations and selected solutions when controlling the nominal plants with $\tau \leq 0.5$ and $\tau > 0.5$ are presented in Figure 3.7 and Figure 3.8, respectively. For comparison purposes, the performances obtained with the second-order LADRC tuned with the rules from [32] (tagged as ADRC_Z) are shown for both groups. The formulae corresponding to this approach are listed in Table 3.3.

Table 3.3: LADRC tuning rules from literature applicable to the control of FOPDT plants in the form of (3.4). The LADRC performance points tagged in Figure 3.7 and Figure 3.8 as ADRC_Z were obtained by tuning the controller (3.3) with the rules from [32]. The tuning method from [30] is used for comparison section 4.1.1.

Tuning method	Tuning rules
LADRC with robustness constraint [32] $\lambda = 1$	$b_0 = \lambda \dfrac{K}{T} \left(\dfrac{5.779}{l} + \dfrac{6.041}{T} \right)$ $\omega_c = \dfrac{3.841}{l} + \dfrac{0.297}{T}$ $\omega_o = \dfrac{1.172}{l} + \dfrac{3.742}{T}$
LADRC for high-order processes* [30] Tuning parameter, k * Applicable to FOPDT plants with $\frac{l}{T} > 1$ after its approximation to $\widetilde{K} \big/ \left(\widetilde{T}s + 1 \right)^n$	$b_0 = \dfrac{\widetilde{K}}{n^2 \widetilde{T}^2} \left(\dfrac{6454.1}{k^3} - \dfrac{1427.26}{k^2} \right)$ $\omega_c = \dfrac{10}{kn\widetilde{T}}$ $\omega_o = \dfrac{100}{kn\widetilde{T}}$
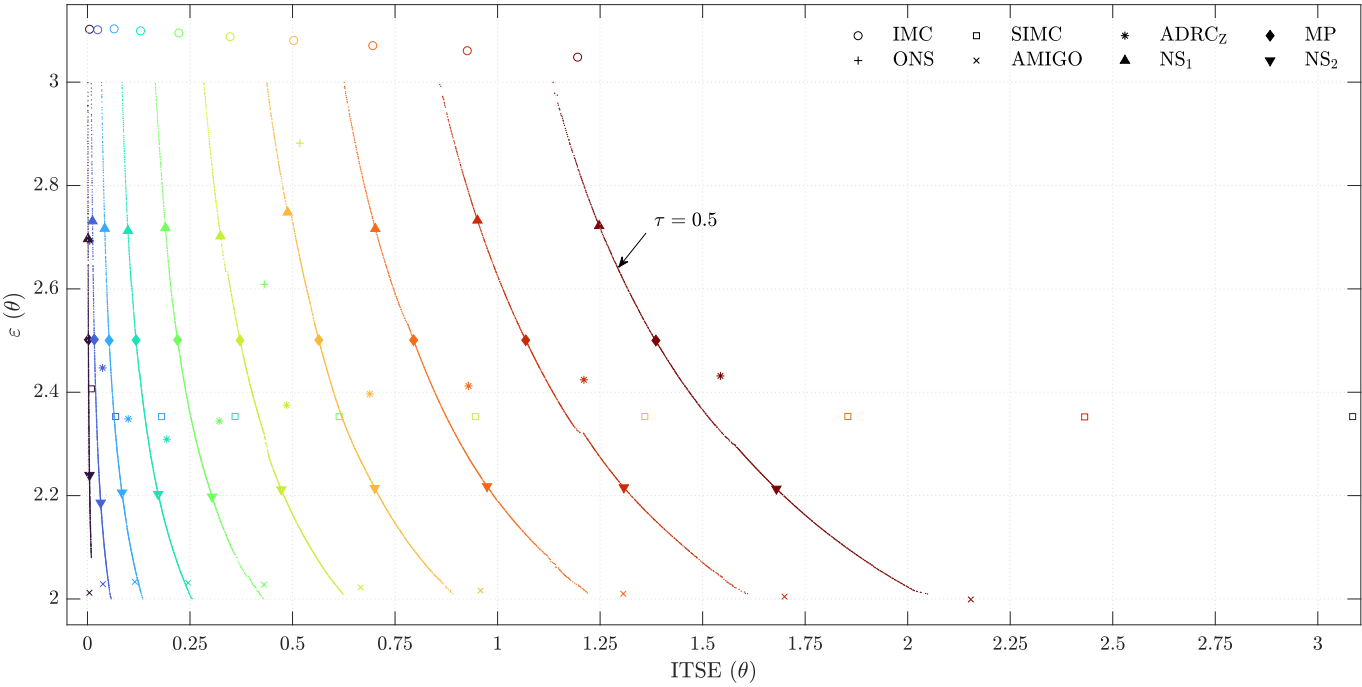
Figure 3.7: Pareto Fronts approximations and selected solutions for controlling nominal plants with normalised delay $\tau \leq 0.5$. The performances obtained with the PID tuning methods IMC, SIMC, AMIGO, and the rules from [92] (ONS), as well as the LADRC tuning rules from [32] (ADRC$_Z$), are included for comparison. The information related to the same plant is plotted in the same colour.
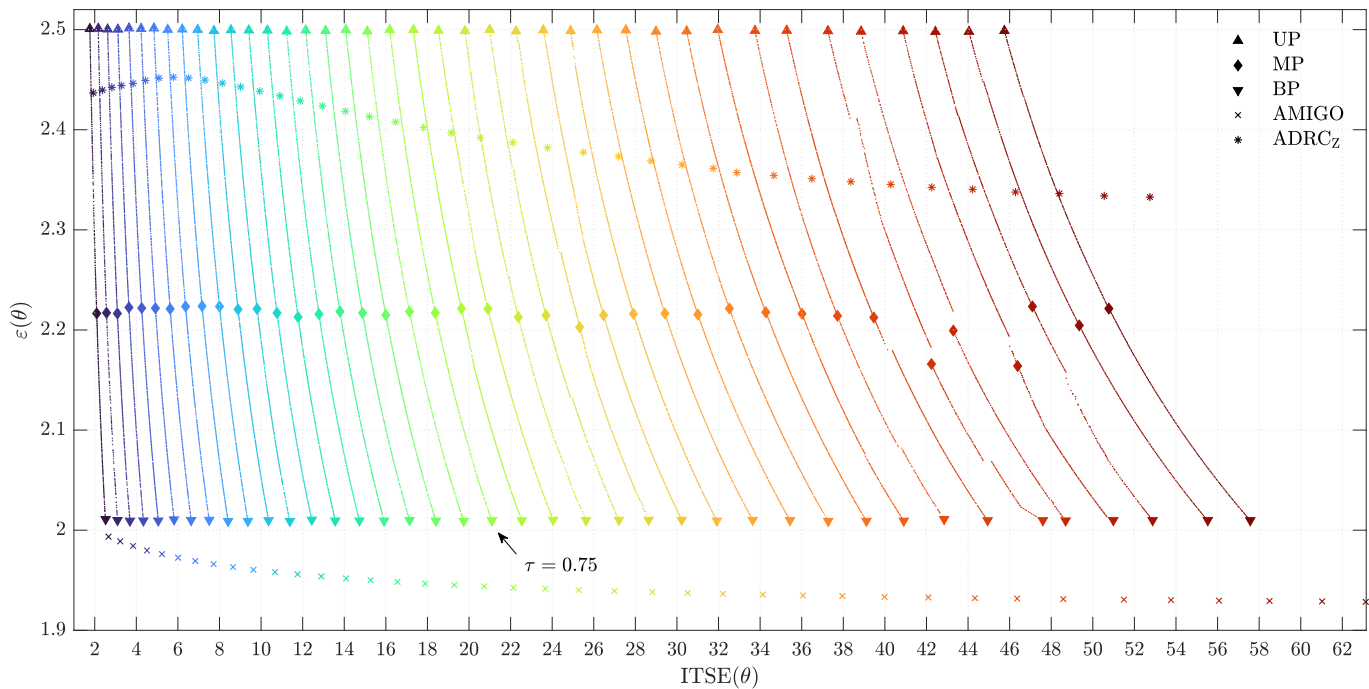
Figure 3.8: Pareto Fronts approximations and selected solutions for controlling nominal plants with normalised delay $\tau > 0.5$. The performances obtained with the PID tuning method AMIGO and the LADRC tuning rules from [32] (ADRC$_Z$) are included for comparison. The SIMC points have been excluded for proper visualisation because the Pareto optimal solutions always dominate these alternatives. The information related to the same plant is plotted in the same colour.

Likewise, the performances obtained with the PID tuning methods IMC, SIMC, AMIGO, and the rules from [92] (labelled as ONS) are also included for *Group 1*. For *Group 2*, the Pareto alternatives are compared with the SIMC and AMIGO approaches.

The Table 3.4 summarises the formulae used to tune the PID controllers and the design considerations that were taken into account over the two-degree-of-freedom configuration

$$
C(s) = K_c \left(b + \frac{1}{T_i s} + c \frac{T_d s}{\frac{T_d}{10} s + 1} \right) R(s)
$$
$$
- K_c \left(1 + \frac{1}{T_i s} + \frac{T_d s}{\frac{T_d}{10} s + 1} \right) Y(s), \quad (3.24)
$$

where $R(s)$ is the Laplace transform of the reference, $Y(s)$ the Laplace transform of the output, K_c the proportional gain, T_i the integral time, T_d the derivative time, and b and c are setpoint weights.

From Figure 3.7 and Figure 3.8, the following remarks are derived. Notice that the Fronts move to the right in the objective space as the normalised delay increases.

- The performances obtained with the PID controllers tuned by the IMC, SIMC and the rules from [92] (ONS) are in the dominance area of the Pareto Fronts belonging to plants from *Group 1*. Notably, the SIMC points are dominated by the Pareto optimal solutions in all cases.

- For plants from *Group 2*, the performances obtained with the AMIGO tuning method are outside the Pareto Fronts approximations due to the constraint imposed on $\varepsilon(\theta)$. However, the alternative solutions corresponding to the bottom end of the fronts have better disturbance rejection with a reasonable level of robustness.

- The performances obtained with the tuning rules from [32] (ADRC$_\text{Z}$) are in the dominance area of the approximated Pareto Fronts for the entire set of nominal plants. Even though the ADRC$_\text{Z}$ points are the results of fitting curves, they tend to move away from the fronts as τ increases, highlighting their suboptimal feature.

Table 3.4: PID tuning rules from literature for the control of FOPDT plants in the form of (3.4). The PID performance points plotted in Figure 3.7 and Figure 3.8 were obtained by tuning the controller (3.24) with these rules.

Tuning method	Tuning rules
IMC [85] $\lambda = 0.25\ l$ as in [32] $b = 1,\ c = 1$	$T_i = T + \dfrac{l^2}{2(\lambda + l)}$ $K_c = \dfrac{T_i}{K(\lambda + l)}$ $T_d = \dfrac{l^2}{2(\lambda + l)}\left[1 - \dfrac{l}{3T_i}\right]$
SIMC [86] $T_c = l$ $b = 1$	$T_i = \begin{cases} \min\left\{T, 4(T_c + l)\right\}, & \tau < 0.7 \\[2mm] \min\left\{T + \frac{l}{3}, 4(T_c + l)\right\}, & \tau \geq 0.7 \end{cases}$ $K_c = \begin{cases} \dfrac{T}{K(T_c + l)}, & \tau < 0.7 \\[3mm] \dfrac{T + \frac{l}{3}}{K(T_c + l)}, & \tau \geq 0.7 \end{cases}$
AMIGO [87] $b = \begin{cases} 0, & \tau \leq 0.5 \\ 1, & \tau > 0.5 \end{cases}$ $c = 0$	$T_i = l\left(\dfrac{0.4\ l + 0.8T}{l + 0.1T}\right)$ $K_c = \dfrac{1}{K}\left(0.2 + 0.45\dfrac{T}{l}\right)$ $T_d = \dfrac{0.5\ l\ T}{0.3\ l + T}$
Optimal-Nash [92] $0.1 \leq \dfrac{l}{T} \leq 2$ $b = 1,\ c = 1$	$T_i = T\left[-0.01197\left(\dfrac{l}{T}\right)^2 + 0.5683\dfrac{l}{T} + 0.4343\right]$ $K_c = \dfrac{1}{K}\left[0.233\left(\dfrac{l}{T}\right)^{0.4582} + 0.7349\left(\dfrac{l}{T}\right)^{-0.9348}\right]$ $T_d = T\left[-0.1206\left(\dfrac{l}{T}\right)^2 + 0.5743\dfrac{l}{T} - 0.01306\right]$

A set of Pareto optimal solutions with a trade-off between disturbance rejection and robustness was obtained with the MOOD procedure developed for the tuning problem of the second-order LADRC applied to FOPDT nominal systems. The distribution of these solutions in the decision search space leads to different fitting curves depending on the preferred level of compromise between objectives. This idea is the core of the fitting procedure presented in the next section.

3.5 Tuning rules for LADRC

The solutions obtained from the MOOD procedure correspond to the Pareto optimal LADRC parameters suitable to control FOPDT plants in the form of (3.5). These data were initially fitted to functions of the normalised delay τ. Afterwards, the resulting expressions were scaled to obtain the LADRC tuning rules applicable to the control of the general FOPDT system (3.4).

Data were fitted separately for the two previously defined groups of plants. This was mainly because of the behaviour observed in the rate of change of the parameters concerning the variation in the normalised delay (see Figure 3.4b, Figure 3.5b). Additionally, in each group, the three optimal solutions selected were used to fit three curves related to different levels of robustness, taking τ as independent variable. These levels of robustness were defined as follows.

- Low level (ε_{low}): The LADRC tuned by this approximation will offer robustness of about 2.7 for processes with $\tau \leq 0.5$ and about 2.5 for plants with $\tau > 0.5$. For *Group 1*, the tuning rule was approximated using the Nash solutions of the upper regions of the Pareto Fronts (NS_1). For *Group 2*, the curve was fitted using the upper ends of the Fronts (UP).

- Medium level (ε_{med}): Processes with $\tau \leq 0.5$ controlled by LADRC tuned according to this formulae will have robustness of approximately 2.5. In the case of plants with $\tau > 0.5$, the robustness of the closed-loop will be about 2.3. The midpoints of the Pareto Fronts (MP) were used to approximate the tuning function in the first group of systems and the Nash solutions (NS) were used for the second group.

- High level ($\varepsilon_{\text{high}}$): The highest robustness of the closed-loop will be approximately 2.2 for systems with $\tau \leq 0.5$ and 2.0 for plants meeting $\tau > 0.5$. In *Group 1* the approximation was made using the Nash solutions of the lower regions of the Pareto Fronts (NS_2), and in *Group 2*, the bottom ends of the Fronts (BP) were used instead.

The nominal values for the critical gain were fitted to power functions in the case of systems with $\tau \leq 0.5$. The relevance of this type of adjustment was validated by plotting the logarithm of the nominal critical gain values obtained in the decision-making phase versus the logarithm of the normalised delay as a linear relationship was observed. However, for systems with $\tau > 0.5$, it was concluded that fitting the b_0 values to polynomial functions was more appropriate.

Therefore, the corresponding tuning rule for the nominal value of the critical gain when the second-order LADRC is used to control the FOPDT system is given by (3.25) with k_b, n_b, a_b, b_b, and c_b as constants.

$$b_0 = \begin{cases} k_b \left(\dfrac{\tau}{1-\tau} \right)^{n_b}, & \tau \leq 0.5 \\[4mm] a_b \left(\dfrac{\tau}{1-\tau} \right)^2 + b_b \left(\dfrac{\tau}{1-\tau} \right) + c_b, & \tau > 0.5 \end{cases} \tag{3.25}$$

On the other hand, the controller bandwidth values were fitted for both groups to power functions. Consequently, the tuning rule for ω_c is in the form of (3.26), where k_ω and n_ω are constants.

$$\omega_c = k_\omega \left(\frac{\tau}{1-\tau} \right)^{n_\omega} \tag{3.26}$$

The resultant fitting functions for the three specified levels of robustness are presented in Figure 3.9 and Figure 3.10, and the corresponding parameters for (3.25) and (3.26) are reported in the guide 3.5.1.

As the last step in the data processing, (3.25) and (3.26) were substituted in the corresponding scaled parameters of (3.10) to obtain the general LADRC tuning rules (3.27)-(3.29), which are now dependent on the three FOPDT plant parameters, obtained straightforwardly by identification techniques for many processes.

$$\bar{b}_0 = \begin{cases} \dfrac{K}{T^2} \left[k_b \left(\dfrac{\tau}{1-\tau} \right)^{n_b} \right], & \tau \leq 0.5 \\[4mm] \dfrac{K}{T^2} \left[a_b \left(\dfrac{\tau}{1-\tau} \right)^2 + b_b \left(\dfrac{\tau}{1-\tau} \right) + c_b \right], & \tau > 0.5 \end{cases} \tag{3.27}$$

$$\overline{\omega}_c = \frac{1}{T} \left[k_\omega \left(\frac{\tau}{1 - \tau} \right)^{n_\omega} \right] \tag{3.28}$$

$$\overline{\omega}_o = \frac{10}{T} \left[k_\omega \left(\frac{\tau}{1 - \tau} \right)^{n_\omega} \right] \tag{3.29}$$

In summary, the guide 3.5.1 for tuning the LADRC to control FOPDT plants is presented. Each of the defined levels of robustness represents a compromise between this objective and the disturbance rejection performance. This way, the designer is provided with three closed-loop stable candidate controllers that could be tested on the system for the final decision.

Furthermore, the designer could vary the values of the LADRC parameters in the intervals obtained from the proposed rules to adjust the performance according to the preferences. To help in this task, a tuning tool was developed using App Designer from MATLAB$^{\circledR}$ and is available at Matlab Central [64]. This app requires as input the FOPDT model. Through interaction with robustness level and manual tuning sliders, the user can visualise the closed-loop response and evaluate the second-order LADRC performance with the aid of some measures.

The tuning rules proposed in this section and the developed tuning tool allow some degree of designer involvement in the final selection of the LADRC parameters but eliminate the time and complexity of performing the entire optimisation process. It is highlighted that

The proposed tuning rules allow the computation of the three main LADRC parameters: nominal critical gain b_0, controller bandwidth ω_c, and observer bandwidth ω_o. A range of values can be obtained for each parameter whose limits are defined by the achievable robustness quality $2 \leq \varepsilon \leq 3$. Thus, no additional tuning parameters are provided. The LADRC designed with the tuning method proposed here ensures closed-loop stability and a reasonable compromise between disturbance rejection and loop robustness such that $1.3 \leq M_S \leq 2$ and $1 \leq M_T \leq 1.4$.
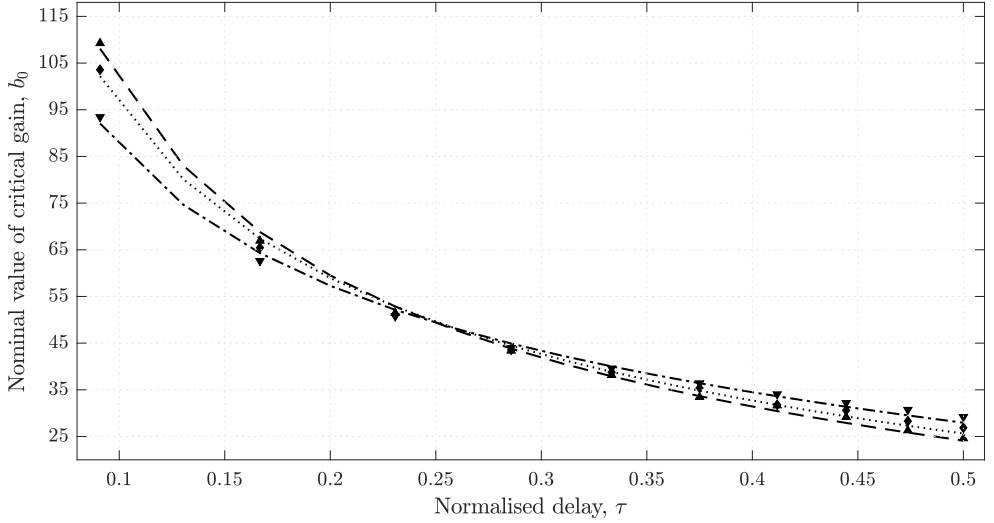
(a) Fitting for *Group 1*, $\tau \leq 0.5$
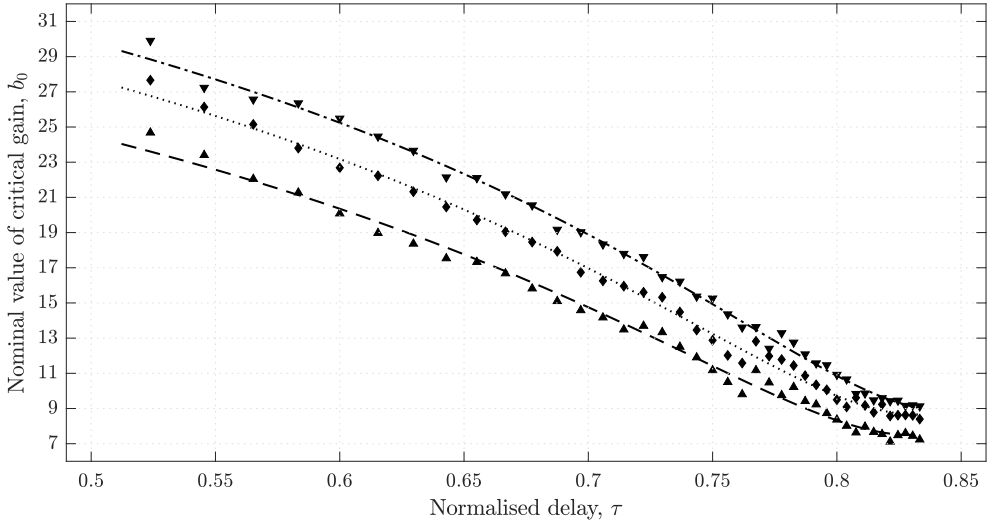
(b) Fitting for *Group 2*, $\tau > 0.5$

Figure 3.9: Tuning for the nominal values of the second-order LADRC critical gain. Markers indicate the Pareto optimal solutions NS_1 (▲), MP (♦), NS_2 (▼). Lines are the fitting functions for the robustness levels ε_{low} (— —), ε_{med} (· · ·), $\varepsilon_{\text{high}}$ (-··-).
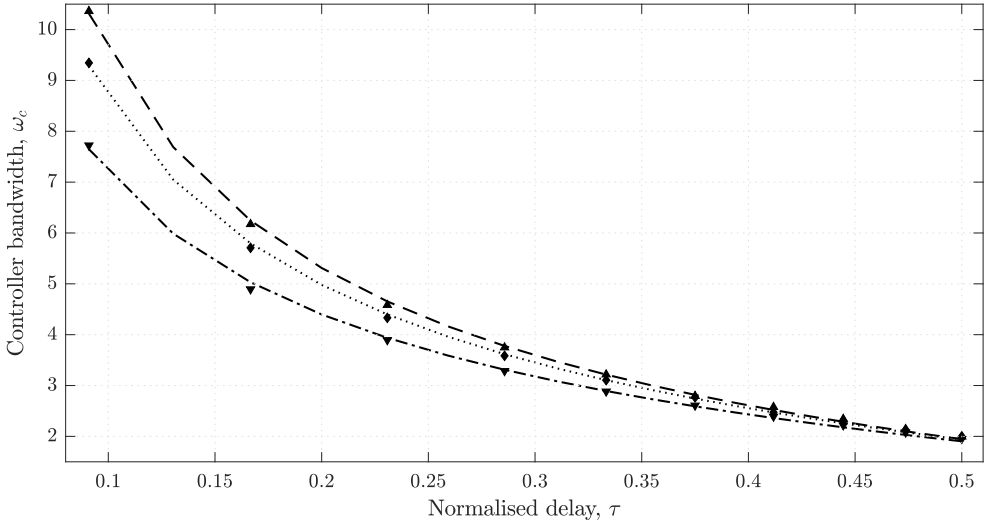
(a) Fitting for *Group 1*, $\tau \leq 0.5$
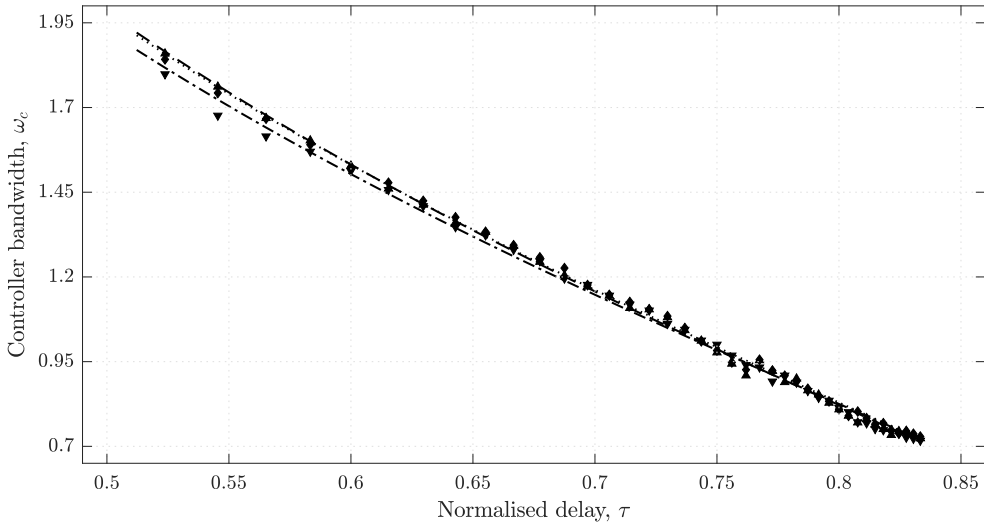
(b) Fitting for *Group 2*, $\tau > 0.5$

Figure 3.10: Tuning for the second-order LADRC controller bandwidth. Markers indicate the Pareto optimal solutions UP (▲), NS (◆), and BP (▼). Lines are the fitting functions for the robustness levels ε_{low} (− −), ε_{med} (· · ·), and $\varepsilon_{\text{high}}$ (-··-).

Guide 3.5.1: Tuning guide for the Linear Active Disturbance Rejection Control (LADRC) of First Order Plus Dead Time (FOPDT) systems

1. Approximate the process dynamics with the FOPDT model

$$G(s) = \frac{K}{Ts+1}e^{-ls}.$$

2. Compute the normalised dead time, $0 \leq \tau \leq 1$, as

$$\tau = \frac{l}{T+l}.$$

3. Decide whether the process belongs to Group 1: $\tau \leq 0.5$ or Group 2: $\tau > 0.5$ according to the normalised dead time computed in step 2.

4. Use the tables given below to select the appropriate coefficients for the tuning rules according to preferences on the achievable approximated robustness quality ε.

Group 1: $\tau \leq 0.5$				Group 2: $\tau > 0.5$			
	ε_{low}	ε_{med}	$\varepsilon_{\text{high}}$		ε_{low}	ε_{med}	$\varepsilon_{\text{high}}$
ε	2.7	2.5	2.2	ε	2.5	2.3	2.0
k_b	24.129	25.632	27.952	a_b	1.145	1.238	1.121
n_b	-0.651	-0.601	-0.518	b_b	-11.110	-12.192	-11.921
k_ω	1.946	1.938	1.903	c_b	34.443	38.682	40.601
n_ω	-0.724	-0.681	-0.604	k_ω	1.982	1.972	1.927
				n_ω	-0.635	-0.625	-0.612

5. Substitute the coefficients selected in step 4, the static gain K, and the apparent time constant T in the following rules to compute the nominal value of the critical gain $\bar{b}_0$, the controller bandwidth $\bar{\omega}_c$, and the observer bandwidth $\bar{\omega}_o$ for the second-order LADRC.

$$\bar{b}_0 = \begin{cases} \dfrac{K}{T^2}\left[k_b\left(\dfrac{\tau}{1-\tau}\right)^{n_b}\right], & \tau \leq 0.5 \\[2em] \dfrac{K}{T^2}\left[a_b\left(\dfrac{\tau}{1-\tau}\right)^2 + b_b\left(\dfrac{\tau}{1-\tau}\right) + c_b\right], & \tau > 0.5 \end{cases}$$

$$\bar{\omega}_c = \frac{1}{T}\left[k_\omega\left(\frac{\tau}{1-\tau}\right)^{n_\omega}\right] \qquad \bar{\omega}_o = \frac{10}{T}\left[k_\omega\left(\frac{\tau}{1-\tau}\right)^{n_\omega}\right]$$

3.6 Validation of the LADRC tuning rules

This section presents two examples to validate the proposed tuning rules. The load disturbance and setpoint responses to the unit step are compared with the performances obtained with other controllers such as PID and LADRC tuned by different methods.

The performances are quantified by the indices in the frequency domain M_S, M_T, and ε, and the indices in the time domain ITSE, TV, and settling time ($t_{98\%}$, in seconds).

EXAMPLE 3.6.1 Consider the FOPDT lag-dominated system

$$G_1(s) = \frac{1}{10s+1}e^{-2s} \tag{3.30}$$

The tuning guide 3.5.1 is used to illustrate the computation of the parameters for the second-order LADRC according to the three levels of robustness. The performances obtained with the resultant controllers are compared with those achieved by the LADRC tuned with the rules from [32] and the IMC-PID, SIMC-PID, AMIGO-PID, and the optimal-Nash-PID (ONS). Some further analysis related to the loop frequency response and the closed-loop stability is done.

Following the steps from Guide 3.5.1

1. From (3.30), the static gain is $K = 1$, the apparent time constant is $T = 10$, and the apparent delay is $l = 2$.

2. The normalised dead time is

$$\tau = \frac{2}{10+2} = 0.17 \tag{3.31}$$

3. According to the normalised dead time from step 2, the system (3.30) belongs to *Group 1*. Therefore, the three candidate controllers have robustness values of approximately 2.7 (ε_{low}), 2.5 (ε_{med}), and 2.2 ($\varepsilon_{\text{high}}$).

4. For example, if a controller with high robustness is preferred, the corresponding coefficients for the tuning rules are $k_b = 27.952$ and $n_b = -0.518$ for computation of b_0, and $k_\omega = 1.903$ and $n_\omega = -0.604$ for computation of ω_c and ω_o.

5. The nominal value of the critical gain, the controller bandwidth, and the observer bandwidth are calculated by substituting the coefficients from step 4 and the FOPDT parameters in the tuning rules. This is,

$$\bar{b}_0 = \frac{1}{100}\left[27.952\left(\frac{0.17}{1-0.17}\right)^{-0.518}\right] = 0.643 \qquad (3.32)$$

$$\bar{\omega}_c = \frac{1}{10}\left[1.093\left(\frac{0.17}{1-0.17}\right)^{-0.604}\right] = 0.503 \qquad (3.33)$$

$$\bar{\omega}_o = 1.903\left(\frac{0.17}{1-0.17}\right)^{-0.604} = 5.031 \qquad (3.34)$$

Steps 4 and 5 from the above procedure should be repeated if different robustness is desired. Consequently, the LADRC parameters for the three levels of robustness (ε_{low}, ε_{med}, $\varepsilon_{\text{high}}$) are listed in Table 3.5. Additionally, the parameters computed with the tuning rules proposed in [32] (labelled as ADRC_{Z}) and those corresponding to the PID controllers are included.

Table 3.5: Parameters for the control of plant $G_1(s)$. The PID parameters were calculated according to the rules from Table 3.4, the ADRC_{Z} values were computed with the formulae from Table 3.3, and the remaining LADRC parameters were obtained following Guide 3.5.1.

LADRC	b_0	ω_c	ω_o	PID	K_c	T_i	T_d
ε_{low}	0.688	0.624	6.243	IMC	4.320	10.8	0.751
ε_{med}	0.674	0.580	5.795	SIMC	2.500	10	0
$\varepsilon_{\text{high}}$	0.643	0.503	5.031	AMIGO	2.450	5.867	0.943
ADRC_{Z}	0.349	1.950	0.960	ONS	3.420	5.475	0.970

Figure 3.11 shows the closed-loop time responses of (3.30) with the three candidate controllers and the PID configurations. The resulting values for the performance indices are reported in Table 3.6. On the one hand, it can be seen that each of the proposed controllers offers a robustness level similar to one of the PID alternatives with a lower ITSE for disturbance rejection. Likewise, the LADRC candidates drive the output back to the steady state faster than the PID tuned with the IMC and the SIMC methods. This behaviour is appreciated in Figure 3.11b.
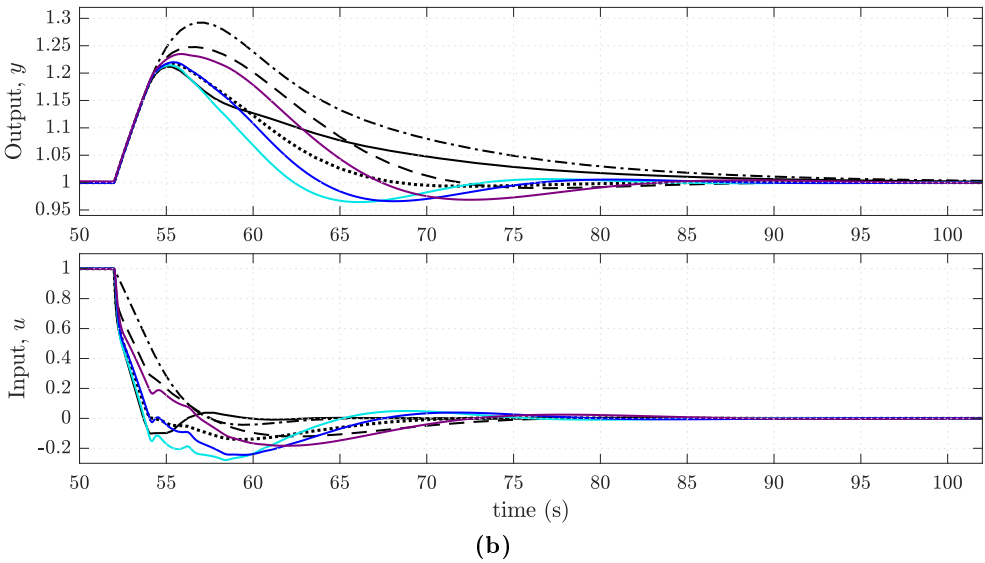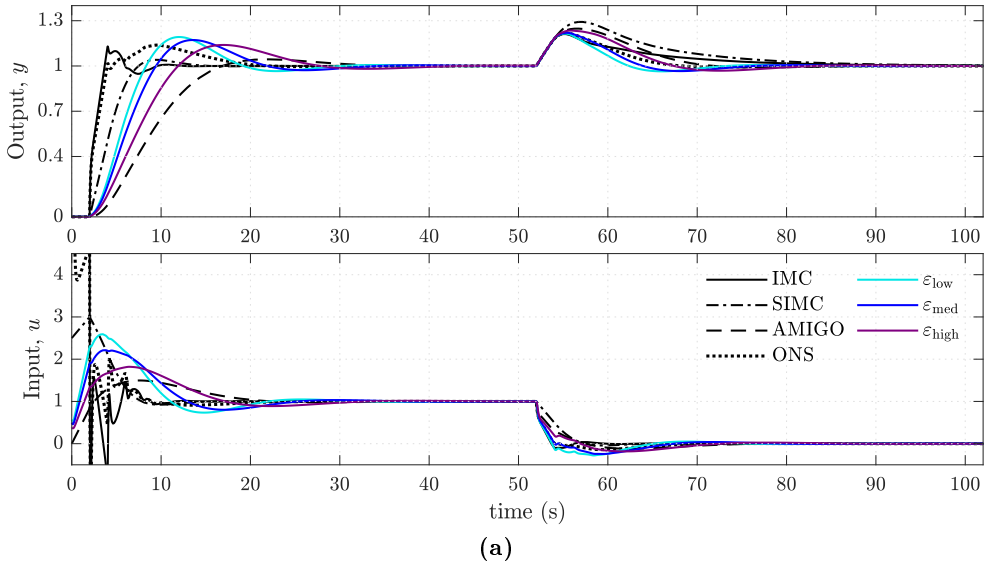
Figure 3.11: Closed-loop time responses of $G_1(s)$ when controlled with the second-order LADRC tuned with the proposed rules. Comparison with the performance of the closed-loop with PID controllers. **(a)** Unit step response and disturbance rejection response when a unit step disturbance is applied to the input at $t = 50\,\text{s}$. **(b)** Inset to the disturbance rejection response in the time window $t \in [50, 100]\,\text{s}$.

Table 3.6: Performance indices obtained when the plant $G_1(s)$ is controlled with PID configurations and LADRC. The $\varepsilon_{\text{high}}$ controller is more robust and produces lower ITSE in disturbance rejection than the ADRC$_\text{Z}$ controller.

	M$_\text{S}$	M$_\text{T}$	ε	Disturbance rejection			Setpoint following		
				ITSE	TV	$t_{98\%}$	ITSE	TV	$t_{98\%}$
IMC	2.032	1.097	3.103	2.493	1.390	44.1	2.794	61.353	8.7
SIMC	1.590	1	2.353	6.871	1.087	46.2	6.235	2.662	12.1
AMIGO	1.446	1.135	2.029	3.774	1.250	33.6	26.096	2.038	28.7
ONS	1.767	1.181	2.545	1.741	1.370	26.7	4.029	48.374	18.5
ADRC$_\text{Z}$	1.583	1.345	2.447	3.692	1.549	43.3	12.542	14.762	35.4
ε_{low}	1.842	1.489	2.771	1.241	1.804	29.9	12.753	4.370	26.4
ε_{med}	1.735	1.392	2.544	1.665	1.657	33.1	14.662	3.510	29.1
$\varepsilon_{\text{high}}$	1.598	1.258	2.236	2.977	1.470	31.4	19.496	2.564	25.9

On the other hand, in Figure 3.12, the closed-loop time responses of (3.30) with the three LADRC candidates and the LADRC tuned with the rules from [32] are plotted. According to the indices in Table 3.6, the proposed controllers produce lower ITSE and settling times than the ADRC$_\text{Z}$ controller in the case of a load disturbance, as shown in Figure 3.12b. Notice that the $\varepsilon_{\text{high}}$ candidate achieves a higher robustness level and better disturbance rejection. In addition, the total variation of the control action is lower for this alternative.

In the case of setpoint following, the ε_{low} controller produces a similar ITSE to the ADRC$_\text{Z}$. However, it is worth noting that the control actions produced by the three alternatives are smoother, which is reflected in the total variations indices calculated. This is mainly because the initial values of the control signals (sometimes referred to in the literature as *proportional kick*) are significantly lower than those reached by the ADRC$_\text{Z}$ controller.

The frequency measures reported in Table 3.6 for the control of $G_1(s)$ with the $\varepsilon_{\text{high}}$ LADRC are marked in Figure 3.13 which shows the magnitude of the frequency response of the sensitivity function, the complementary sensitivity function, and the sum of the above frequency responses, from which the robustness index ε is computed. With this candidate controller, the maximum peaks M$_\text{S}$ and M$_\text{T}$ are within the ranges given by common design rules, and their values vary in such ranges for any other controller whose parameters are obtained from the proposed rules.

Let the $\varepsilon_{\text{high}}$ controller be also used to validate Theorem 3.2.1 and Lemma 3.4.1.

(a)

(b)
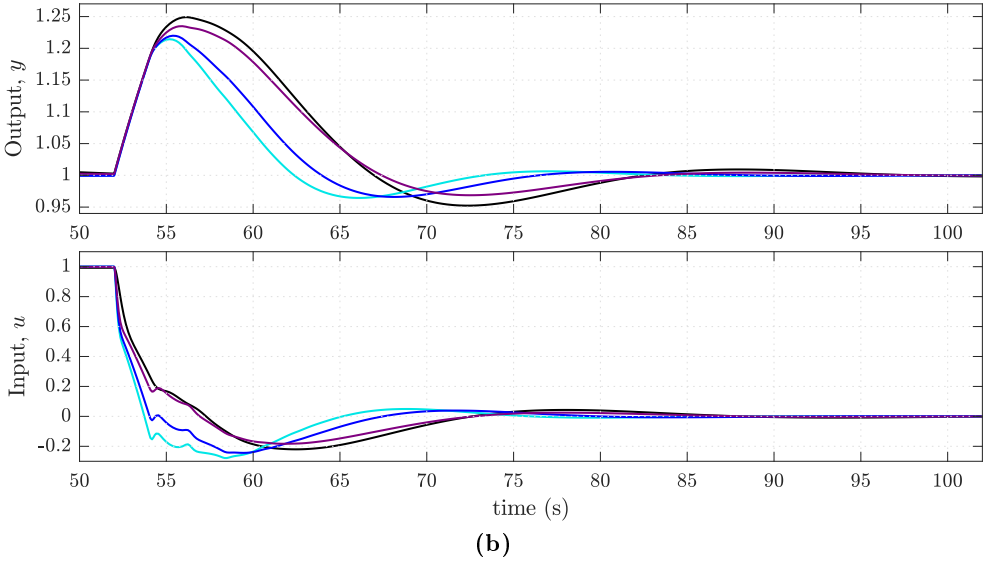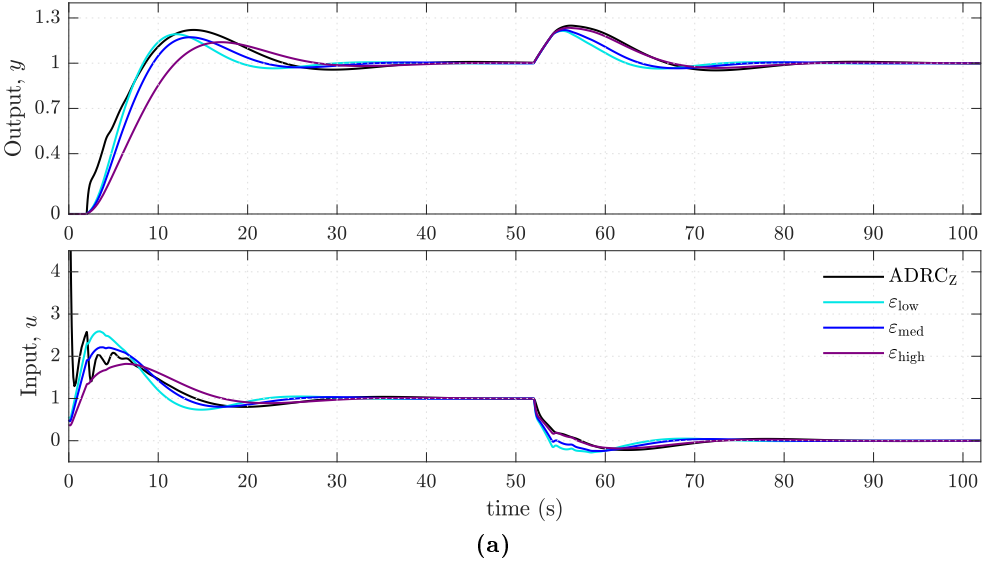
Figure 3.12: Closed-loop time responses of $G_1(s)$ when controlled with the second-order LADRC tuned with the proposed rules. Comparison with the performance of the closed-loop with the LADRC tuned using the rules from [32]. **(a)** Unit step response and disturbance rejection response when a unit step disturbance is applied to the input at $t = 50\,\mathrm{s}$. **(b)** Inset to the disturbance rejection response in the time window $t \in [50, 100]$ s.
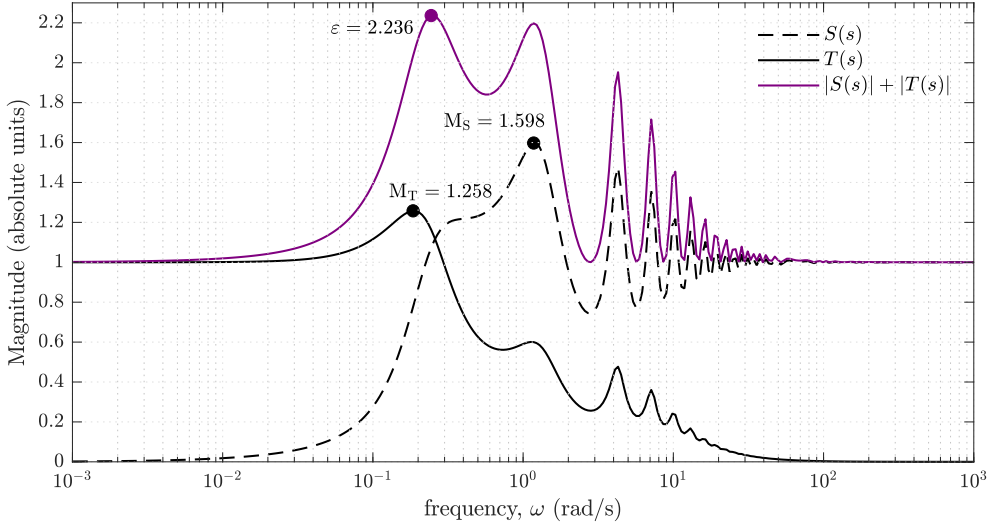
Figure 3.13: Magnitudes of the frequency responses of the sensitivity function, complementary sensitivity function, and sum of the above frequency responses when the plant $G_1(s)$ is controlled by the $\varepsilon_{\text{high}}$ LADRC. The robustness indices M_S, M_T, and ε are marked.

Comparing (3.30) with (3.6), the gain scaling $k = 1$, the frequency scaling $\omega_p = 1/10$, and nominal delay $\Theta = 2/10$ are identified. Therefore, $G_1(s)$ is a scaled version of the nominal plant

$$G_n(s) = \frac{1}{s+1}e^{-0.2s}, \tag{3.35}$$

which was included in the batch of processes used in the MOOD procedure addressed in section 3.4. For (3.35), the LADRC with the highest achievable robustness has parameters $b_0 = 64.294$, $\omega_c = 5.031$, and $\omega_o = 50.312$ (computed using (3.35) in Guide 3.5.1). The corresponding open-loop transfer function is

$$\mathcal{L}(s) = G_A(s)G_n(s) = \frac{3228.8\,(s^2 + 7.099s + 15.53)}{s\,(s+1)\,(s^2 + 161s + 9138)}e^{-0.2s}, \tag{3.36}$$

where $G_A(s)$ is the stabilising LADRC obtained by substituting its associated parameters in (3.15).

85
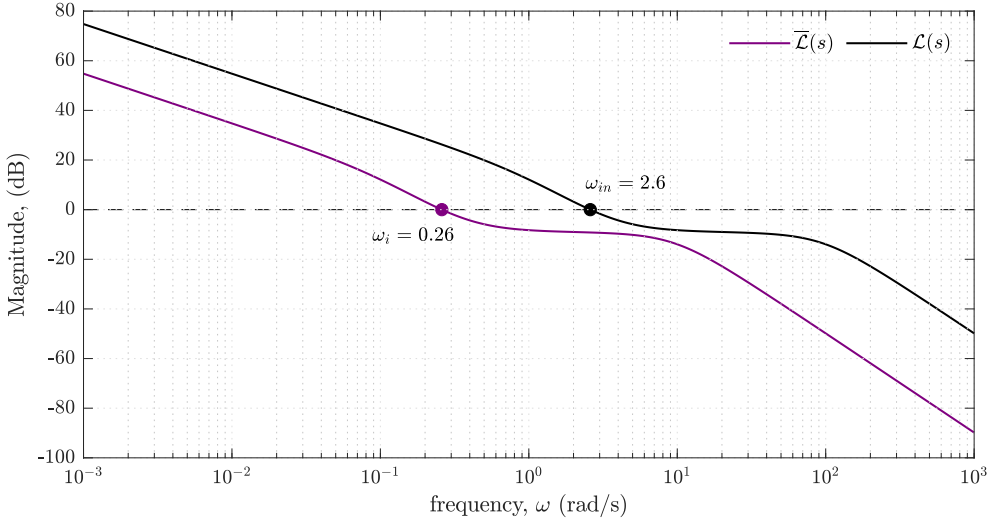
Figure 3.14: Magnitudes of the frequency responses of the open-loop transfer functions $\overline{\mathcal{L}}(s) = \overline{G}_A(s)G_1(s)$ and $\mathcal{L}(s) = G_A(s)G_n(s)$. The scaled loop $\overline{\mathcal{L}}(s)$ has a crossover frequency $\omega_i = \omega_{in}\omega_p$, with ω_{in} the crossover frequency of the nominal loop $\mathcal{L}(s)$.

Correspondingly, the open-loop transfer function involving the $\varepsilon_{\text{high}}$ LADRC and $G_1(s)$ is (3.37) with $\overline{G}_A(s)$ as the scaled controller.

$$\overline{\mathcal{L}}(s) = \overline{G}_A(s)G_1(s) = \frac{322.88\,(s^2 + 0.710s + 0.155)}{s\,(10s + 1)\,(s^2 + 16.1s + 91.38)}e^{-2s}. \tag{3.37}$$

The magnitudes of the frequency responses of (3.36) and (3.37) are presented in Figure 3.14. As stated in Theorem 3.2.1, the nominal loop $\mathcal{L}(s)$ has a crossover frequency $\omega_{in} = 2.6\,\text{rad/s}$, and consequently, the crossover frequency of the new scaled loop $\overline{\mathcal{L}}(s)$ is $\omega_i = \omega_{in}\omega_p = 0.26\,\text{rad/s}$. Moreover, both loops have the same stability margins and robustness properties.

Finally, the closed-loop stability is validated by evaluating the conditions of Lemma 3.4.1. Let $H(s)$ be the delay-free open-loop transfer function such that $H(s) = \overline{G}_A(s)G_0(s)$ and $G_0(s)$ is equivalent to (3.30) with $l = 0$. Due to the delay does not affect the magnitude of the frequency response of an open-loop transfer function, from Figure 3.14 is deduced that the magnitude of $H(s)$ equals 1 (0 dB) at $\omega_i = 0.26\,\text{rad/s}$, and from Figure 3.15 is clear that the phase of $H(s)$ is greater than the phase of $-e^{2s}$ at the crossover frequency.
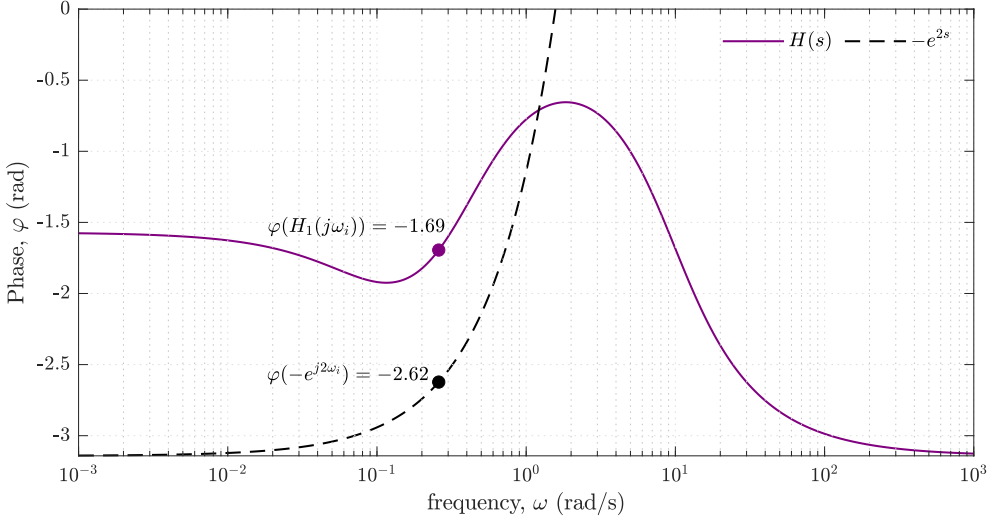
Figure 3.15: Phases of the frequency responses of the delay-free open-loop transfer function $H(s)$ and $-e^{2s}$. The phase $\varphi(H(j\omega_i))$ of $H(s)$ at $\omega_i = 0.26\,\text{rad/s}$ is greater than the phase $\varphi\left(-e^{j2\omega_i}\right)$ at the same crossover frequency.

EXAMPLE 3.6.2 The FOPDT delay-dominated system is controlled.

$$G_2(s) = \frac{3}{0.25s + 1}e^{-s} \tag{3.38}$$

The static gain for this plant is $K = 3$, the apparent time constant $T = 0.25$, and the normalised delay $\tau = 0.80$. The performances achieved by the second-order LADRC designed with the proposed rules are compared with PID controllers tuned with the rules IMC, SIMC and AMIGO, and the LADRC adjusted with the rules from [32] (labelled as ADRC_z). In addition, a second-order LADRC tuned using the formulae from [30] (tagged as ADRC_H) was also considered for comparison. The latter tuning method is proposed for the control of high-order plants, but it can be used for self-regulatory FOPDT systems with τ/T above 0.46 by approximating the plant into the form $\widetilde{K}/(\widetilde{T}s + 1)^n$. These tuning rules are listed in Table 3.3.

According to the empirical two-point method suggested in [30], the system (3.38) is approximated to a high-order process by substituting in (3.39) the steady-state value y_∞ and the times $t_{40\%}$ and $t_{80\%}$ at which the step response reaches 40% and 80% of the final value, respectively.

87

$$
\begin{cases}
\widetilde{K} = y_\infty/u \\[2ex]
n = \left(\dfrac{1.075 t_{40\%}}{t_{80\%} - t_{40\%}} + 0.5 \right)^2 \\[2ex]
\widetilde{T} = \dfrac{t_{40\%} + t_{80\%}}{2.16 n}
\end{cases}
\tag{3.39}
$$

From the step response of (3.38) with $u = 1$, $y_\infty = 3$, $t_{40\%} = 1.12\,\text{s}$, and $t_{80\%} = 1.40\,\text{s}$. Therefore,

$$
G_2(s) \approx \frac{3}{(0.051s + 1)^{23}}.
\tag{3.40}
$$

Comparing the proposed LADRC candidates with the PID controllers is considered first. Table 3.7 lists the corresponding parameters, and the closed-loop responses obtained with such a set of controllers are presented in Figure 3.16. Likewise, the performance indices computed are reported in Table 3.8. These indices show that the robustness of the LADRC tuned with the proposed rules is within the robustness quality achievable with PID configurations, and the disturbance rejection can be improved. For example, the $\varepsilon_{\text{high}}$ candidate is more robust and produces lower ITSE than the SIMC-PID. Even a relaxation in robustness, i.e. a controller whose robustness index is close to ε_{med}, will naturally improve the ITSE for disturbance rejection.

Table 3.7: Parameters for the control of plant $G_2(s)$. The PID parameters were calculated according to the rules from Table 3.4, the ADRC_Z and ADRC_H values were computed with the formulae from Table 3.3 and the remaining LADRC parameters were obtained following Guide 3.5.1.

LADRC	b_0	ω_c	ω_o	PID	K_c	T_i	T_d
ε_{low}	399.747	3.288	32.876	IMC	0.173	0.650	0.195
ε_{med}	466.508	3.317	33.172	SIMC	0.097	0.583	0
$\varepsilon_{\text{high}}$	521.205	3.301	33.007	AMIGO	0.104	0.585	0.227
ADRC_{Z1}	316.198	5.029	16.140				
ADRC_{Z2}	434.772	5.029	16.140				
ADRC_{H1}	535.722	3.663	36.630				
ADRC_{H2}	11079	8.571	85.714				
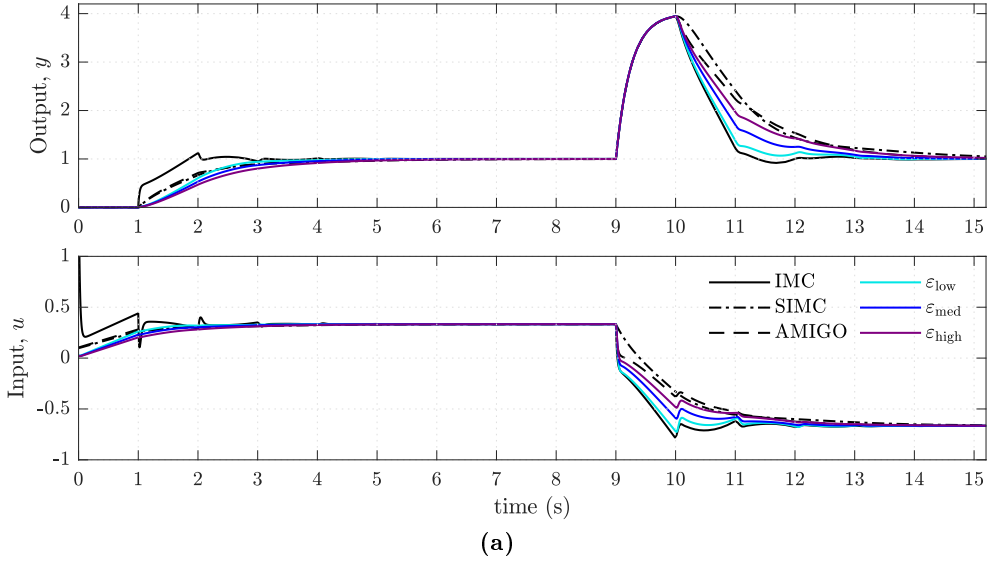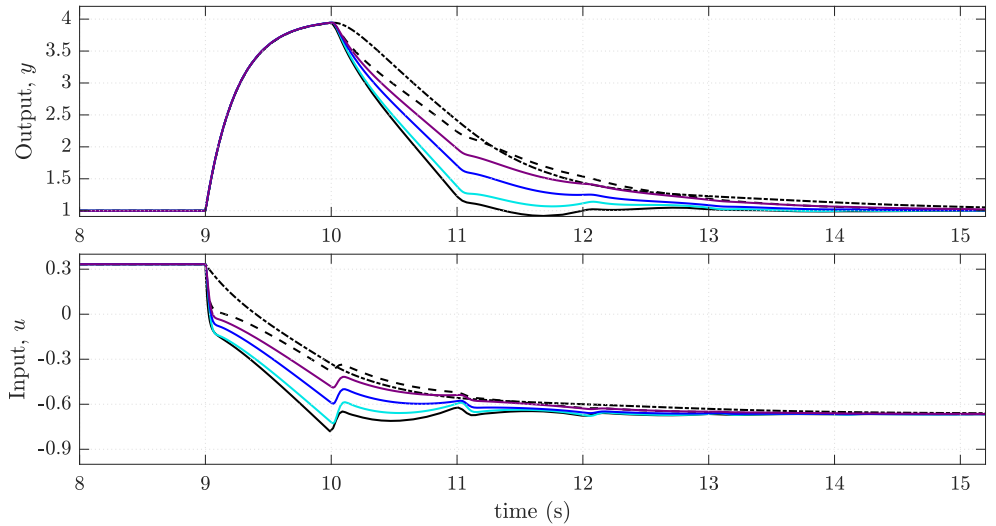
Figure 3.16: Closed-loop time responses of $G_2(s)$ when controlled with the second-order LADRC tuned with the proposed rules. Comparison with the performance of the closed-loop with PID controllers. **(a)** Unit step response and disturbance rejection response when a unit step disturbance is applied to the input at $t = 8$ s. **(b)** Inset to the disturbance rejection response in the time window $t \in [8, 15]$ s.

Table 3.8: Performance indices obtained when the plant $G_2(s)$ is controlled with PID and LADRC designs. For all controllers, $M_T = 1$. Under the same robustness requirement, the LADRC designs tuned with the proposed rules offer lower ITSE in disturbance rejection than the LADRC tuned with other rules from the literature.

	M_S	ε	Disturbance rejection			Setpoint following		
			ITSE	TV	$t_{98\%}$	ITSE	TV	$t_{98\%}$
IMC	1.873	2.774	15.461	1.562	3.9	0.644	2.915	3.7
SIMC	1.568	2.187	25.191	1	7	1.205	0.236	5.7
AMIGO	1.401	1.933	22.618	1.081	6	1.129	0.275	4.4
$ADRC_{Z1}$	1.761	2.624	17.256	1.340	5.3	1.208	0.362	4.5
$ADRC_{Z2}$	1.472	2.079	22.016	1.035	5.2	1.595	0.331	4.7
$ADRC_{H1}$	1.781	2.618	16.629	1.379	4.0	1.344	0.331	2.9
$ADRC_{H2}$	1.521	2.229	31.763	1.049	7.1	2.052	0.344	6.1
ε_{low}	1.798	2.615	16.033	1.544	4.9	1.380	0.318	4.1
ε_{med}	1.638	2.296	17.834	1.272	5.3	1.552	0.313	4.7
ε_{high}	1.526	2.073	20.123	1.158	6.1	1.776	0.316	5.5

The proposed controllers are compared with other LADRC designs next. For this purpose, consider the LADRC parameters reported in Table 3.7, labelled $ADRC_{Z1}$ and $ADRC_{Z2}$. These controllers were designed by adjusting the λ additional tuning parameter of the rules from [32] to $\lambda = 0.88$ to obtain a low robustness LADRC and to $\lambda = 1.21$ to get a high robustness LADRC, respectively, as quantified in the ε column.

Similarly, the $ADRC_{H1}$ and $ADRC_{H2}$ parameters correspond to those calculated with the rules from [30] and the approximation (3.40). In this case, the low robustness LADRC was obtained by adjusting the associated additional tuning parameter to $k = 2.34$, and the high robustness LADRC was designed with $k = 1$. A value of k above 2.77 leads the loop to instability.

With the above designs, the performances of the proposed controllers are contrasted with the ones of the LADRC with the same robustness. For example, suppose the robustness requirement is relaxed. In that case, a robustness measure $\varepsilon \approx 2.6$ is allowed, and the ε_{low} controller improves (reduces) the ITSE values of the disturbance rejection responses obtained with the $ADRC_{Z1}$ and $ADRC_{H1}$ parameters, although the latter drives the output back to the steady-state faster.
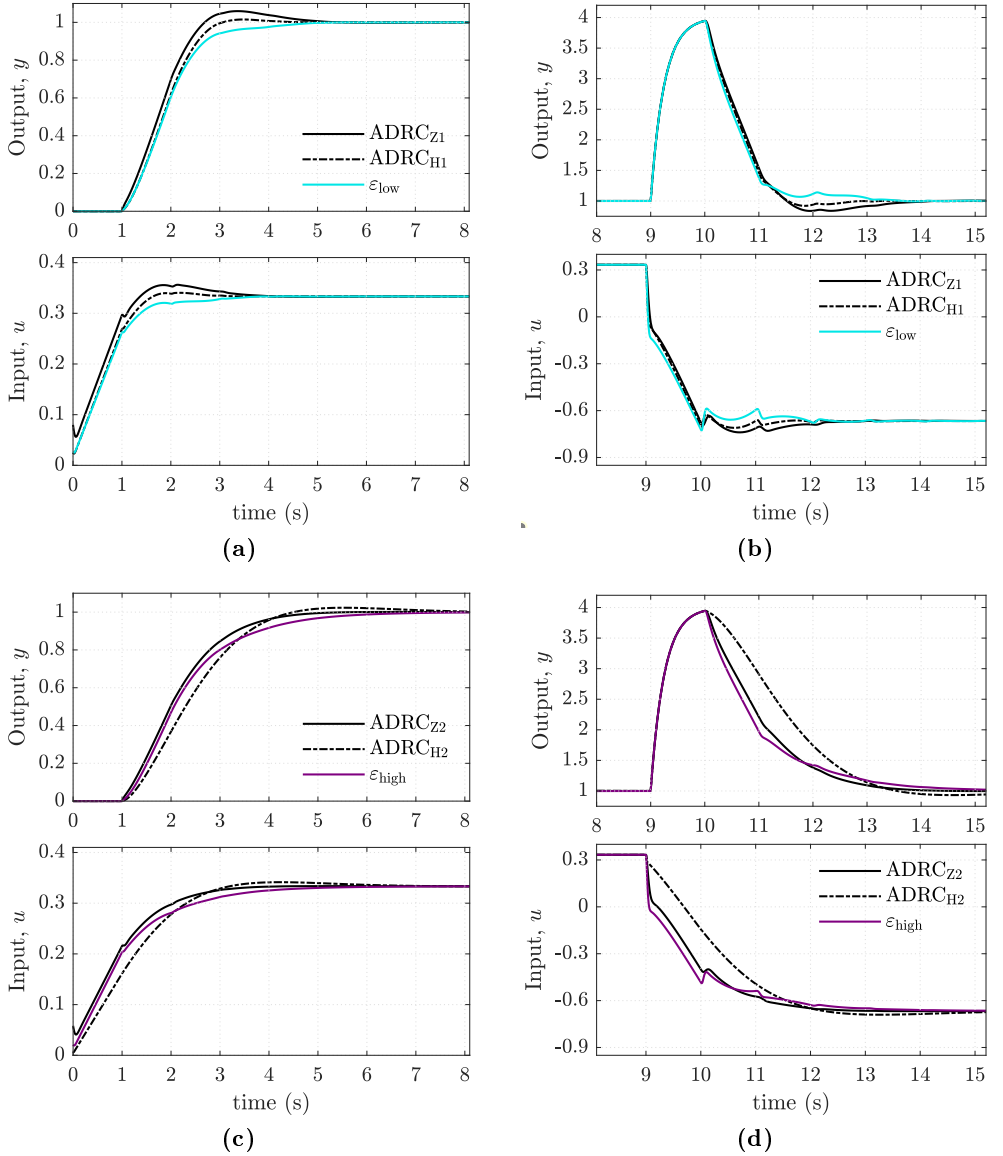
Figure 3.17: Unit step and disturbance rejection responses of $G_2(s)$ when controlled with the LADRC tuned with the proposed rules. Comparison with the responses to the LADRC designed with the rules from [32] (ADRC$_{Z1}$ and ADRC$_{Z2}$) and [30] (ADRC$_{H1}$ and ADRC$_{H2}$). A unit step disturbance is applied to the input at $t = 8\,\text{s}$. **(a)-(b)** Controllers with low robustness $\varepsilon \approx 2.6$. **(c)-(d)** Controllers with high robustness $\varepsilon \approx 2.1 - 2.2$.

On the other hand, with a high robustness objective of $\varepsilon \approx 2.1$, the $\varepsilon_{\text{high}}$ candidate also produces lower ITSE than the ADRC_{Z2} and the ADRC_{H2} controllers, offering a better setpoint tracking than the latter. It should be pointed out that the lower robustness index computed with the rules from [30] is the value reported in Table 3.8. Notice that the ε_{med} LADRC, which has a closer robustness measure to the ADRC_{H2}, still improves the servo-regulatory operation. The above discussion is supported by the unit step and disturbance rejection responses shown in Figure 3.17.

End of example 3.6.2 ■

The tuning rules for the LADRC, summarised in Guide 3.5.1, were used to design control loops for lag-dominated and delay-dominated systems. The results obtained were contrasted with those generated by the PID configuration tuned following widely accepted rules, and the LADRC adjusted with other rules from the literature. It is concluded

The second-order LADRC designed with the proposed rules is a control strategy alternative to PID control for FOPDT systems, potentially improving the step-type input disturbance rejection response. The designers are provided directly with LADRC candidates that cover the robustness range of the PID controllers tuned with classical rules that keep the trade-off between disturbance rejection and robustness.

The second-order LADRC designed with the proposed rules potentially improves the step-type input disturbance rejection obtained with the LADRC tuned with the rules from [32] and [30] (when applicable), even under the same robustness requirement.

The LADRC tuned with the proposed rules may produce smoother control actions than those of the LADRC adjusted according to [32] due to the computed controller and observer bandwidths holding the relation $\omega_c < \omega_o$.

The proposed rules allow the computation of the LADRC parameters for a broader family of FOPDT plants in contrast to the rules presented in [30], applicable only to control FOPDT systems meeting $l/T \leq 0.46$ and with which the closed-loop stability is dependent on an additional tuning parameter.

3.7 Control of the Peltier thermoelectric module

In Example 2.6.1, it was demonstrated that the second-order LADRC is capable of controlling the temperature of the cold face of a thermoelectric module. In the following, the control performance of the LADRC when tuned with the rules presented in this chapter is addressed.

The Peltier cell behaviour, described by (2.44)-(2.57), in the freezing zone ($\approx -8\,°\text{C}$) is approximated by the FOPDT model [93]

$$G_p(s) = \frac{-0.315}{3.192s + 1} e^{-0.4s}. \tag{3.41}$$

Consequently, for (3.41) the static gain is $K = -0.315\,°\text{C}/\%$, the time constant $T = 3.192\,\text{s}$, the apparent dead time $l = 0.4\,\text{s}$, and the normalised delay is $\tau = 0.11$. The parameters of the three LADRC candidates obtained using the above information in Guide 3.5.1 are reported in Table 3.9. Two additional controllers are included for comparison purposes: the LADRC tuned with the proposal from [32] (ADRC_Z) and a PID whose parameters were calculated using the SIMC method.

Table 3.9: Parameters for the control of the thermoelectric module. The ADRC_Z values were computed with the formulae from Table 3.3, the PID parameters were calculated according to the rules from Table 3.4, and the remaining LADRC parameters were obtained following Guide 3.5.1.

LADRC	b_0	ω_c	ω_o	PID	K_c	T_i	T_d
ε_low	-2.885	2.744	27.440	SIMC	-12.667	3.192	0
ε_med	-2.758	2.496	24.957				
ε_high	-2.532	2.090	20.905				
ADRC_Z	-1.613	9.696	4.102				

Consider that the cold face of the module is stable at $-5\,°\text{C}$, and a fault in the power system reduces the input voltage by $10\,\%$ of its nominal value. The evolution of the temperature T_c and the required voltage to reject the disturbance are shown in Figure 3.18. The corresponding performance indices ITSE ($°\text{C}^2\,\text{s}$), TV ($\%$) and $t_{98\%}(\text{s})$ are included in Table 3.10.
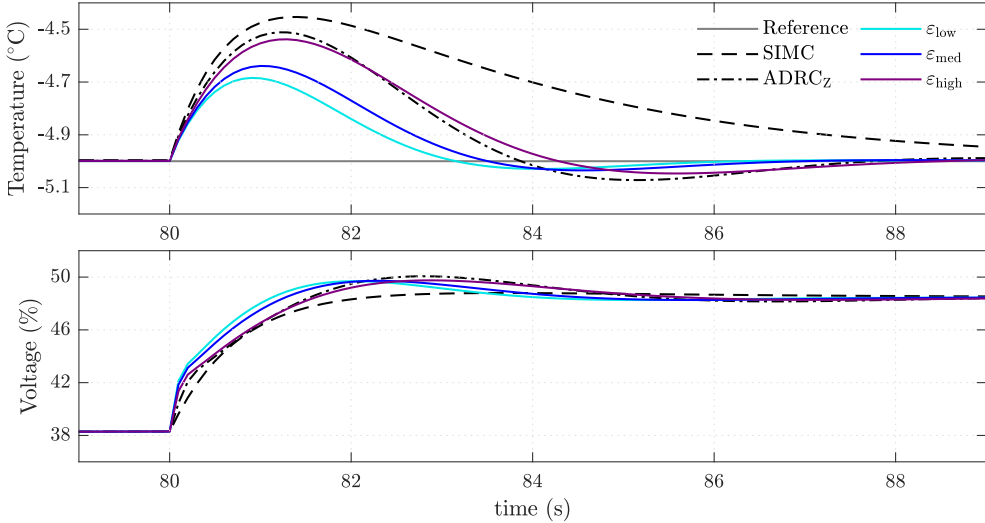
Figure 3.18: Disturbance rejection response of the Peltier thermoelectric module with the second-order LADRC tuned with the proposed rules. Comparison with the performance of the LADRC adjusted according to [32] (ADRC$_Z$) and the SIMC-PID.

Table 3.10: Performance indices obtained from the disturbance rejection response of the thermoelectric module controlled with PID and LADRC designs.

	M_S	M_T	ε	ITSE	TV	$t_{98\%}$
SIMC	1.590	1	2.353	2.190	10.807	11.9
ADRC$_Z$	1.545	1.455	2.607	0.679	13.984	6.9
ε_{low}	1.848	1.516	2.721	0.159	13.094	4.9
ε_{med}	1.749	1.425	2.511	0.258	13.126	5.6
ε_{high}	1.613	1.299	2.232	0.639	13.153	7.2

As expected, the ε_{low} controller produces the response with lower ITSE due to the relaxation in the robustness requirement. In addition, the total variation of control action and settling time are the lowest among the three proposals.

On the other hand, the ε_{med} controller improves the performance obtained with the ADRC$_Z$ parameters. The robustness index is slightly lower, indicating a more robust closed-loop system, and the ITSE value reflects that the output stabilises faster with less overshoot.
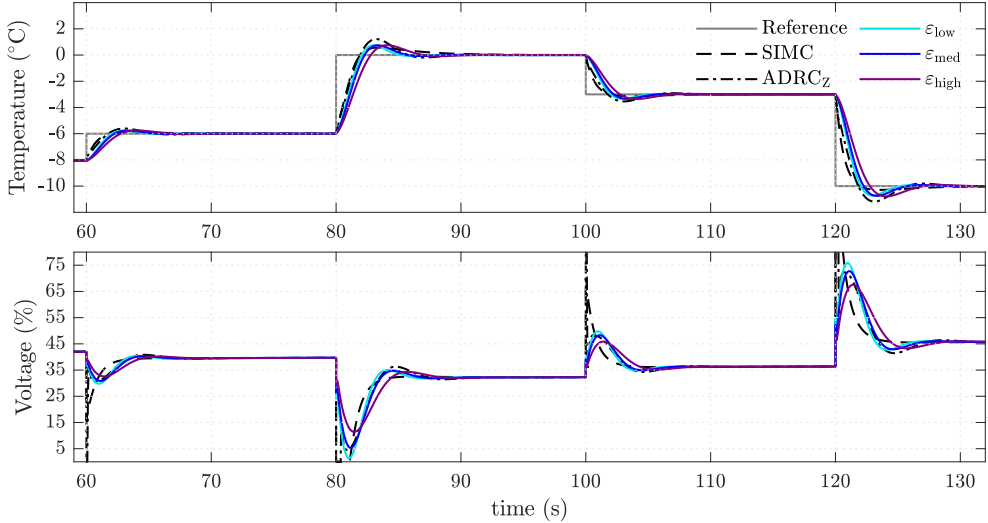
Figure 3.19: Setpoint following response of the Peltier thermoelectric module controlled by the second-order LADRC tuned with the proposed rules. Comparison with the performance of the LADRC adjusted according to [32] (ADRC$_Z$) and the SIMC-PID.

The most robust controller ε_{high} produces a time response similar to that of the ADRC$_Z$, but the ITSE and TV values are slightly lower. Notice that this controller also has a better disturbance rejection and robustness level than the PID tuned by the SIMC method.

The thermoelectric module can be operated at different temperatures. Due to the non-linearities, the transient temperature response shows a different behaviour depending on the magnitude and direction of the setpoint changes. An additional simulation was performed to test the LADRC alternatives under this scenario. Figure 3.19 presents the time response of the cold face temperature with different setpoints, and the indices from Table 3.11 quantify the performance.

The controllers tuned with the proposed rules guarantee the setpoint following, and the steady state is reached in less time than with the other designs. However, the ITSE values are above those calculated for the SIMC and the ADRC$_Z$ controllers. To clarify this behaviour, the output overshoot (in % of the setpoint change) has been included in Table 3.11. As shown, the SIMC method produces the lowest overshoot followed by the ε_{low}, ε_{med} and ε_{high} tunings. As expected, the overshoot in output increases for significant changes in the magnitude of the setpoint due to the non-linear nature of the system.

Table 3.11: Performance indices obtained from the setpoint following response of the thermoelectric module controlled with PID and LADRC designs.

Setpoint (°C)	SIMC	ADRC$_\mathrm{Z}$	ε_low	ε_med	$\varepsilon_\mathrm{high}$
	Integral of Time Weighted Squared Error				
−8 to −6	0.515	1.781	1.623	2.037	3.118
−6 to 0	10.230	19.467	14.784	18.247	27.329
0 to −3	0.922	3.508	3.346	4.214	6.464
−3 to −10	5.046	19.061	17.826	22.481	34.683
	Total Variation of control action				
−8 to −6	49.838	96.288	24.025	21.689	17.908
−6 to 0	32.597	58.728	61.296	54.530	44.258
0 to −3	34.185	92.800	28.584	25.894	21.442
−3 to −10	54.506	96.285	60.307	55.708	47.510
	Output overshoot				
−8 to −6	2.769	21.463	8.825	9.031	9.332
−6 to 0	7.309	22.777	9.931	10.016	10.191
0 to −3	2.294	20.546	8.845	8.926	9.357
−3 to −10	2.113	19.366	8.033	8.313	8.872
	Settling time				
−8 to −6	7.2	7.9	4.6	5.1	6.3
−6 to 0	8.9	8.1	4.7	5.2	6.4
0 to −3	6.9	7.8	4.6	5.1	6.3
−3 to −10	6.9	7.9	4.6	5.1	6.3

In Figure 3.19, it is also shown that the three design alternatives can lead to a lower variation of the control action in contrast with the abrupt change produced by the other controllers when the setpoint changes. This kind of peak may be damaging to the system. The corresponding TV indices from Table 3.11 reflect the above.

Finally, as in Example 2.6.1, the LADRC is tested when the thermoelectric module is operated in the cool zone ($\approx 4\,°\mathrm{C}$). In this case, random noise with variance $\sigma^2 = 0.005$ and sampling frequency of $100\,\mathrm{Hz}$ is added to the output to emulate a temperature measured in the range $T_c \pm 0.225\,°\mathrm{C}$.
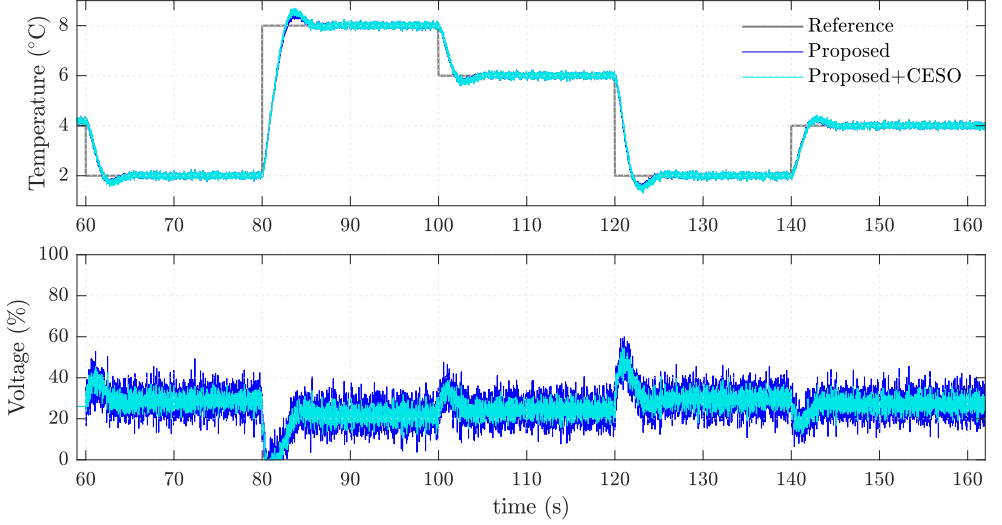
Figure 3.20: Setpoint following response of the Peltier thermoelectric module controlled by the second-order LADRC tuned with the ε_{low} set of parameters. Comparison with the performance of the LADRC implemented with the Cascade Extended State Observer (CESO).

Figure 3.20 shows the temperature changes in the cool face produced by the LADRC tuned with the ε_{low} set of parameters and the corresponding changes in the voltage. As can be seen, the LADRC achieves proper control in the cool zone despite the noisy output. However, the control signal exposes the inherent sensibility of the ESO to the high-frequency noise. The higher the observer bandwidth, the better the state estimation at the cost of higher noise impact in the control signal.

An alternative to reduce the noise influence in the input of a loop controlled with LADRC is to replace the standard ESO with a cascade configuration, as recently proposed in [94]. The idea of the Cascade Extended State Observer (CESO), in its most general configuration, is to implement a cascade structure of p levels, where each level is an ESO with associated observer bandwidth $\omega_{o,i}$, such that $\omega_{o,i-1} < \omega_{o,i} < \cdots < \omega_{o,p}$ $(i = 1, 2, \ldots, p)$.

According to [94], the number of levels and the observers bandwidths need to be tailored to achieve noise suppression without worsening the tracking accuracy. Therefore, consider that, for the thermoelectric module operating in the cool zone, the LADRC is now implemented replacing the standard ESO with a CESO of $p = 3$ levels. To clarify the LADRC with this CESO implementation, the associated block diagram is presented in Figure 3.21.
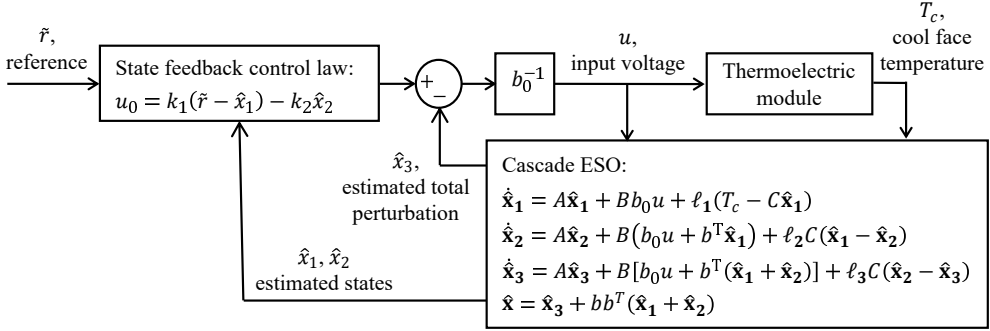
Figure 3.21: Block diagram for the control of the Peltier thermoelectric module using LADRC with the three-level CESO.

The observers bandwidths (rad/s) were chosen as $\omega_{o,1} = 20.905$, $\omega_{o,2} = 24.957$, and $\omega_{o,3} = 27.440$. Notice that these values correspond to the three observer bandwidths computed with the proposed rules. The remaining LADRC parameters were tuned as $b_0 = -2.885$ and $\omega_c = 2.744\,\text{rad/s}$ from the ε_{low} set.

The results of the LADRC with CESO are included in Figure 3.20. From a qualitative comparison with the performance produced by the ε_{low} controller, noise suppression exists in the control action and the setpoint following performance is preserved. That being the case, the LADRC with the three-level CESO was straightforwardly designed using the sets of parameters computed with the proposed rules, which points out that the proposed tuning method can be used as starting point for the design of the LADRC loop with the CESO.

Chapter 4

Modified Active Disturbance Rejection Predictive Control: a fixed-order state-space formulation for SISO systems

This chapter describes the Modified Active Disturbance Rejection Predictive Control (MADRPC): a discrete-time algorithm that merges the estimation-rejection capability of the ADRC with the receding horizon feature of the MPC. The first section introduces the approach together with its main highlights. The second section briefly describes the state-space MPC, and the third section presents the discrete-time formulation of LADRC as preliminaries to the fourth section, which introduces the proposed control architecture. The disturbance rejector and the modified predictive controller, the main comprising structures of the proposed loop, are also described in detail in the fourth section, together with the conditions for feasibility and nominal stability of the overall loop. Finally, the fifth section addresses the validation of the proposal through the control of linear benchmark systems. The performance validation is expanded to a non-linear benchmark with the control of a Continuous Stirred Tank Reactor (CSTR).

4.1   Introduction

This chapter presents a new control strategy that combines ADRC with state-space MPC and it aims at controlling systems where a precise mathematical model is not available. The proposed loop controls a system by applying a receding horizon strategy on an assumed plant of first-order plus integrator whose mismatch with the real process is compensated in the loop. The model mismatch, external perturbations, and assumed plant states are obtained by a third-order ESO, and the system constraints are directly considered in the optimisation problem. The proposed loop is implemented as a discrete-time algorithm with the following highlights.

- The estimation-rejection mechanism of the ADRC as an internal loop is maintained to enforce the real plant dynamics to behave like a first-order plus integrator modified plant. Consequently, the predictive control problem is solved based on a fixed discrete state-space model of second-order, despite the nature of the controlled system. This differs from the control formulations of MPC with state observation, in which a complete-order model still needs to be identified, and the ESO is used to estimate the model states and the state disturbance vector required for the computation of the predictive control law. Moreover, conditions for the feasibility of the optimisation problem and the nominal stability are given.

- The modelling requirements on the real plant are reduced to natural system characteristics such as static gain and apparent time constant due to the ADRC estimation-rejection mechanism. Therefore, the model-based feature of predictive control is relaxed, and the need for the detailed identification of the real system is eliminated.

- The constraints on the manipulated and controlled variables are directly taken into account by reformulating the constraints of the optimisation problem to incorporate the compensation term. The above addresses the challenging handling of constraints in the ADRC configurations and avoids that the manipulated variable acting on the system violates the desired constraint after the predictive control law is compensated in the loop.

- The proposed control strategy offers a closed-loop response that meets performance criteria and system constraints, which is also robust against model mismatch and general process variations encountered when controlling highly non-linear processes.

4.2   State-Space Model Predictive Control

Model Predictive Control refers to a set of advanced control methods in which the control action is computed based on predictions of the output behaviour, hence the importance of accurate modelling of the process to be controlled. [35]. The most commonly used models are the step response (in Dynamic Matrix Control, DMC), the transfer function (in GPC), and the discrete state-space realisation of order n

$$\mathbf{x}_{k+1} = A\mathbf{x}_k + Bu_k + \boldsymbol{\nu}_k$$
$$y_k = C\mathbf{x}_k, \tag{4.1}$$

where $\mathbf{x}_k \in \mathbb{R}^{n \times 1}$ is the state vector, $\boldsymbol{\nu} \in \mathbb{R}^{n \times 1}$ is a state disturbance vector, y is the controlled variable, u is the manipulated variable, and $A \in \mathbb{R}^{n \times n}$, $B \in \mathbb{R}^{n \times 1}$, and $C \in \mathbb{R}^{1 \times n}$ are the system matrices.

The MPC algorithm solves for each instant k an optimisation problem that minimises the cost function (4.2), along a prediction horizon p, subject to none, some or all of the constraints (4.3)-(4.5). Notation $y_{f,i|k}$ indicates that future output at instant $k + i$ is calculated based on conditions at instant k; The same holds for the reference trajectory $y_{r,i|k}$ and the rate of input $\Delta u_{i|k} = u_{i|k} - u_{i-1}$. It is always assumed that the control horizon c satisfies $c \leq p$ and that $\Delta u_{i|k} = 0$ for $i \geq c$.

The cost function (4.2) considers the quadratic forms of the tracking error $\|y_{r,i|k} - y_{f,i|k}\|_{\gamma}^2$ and the rate of manipulated variable $\|\Delta u_{i|k}\|_{\lambda}^2$ with scaling factors γ and λ, respectively, and subject to the variables constrained between their allowed lower and upper limits represented by the bar notations $\underline{w}$ and $\overline{w}$, correspondingly.

$$J = \sum_{i=1}^{p} \|y_{r,i|k} - y_{f,i|k}\|_{\gamma}^2 + \sum_{i=0}^{c-1} \|\Delta u_{i|k}\|_{\lambda}^2 \tag{4.2}$$

$$\underline{\Delta u} \leq \Delta u_{i|k} \leq \overline{\Delta u}, \qquad i = 0, \dots, c - 1, \tag{4.3}$$
$$\underline{u} \leq u_{i|k} \leq \overline{u}, \qquad i = 0, \dots, c - 1, \tag{4.4}$$
$$\underline{y} \leq y_{f,i|k} \leq \overline{y}, \qquad i = 1, \dots, p. \tag{4.5}$$

When the discrete state-space model (4.1) is used to formulate the predictive control problem, the objective function (4.2) can be written as (4.6) with the variables defined as (4.7)-(4.11).

$$J = \|\mathbf{y_r} - \mathbf{y_f}\|_\Gamma^2 + \|\mathbf{\Delta u}\|_\Lambda^2 \tag{4.6}$$

$$\mathbf{y_r} = \left[y_{r,1|k}, y_{r,2|k}, \ldots, y_{r,p|k} \right]^\top \tag{4.7}$$

$$\mathbf{y_f} = \left[y_{f,1|k}, y_{f,2|k}, \ldots, y_{f,p|k} \right]^\top \tag{4.8}$$

$$\mathbf{\Delta u} = \left[\Delta u_{0|k}, \Delta u_{1|k}, \ldots, \Delta u_{c-1|k} \right]^\top \tag{4.9}$$

$$\Gamma = \mathrm{diag}(\gamma) \in \mathbb{R}^{p \times p} \tag{4.10}$$

$$\Lambda = \mathrm{diag}(\lambda) \in \mathbb{R}^{c \times c} \tag{4.11}$$

In index (4.6), the deviation of p future outputs $\mathbf{y_f}$ from the reference trajectory $\mathbf{y_r}$ is penalised through the diagonal weighting matrix Γ. Likewise, penalisation of the actual and $c-1$ future control efforts $\mathbf{\Delta u}$ is introduced using the matrix Λ. The output predictions are computed based on the current state (or an estimation of it), the last applied input, and the unknown actual and future input changes according to

$$\mathbf{y_f} = \underbrace{P\mathbf{x}_k + VBu_{k-1} + \mathbf{w}_k + V\boldsymbol{\nu}_k}_{\mathbf{y_{free}}} + G\mathbf{\Delta u}, \tag{4.12}$$

where matrices $P \in \mathbb{R}^{p \times p}$, $V \in \mathbb{R}^{p \times 1}$, and $G \in \mathbb{R}^{p \times c}$ are defined as

$$P = \begin{bmatrix} CA \\ CA^2 \\ \vdots \\ CA^p \end{bmatrix}, \tag{4.13}$$

$$V = \begin{bmatrix} C \\ C(A+I) \\ \vdots \\ C(A^{p-1} + \cdots + A + I) \end{bmatrix}, \tag{4.14}$$

$$G = \begin{bmatrix} CB & \cdots & 0 \\ C(A+I)B & \cdots & 0 \\ \vdots & \ddots & \vdots \\ C(A^{p-1} + \cdots + A + I)B & \cdots & C(A^{p-c} + \cdots + A + I)B \end{bmatrix}. \quad (4.15)$$

In addition, the correction term $\mathbf{w}_k \in \mathbb{R}^{p \times 1}$ (4.16) and the state disturbance prediction model $\boldsymbol{\nu}_k \in \mathbb{R}^{p \times 1}$ (4.17) are included in (4.12) to provide offset-free control (OF-MPC) [95].

$$\mathbf{w}_k = \begin{bmatrix} w_{1|k} \\ w_{2|k} \\ \vdots \\ w_{p|k} \end{bmatrix} = (y_k - C\mathbf{x}_k) \begin{bmatrix} 1 \\ 1 \\ \vdots \\ 1 \end{bmatrix} \quad (4.16)$$

$$\boldsymbol{\nu}_k = \begin{bmatrix} \nu_{1|k} \\ \nu_{2|k} \\ \vdots \\ \nu_{p|k} \end{bmatrix} = (\mathbf{x}_k - A\mathbf{x}_{k-1} - Bu_{k-1}) \begin{bmatrix} 1 \\ 1 \\ \vdots \\ 1 \end{bmatrix} \quad (4.17)$$

When no constraints are imposed, the minimum of (4.6) can be directly calculated as the matrix product (4.18). However, when constraints are active, there is no explicit solution and the standard approach is to treat the new problem as a standard quadratic one which is easily handled by solvers like *quadprog* from Matlab or Mosek [96].

$$\boldsymbol{\Delta}\mathbf{u} = \left(G^\top \Gamma G + \Lambda\right)^{-1} G^\top \Gamma \left(\mathbf{y_r} - \mathbf{y_{free}}\right) \quad (4.18)$$

4.3 Discrete Linear Active Disturbance Rejection Control

It has been previously stated that the LADRC is a control algorithm based on the idea that a detailed process model is unnecessary to control it. What is more, in chapter 2, it was explained how LADRC relies on input-output information to estimate the existing mismatch between the real system and an assumed integrator-chain modified plant used to design a linear state feedback control law.

Until this point, the LADRC formulation was presented in the continuous time domain. However, its practical implementation requires the discretisation of its main comprising block: the LESO. According to [97], the current-observer configuration offers improvement in terms of estimation accuracy and closed-loop stability compared to the classical predictive-observer.

Let the extended state space model (2.32) of the second-order SISO system introduced in section 2.4 be recalled here for convenience as (4.19), and let $\hat{\mathbf{x}}_k = \begin{bmatrix} \hat{x}_{1,k}, \hat{x}_{2,k}, \hat{x}_{3,k} \end{bmatrix}^\top$ be its discrete-time estimated state vector.

$$
\begin{bmatrix} \dot{x}_1 \\ \dot{x}_2 \\ \dot{x}_3 \end{bmatrix} = \underbrace{\begin{bmatrix} 0 & 1 & 0 \\ 0 & 0 & 1 \\ 0 & 0 & 0 \end{bmatrix}}_{A} \begin{bmatrix} x_1 \\ x_2 \\ x_3 \end{bmatrix} + \underbrace{\begin{bmatrix} 0 \\ b_0 \\ 0 \end{bmatrix}}_{B} u + \underbrace{\begin{bmatrix} 0 \\ 0 \\ 1 \end{bmatrix}}_{E} h \qquad (4.19)
$$

$$
y = \underbrace{\begin{bmatrix} 1 & 0 & 0 \end{bmatrix}}_{C} \begin{bmatrix} x_1 \\ x_2 \\ x_3 \end{bmatrix}
$$

In the current-ESO implementation, the estimation of the state vector and the previous instant control input are used to compute (4.20), which is a prediction of $\hat{\mathbf{x}}_k$. Next, the current estimation of the state vector is obtained according to (4.21) where y_k has been incorporated to update the current estimation with the most recent output measurement.

$$
\mathbf{z}_k = A_d \hat{\mathbf{x}}_{k-1} + B_d u_{k-1} \qquad (4.20)
$$
$$
\hat{\mathbf{x}}_k = \mathbf{z}_k + \boldsymbol{\ell_d} \left(y_k - C_d \mathbf{z}_k \right) \qquad (4.21)
$$

In equations (4.20)-(4.21) A_d, B_d, and C_d are the discrete versions of matrices A, B, and C from (4.19) obtained through zero-order hold discretisation with sampling time t_s. This is,

$$
A_d = \begin{bmatrix} 1 & t_s & \dfrac{t_s^2}{2} \\ 0 & 1 & t_s \\ 0 & 0 & 1 \end{bmatrix} \quad B_d = \begin{bmatrix} \dfrac{b_0 t_s^2}{2} \\ b_0 t_s \\ 0 \end{bmatrix} \quad C_d = \begin{bmatrix} 1 & 0 & 0 \end{bmatrix}. \qquad (4.22)
$$

Notice that substituting (4.20) in (4.21), the general update equation (4.23) for the current-ESO is obtained with $\boldsymbol{\ell_d} = [\ell_{d1}, \ell_{d2}, \ell_{d3}]^\top$ as the vector of observer gains.

$$\hat{\mathbf{x}}_k = (A_d - \boldsymbol{\ell_d} C_d A_d) \hat{\mathbf{x}}_{k-1} + (B_d - \boldsymbol{\ell_d} C_d B_d) u_{k-1} + \boldsymbol{\ell_d} y_k \tag{4.23}$$

Similarly to the continuous time ESO, $\boldsymbol{\ell_d}$ can be computed by equating the observer characteristic equation with the desired characteristic equation for the estimation error such that

$$|zI - (A_d - \boldsymbol{\ell_d} C_d A_d)| = (z - z_d)^3. \tag{4.24}$$

Therefore, if the three observer poles are located in the same position inside the unit circle [22], $z_d = \exp(-\omega_o t_s)$, the corresponding observer gains are given by (4.25)-(4.27), with ω_o denoting the observer bandwidth.

$$\ell_{d1} = 1 - \exp(-3\omega_o t_s) \tag{4.25}$$

$$\ell_{d2} = \frac{3}{2t_s} \left[\exp(-\omega_o t_s) - 1\right]^2 \left[\exp(-\omega_o t_s) + 1\right] \tag{4.26}$$

$$\ell_{d3} = \frac{1}{t_s^2} \left[1 - \exp(-\omega_o t_s)\right]^3 \tag{4.27}$$

Finally, the estimated state vector is used in (2.7) and (2.9) to obtain the discrete control law

$$u_k = \frac{\omega_c^2 \left[y_{r,k} - \hat{x}_{1,k}\right] - 2\omega_c \hat{x}_{2,k} - \hat{x}_{3,k}}{b_0}. \tag{4.28}$$

In this sense, for each instant, $\hat{x}_{3,k} \approx f$, and the total perturbation is cancelled out from the system dynamics allowing the closed-loop response to be governed by the proportional gains dependent on the controller bandwidth ω_c.

4.4 Constrained control loop with active disturbance rejection and output predictions

In the previous sections, OF-MPC and LADRC were briefly described. Let the following comments about both algorithms be the introduction to this section.

On the one hand, if a proper model is available, OF-MPC becomes a robust algorithm with an optimal control action that directly satisfies the process constraints according to the optimisation problem feasibility. However, this model-based feature plays against the system performance when a significant model mismatch arises, for example, in processes with challenging dynamics and different operating points.

On the other hand, LADRC locates itself almost on the opposite side of the spectrum by keeping the information required from modelling to a minimum and relying on its rejector mechanism to perform the disturbance rejection. This configuration offers proper control because it actively combines the non-modelled dynamics in an estimated state without needing further knowledge. Nevertheless, additional characteristic information about the system behaviour may be beneficial, resulting in an assumed plant different from the conventional integrator-chain form. Moreover, some important control aspects, such as the system constraints, mainly handled by limiters inside the loop, could be incorporated into a more dedicated control law.

To take advantage of the unique benefits of the aforementioned control schemes whilst enhancing each other, the control architecture of Figure 4.1 that merges the LADRC disturbance rejector and the receding horizon feature of MPC is proposed. Three main structures are identified.

① The system, which corresponds to the real process to be controlled and whose precise mathematical model is unknown.

② The disturbance rejector representing the active disturbance rejection component of the loop. It includes a current-ESO intended for correctly estimating system states and total perturbation and the sum-gain configuration that uses the estimated total perturbation to compensate for the existing differences between the real and modified plants. A general first order plus integrator model is assumed as the modified plant. Therefore, the disturbance rejector is designed to overcome the possible structural and parametric mismatch and the external disturbances acting on the loop.
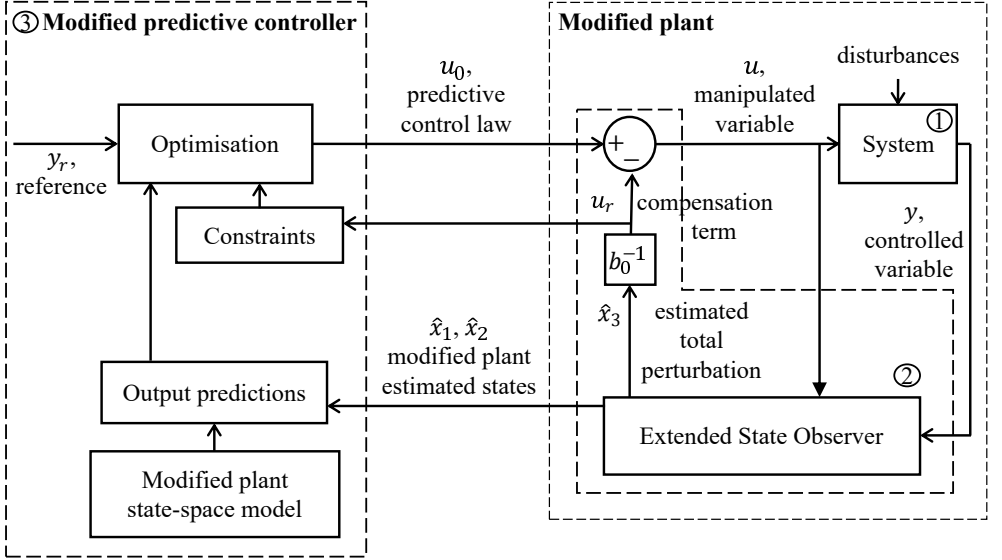
Figure 4.1: Proposed control architecture. The system dynamics ① is enforced by the disturbance rejector ② into a first order plus integrator plant (modified plant) governed by a modified predictive controller ③.

③ The modified predictive controller designed to provide a control law for the disturbance-free modified plant. This control law results from a constrained optimisation process where a cost function involving the tracking error and changes in input is minimised. By incorporating the predictive control algorithm into the loop, the receding horizon characteristic of this advanced control method is exploited in the servo-regulatory operation, and constraints are directly considered.

4.4.1 The disturbance rejector

Let the first order plus integrator model (4.29) represent the dynamics of the assumed modified plant into which the disturbance rejector is expected to enforce the real dynamics. The controlled variable is y, the manipulated variable is u, K represents the static gain, T is the apparent time constant, and f is the total perturbation.

$$\ddot{y} = -\frac{1}{T}\dot{y} + \frac{K}{T}u + f \tag{4.29}$$

Selection of a first-order plus integrator system as the modified plant mainly offers the following advantages: it constitutes a fixed mathematical representation of known order for the process to be controlled with a lower complexity involved in the identification of its parameters; It models the integral effect commonly present in industrial processes and approximate other types of dominant dynamics through a term with a time constant. Compared to the conventional chain-integrator form of LADRC, the additional dynamic information represented by the time constant enhances the estimation ability of the observer and increases the ESO efficiency [98].

A continuous state-space realisation of (4.29) is

$$
\begin{bmatrix} \dot{x}_1 \\ \dot{x}_2 \end{bmatrix} = \begin{bmatrix} 0 & 1 \\ 0 & -1/T \end{bmatrix} \begin{bmatrix} x_1 \\ x_2 \end{bmatrix} + \begin{bmatrix} 0 \\ K/T \end{bmatrix} u + \begin{bmatrix} 0 \\ 1 \end{bmatrix} f
$$

$$
y = \begin{bmatrix} 1 & 0 \end{bmatrix} \begin{bmatrix} x_1 \\ x_2 \end{bmatrix}. \tag{4.30}
$$

If zero-order hold discretisation with sampling time t_s is used on (4.30), the discrete state-space model obtained is (4.31) with $a = \exp(-t_s/T)$, and $b_0 = K/T$ as the nominal value of critical gain.

$$
\begin{bmatrix} x_{1,k+1} \\ x_{2,k+1} \end{bmatrix} = \begin{bmatrix} 1 & T(1-a) \\ 0 & a \end{bmatrix} \begin{bmatrix} x_{1,k} \\ x_{2,k} \end{bmatrix}
$$

$$
+ b_0 \begin{bmatrix} Tt_s - T^2(1-a) \\ T(1-a) \end{bmatrix} u_k + \begin{bmatrix} Tt_s - T^2(1-a) \\ T(1-a) \end{bmatrix} f_k \tag{4.31}
$$

$$
y_k = \begin{bmatrix} 1 & 0 \end{bmatrix} \begin{bmatrix} x_{1,k} \\ x_{2,k} \end{bmatrix}
$$

Assigning f_k to a third state, the extended state vector $\hat{\mathbf{x}}_k = [\hat{x}_{1,k}, \hat{x}_{2,k}, \hat{x}_{3,k}]^\top$ is updated according to (4.32), where the observer matrices A_o, B_o, and C_o are defined as (4.33)-(4.35).

$$
\hat{\mathbf{x}}_k = (A_o - \boldsymbol{\ell}_o C_o A_o) \hat{\mathbf{x}}_{k-1} + (B_o - \boldsymbol{\ell}_o C_o B_o) u_{k-1} + \boldsymbol{\ell}_o y_k \tag{4.32}
$$

$$A_o = \begin{bmatrix} 1 & T(1-a) & Tt_s - T^2(1-a) \\ 0 & a & T(1-a) \\ 0 & 0 & 1 \end{bmatrix} \tag{4.33}$$

$$B_o = b_0 \begin{bmatrix} Tt_s - T^2(1-a) \\ T(1-a) \\ 0 \end{bmatrix} \tag{4.34}$$

$$C_o = \begin{bmatrix} 1 & 0 & 0 \end{bmatrix} \tag{4.35}$$

Likewise, the observer gain vector $\boldsymbol{\ell}_o$ is determined based on the desired location of the observer poles inside the unit circle [22]. By following the same approach used in the design of conventional current-ESO, the corresponding gains are (4.36)-(4.38), with $z_o = \exp\left(-\omega_o t_s\right)$.

$$\ell_{o1} = 1 - \frac{z_o^3}{a} \tag{4.36}$$

$$\ell_{o2} = \frac{2a - \ell_{o1}(1+a) + \ell_{o3}\left[T^2(1-a) - aTt_s\right] - 3z_o^2 + 1}{T(1-a)} \tag{4.37}$$

$$\ell_{o3} = \frac{(1-z_o)^3}{Tt_s(1-a)} \tag{4.38}$$

Consequently, the design of the current-ESO in the proposed loop is dependent on the apparent time constant of modified plant T, the sampling time t_s, and the desired bandwidth ω_o.

Let the control action affecting the system to be

$$u_k = u_{0,k} - \frac{\hat{x}_{3,k}}{b_0} \tag{4.39}$$

with $u_{0,k}$ denoting the value for instant k of a control action computed by a predictive control algorithm. If (4.39) is substituted in (4.31), it follows that

$$\begin{aligned} \begin{bmatrix} x_{1,k+1} \\ x_{2,k+1} \end{bmatrix} &= \begin{bmatrix} 1 & T(1-a) \\ 0 & a \end{bmatrix} \begin{bmatrix} x_{1,k} \\ x_{2,k} \end{bmatrix} + b_0 \begin{bmatrix} Tt_s - T^2(1-a) \\ T(1-a) \end{bmatrix} u_{0,k} \\ &- b_0 \begin{bmatrix} Tt_s - T^2(1-a) \\ T(1-a) \end{bmatrix} \frac{\hat{x}_{3,k}}{b_0} + \begin{bmatrix} Tt_s - T^2(1-a) \\ T(1-a) \end{bmatrix} f_k, \end{aligned} \tag{4.40}$$

and, under the premise that $\hat{x}_{3,k} \approx f_k$, the last two terms on the right hand side of (4.40) cancel out, resulting in the disturbance-free modified plant

$$
\begin{aligned}
\begin{bmatrix} x_{1,k+1} \\ x_{2,k+1} \end{bmatrix} &= \underbrace{\begin{bmatrix} 1 & T(1-a) \\ 0 & a \end{bmatrix}}_{A} \underbrace{\begin{bmatrix} x_{1,k} \\ x_{2,k} \end{bmatrix}}_{\mathbf{x}_k} + \underbrace{b_0 \begin{bmatrix} Tt_s - T^2(1-a) \\ T(1-a) \end{bmatrix}}_{B} u_{0,k} \\
y_k &= \underbrace{\begin{bmatrix} 1 & 0 \end{bmatrix}}_{C} \begin{bmatrix} x_{1,k} \\ x_{2,k} \end{bmatrix}
\end{aligned}
\tag{4.41}
$$

Up to this point, it has been shown how the current-ESO estimates the modified plant states and the total perturbation. When the latter is used to compute the manipulated variable acting on the system, the model mismatch and external disturbances are compensated, allowing the discrete-time realisation of the first order plus integrator system from (4.41) to be used as a prediction model to obtain the predictive control law $u_{0,k}$.

4.4.2 The modified predictive controller

Let J_M be the quadratic cost index associated to the optimisation problem of the modified predictive controller such that

$$
J_M = \sum_{i=1}^{p} \|y_{r,i|k} - y_{f,i|k}\|_\gamma^2 + \sum_{i=0}^{c-1} \|\Delta u_{0,i|k}\|_\lambda^2,
\tag{4.42}
$$

which results in

$$
J_M = \|\mathbf{y_r} - \mathbf{y_f}\|_\Gamma^2 + \|\mathbf{\Delta u_0}\|_\Lambda^2,
\tag{4.43}
$$

with $\mathbf{\Delta u_0} = \begin{bmatrix} \Delta u_{0,0|k}, \Delta u_{0,1|k}, \ldots, \Delta u_{0,c-1|k} \end{bmatrix}^\top$ and $\mathbf{y_f}$ as the vector of p output predictions

$$
\mathbf{y_f} = \underbrace{P\mathbf{x}_k + VBu_{0,k-1}}_{\mathbf{y_{free}}} + G\mathbf{\Delta u_0}.
\tag{4.44}
$$

Notice that neither the correction term nor the disturbance prediction model are included in (4.44). This is because the observer is providing the current state vector $\mathbf{x}_k$ of the modified plant and consequently, matrices $P \in \mathbb{R}^{p \times 2}$, $V \in \mathbb{R}^{p \times 1}$, and $G \in \mathbb{R}^{p \times c}$ are computed using the discrete state-space realisation from (4.41).

In order to incorporate the real system constraints in the optimisation problem related to (4.42), the following formulation based on the classical Quadratic Dynamic Matrix Control (QDMC) approach is proposed.

Firstly, consider the constraints on the manipulated variable specified as (4.4). For instant k, it holds that

$$u_{0|k} \leq \overline{u}. \tag{4.45}$$

From (4.39), $u_{0|k}$ can be rewritten as $u_{0|k} = \left[\Delta u_{0,0|k} + u_{0,k-1}\right] - (1/b_0)\hat{x}_{3,k}$ and substituting the latter in (4.45) leads to

$$\Delta u_{0,0|k} \leq \overline{u} - u_{0,k-1} + \frac{\hat{x}_{3,k}}{b_0}. \tag{4.46}$$

Thus, the upper limit constraint on input magnitude $\overline{u}$ has been used to determine the corresponding upper limit constraint for the first decision variable of (4.43), $\Delta u_{0,0|k}$, taking into account the contribution of the disturbance rejector to the manipulated variable $u_{0|k}$.

The above procedure is expanded along the control horizon as follows.

$$
\begin{aligned}
\Delta u_{0,1|k} + \Delta u_{0,0|k} &\leq & \overline{u} - u_{0,k-1} + \frac{\hat{x}_{3,1|k}}{b_0} \\
\Delta u_{0,2|k} + \Delta u_{0,1|k} + \Delta u_{0,0|k} &\leq & \overline{u} - u_{0,k-1} + \frac{\hat{x}_{3,2|k}}{b_0} \\
&\vdots& \\
\Delta u_{0,c-1|k} + \cdots + \Delta u_{0,0|k} &\leq & \overline{u} - u_{0,k-1} + \frac{\hat{x}_{3,c-1|k}}{b_0}
\end{aligned}
\tag{4.47}
$$

From equation (4.47) is evident that future values of the estimated total perturbation are required, which are not available. Still, it can be assumed that $\hat{x}_{3,k}$ remains constant over the control horizon, and its value is updated by the ESO each time the optimisation problem needs to be solved. This is, with $\hat{x}_{3,k} = \hat{x}_{3,1|k} = \cdots = \hat{x}_{3,c-1|k}$, (4.47) turns into (4.48).

$$
\begin{aligned}
\Delta u_{0,1|k} + \Delta u_{0,0|k} &\leq \overline{u} - u_{0,k-1} + \frac{\hat{x}_{3,k}}{b_0} \\
\Delta u_{0,2|k} + \Delta u_{0,1|k} + \Delta u_{0,0|k} &\leq \overline{u} - u_{0,k-1} + \frac{\hat{x}_{3,k}}{b_0} \\
&\vdots \\
\Delta u_{0,c-1|k} + \cdots + \Delta u_{0,0|k} &\leq \overline{u} - u_{0,k-1} + \frac{\hat{x}_{3,k}}{b_0}.
\end{aligned}
\tag{4.48}
$$

A similar development is done to determine the lower limit constraints on $\mathbf{\Delta u_0}$ as a function of the allowed lower limit $\underline{u}$ for the manipulated variable such that

$$
\begin{aligned}
-\Delta u_{0,1|k} - \Delta u_{0,0|k} &\leq -\underline{u} + u_{0,k-1} - \frac{\hat{x}_{3,k}}{b_0} \\
-\Delta u_{0,2|k} - \Delta u_{0,1|k} - \Delta u_{0,0|k} &\leq -\underline{u} + u_{0,k-1} - \frac{\hat{x}_{3,k}}{b_0} \\
&\vdots \\
-\Delta u_{0,c-1|k} - \cdots - \Delta u_{0,0|k} &\leq -\underline{u} + u_{0,k-1} - \frac{\hat{x}_{3,k}}{b_0}.
\end{aligned}
\tag{4.49}
$$

Gathering inequalities from (4.48) and (4.49) results in the matrix form

$$
\underbrace{\begin{bmatrix} I_L \\ -I_L \end{bmatrix}}_{A_u} \underbrace{\begin{bmatrix} \Delta u_{0,0|k} \\ \Delta u_{0,1|k} \\ \vdots \\ \Delta u_{0,c-1|k} \end{bmatrix}}_{\mathbf{\Delta u_0}} \leq \underbrace{\begin{bmatrix} \overline{\mathbf{u}} \\ -\underline{\mathbf{u}} \end{bmatrix} - \begin{bmatrix} \mathbf{1} \\ -\mathbf{1} \end{bmatrix} u_{0,k-1} + \begin{bmatrix} \mathbf{1} \\ -\mathbf{1} \end{bmatrix} u_{r,k}}_{\mathbf{b_u}},
\tag{4.50}
$$

where $I_L \in \mathbb{R}^{c \times c}$ is an all-ones lower triangular matrix; $\overline{\mathbf{u}} \in \mathbb{R}^{c \times 1}$ and $\underline{\mathbf{u}} \in \mathbb{R}^{c \times 1}$ are vectors of repeated elements $\overline{u}$ and $\underline{u}$, respectively; $\mathbf{1} \in \mathbb{R}^{c \times 1}$ is an all-ones vector, and $u_{r,k} = (1/b_0)\hat{x}_{3,k}$ represents the contribution of the disturbance rejector to the manipulated variable.

Attention is now drawn to handling constraints on the rate of change of input given in the form of (4.3). Proceeding as before, for instant k, it holds that

$$
u_{0|k} - u_{k-1} \leq \overline{\Delta u}.
\tag{4.51}
$$

Using (4.39) in (4.51), it follows that

$$\left[\Delta u_{0,0|k} + u_{0,k-1} - \frac{\hat{x}_{3,k}}{b_0} \right] - u_{k-1} \leq \overline{\Delta u}. \tag{4.52}$$

Furthermore, $u_{k-1} = u_{0,k-1} - (1/b_0)\hat{x}_{3,k-1}$. Thus, substituting the latter in (4.52) and reorganising terms

$$
\begin{aligned}
\Delta u_{0,0|k} &\leq \overline{\Delta u} - u_{0,k-1} + u_{0,k-1} + \frac{\hat{x}_{3,k}}{b_0} - \frac{\hat{x}_{3,k-1}}{b_0} \\
\Delta u_{0,0|k} &\leq \overline{\Delta u} + \frac{\hat{x}_{3,k}}{b_0} - \frac{\hat{x}_{3,k-1}}{b_0} \\
\Delta u_{0,0|k} &\leq \overline{\Delta u} + \frac{\Delta \hat{x}_{3,k}}{b_0}.
\end{aligned}
\tag{4.53}
$$

Likewise, for future control moves, constraints become

$$
\begin{aligned}
\Delta u_{0,1|k} &\leq \overline{\Delta u} + \frac{\Delta \hat{x}_{3,1|k}}{b_0} \\
\Delta u_{0,2|k} &\leq \overline{\Delta u} + \frac{\Delta \hat{x}_{3,2|k}}{b_0} \\
&\vdots \\
\Delta u_{0,c-1|k} &\leq \overline{\Delta u} + \frac{\Delta \hat{x}_{3,c-1|k}}{b_0}.
\end{aligned}
\tag{4.54}
$$

However, as it was assumed that $x_{3,k}$ remains constant along the control horizon, $\Delta \hat{x}_{3,1|k} = \Delta \hat{x}_{3,2|k} = \cdots = \Delta \hat{x}_{3,c-1|k} = 0$, indicating that the disturbance rejector contribution to the manipulated variable is only affecting the constraint on the first decision variable $\Delta u_{0,0|k}$.

Constraints for the lower bound of $\mathbf{\Delta u_0}$ based on $\underline{\Delta u}$ are derived similarly to that was performed for the upper bound. Therefore, constraints on the rate of change of input are incorporated into the optimisation problem through the matrix form (4.55), with I as the identity matrix, $\underline{\mathbf{\Delta u}} \in \mathbb{R}^{(c-1)\times 1}$ and $\overline{\mathbf{\Delta u}} \in \mathbb{R}^{(c-1)\times 1}$ as vectors of repeated elements $\underline{\Delta u}$ and $\overline{\Delta u}$ respectively, and $\mathbf{0} \in \mathbb{R}^{(c-1)\times 1}$ as the zero vector.

$$
\underbrace{\left[\begin{array}{c} I \\ -I \end{array}\right]}_{A_{\Delta u}} \underbrace{\left[\begin{array}{c} \Delta u_{0,0|k} \\ \Delta u_{0,1|k} \\ \vdots \\ \Delta u_{0,c-1|k} \end{array}\right]}_{\mathbf{\Delta u_0}} \leq \underbrace{\left[\begin{array}{c} \overline{\Delta u} \\ \overline{\mathbf{\Delta u}} \\ -\underline{\Delta u} \\ -\underline{\mathbf{\Delta u}} \end{array}\right]}_{\mathbf{b_{\Delta u}}} + \left[\begin{array}{c} u_{r,k} \\ \mathbf{0} \\ -u_{r,k} \\ \mathbf{0} \end{array}\right]
\tag{4.55}
$$

Lastly, constraints (4.5) on output are introduced into the optimisation problem in the same fashion as the classical QDMC approach because the prediction vector (4.44) is dependent only on the current state vector $\mathbf{x}_k$ and past input $u_{0,k-1}$. Hence, defining $\overline{\mathbf{y}} \in \mathbb{R}^{p \times 1}$ and $\underline{\mathbf{y}} \in \mathbb{R}^{p \times 1}$ as vectors of p elements $\overline{y}$ and $\underline{y}$, respectively

$$
\underbrace{\left[\begin{array}{c} G \\ -G \end{array}\right]}_{A_y} \leq \underbrace{\left[\begin{array}{c} \Delta u_{0,0|k} \\ \Delta u_{0,1|k} \\ \vdots \\ \Delta u_{0,c-1|k} \end{array}\right]}_{\mathbf{\Delta u_0}} \leq \underbrace{\left[\begin{array}{c} \overline{\mathbf{y}} - \mathbf{y_{free}} \\ -\underline{\mathbf{y}} + \mathbf{y_{free}} \end{array}\right]}_{\mathbf{b_y}}.
\tag{4.56}
$$

In summary, the optimisation problem for the modified predictive controller of the proposed loop is stated as (4.57), with constraints matrices defined in (4.50), (4.55), and (4.56).

$$
\min_{\mathbf{\Delta u_0}} \left\{ \|\mathbf{y_r} - \mathbf{y_f}\|_{\Gamma}^2 + \|\mathbf{\Delta u_0}\|_{\Lambda}^2 \right\}
$$
$$
\text{s.t.} \quad \left[\begin{array}{c} A_{\Delta u} \\ A_u \\ A_y \end{array}\right] \mathbf{\Delta u_0} \leq \left[\begin{array}{c} \mathbf{b_{\Delta u}} \\ \mathbf{b_u} \\ \mathbf{b_y} \end{array}\right]
\tag{4.57}
$$

4.4.3 Stability and feasibility

The closed-loop stability of the control architecture from Figure 4.1 can be addressed based on the separation principle under which the disturbance rejector and the modified predictive controller constitute two cascaded systems that can be independently designed. If the stability of these two comprising structures is assured, then the closed-loop stability is guaranteed [99].

Let $\mathbf{e}_k = \mathbf{x}_k - \hat{\mathbf{x}}_k$ be the discrete-time estimation error such that

$$\mathbf{e}_{k+1} = (A_o - \boldsymbol{\ell}_o C_o A_o)\,\mathbf{e}_k. \tag{4.58}$$

Thus, the discrete ESO from the disturbance rejector is stable if the gains vector $\boldsymbol{\ell}_o$ is designed by assuring that matrix $A_o - \boldsymbol{\ell}_o C_o A_o$, representing the observation error dynamics, has all its eigenvalues inside the unit circle. This principle holds in gains (4.36)-(4.38), which are only dependent on the sampling time and the observer bandwidth. A detailed presentation of the Input-to-State stability properties of the discrete ESO is presented in [47]. Notice that the ESO comprising the proposed loop can be seen as a particular realisation of the discrete generalised ESO addressed in [47] in which the matrices are always defined by (4.33)-(4.35).

On the other hand, the asymptotic stability of the modified predictive controller can be assured by including a terminal constraint in the optimisation problem (4.57) [100], such that the predicted outputs are forced to converge to the desired reference at the end of the prediction horizon and to remain at this setpoint for several desired additional instants. For this purpose, consider the vector of additional n future outputs over the prediction horizon p

$$\tilde{\mathbf{y}}_{\mathbf{f}} = \left[y_{f,p+1|k}, y_{f,p+2|k}, \dots, y_{f,p+n|k} \right]^\top, \tag{4.59}$$

which is recursively computed as

$$\tilde{\mathbf{y}}_{\mathbf{f}} = \underbrace{\widetilde{P}\hat{\mathbf{x}}_k + \widetilde{V}Bu_{0,k-1}}_{\tilde{\mathbf{y}}_{\mathbf{free}}} + \widetilde{G}\boldsymbol{\Delta}\mathbf{u_0}, \tag{4.60}$$

with $\widetilde{P} \in \mathbb{R}^{n \times 2}$, $\widetilde{V} \in \mathbb{R}^{n \times 1}$, and $\widetilde{G} \in \mathbb{R}^{n \times c}$ also obtained by using the assumed disturbance-free state space (4.41) in expressions (4.13)-(4.15). Using this formulation, (4.57) is additionally subject to the equality constraint

$$\widetilde{G}\boldsymbol{\Delta}\mathbf{u_0} = \tilde{\mathbf{y}}_{\mathbf{r}} - \tilde{\mathbf{y}}_{\mathbf{f}}, \tag{4.61}$$

where $\tilde{\mathbf{y}}_{\mathbf{r}} \in \mathbb{R}^{n \times 1}$ is a vector with all its components equal to the desired reference value $y_{r,p|k}$.

The approach in which a constraint in the form of (4.61) is included in the MPC optimisation problem is usually referred to in the literature as the Constrained Receding-Horizon Predictive Control (CRHPC) [101], and if (4.61) holds, then $y_{f,p+i|k} = y_{r,p|k}$ for $i = 1, 2, \ldots, n$, which brings a monotonically convergent cost and guarantees the closed-loop stability for finite horizons [102]. The number of additional n output predictions is related to the system order. Therefore, for the modified predictive controller, $n = 2$ always as the prediction model is a fixed second-order state space realisation resembling the assumed modified plant of first-order plus integrator. Moreover, imposing this constraint on the optimisation problem leads to the condition that the control horizon must be selected according to $c \geq n = 2$, setting a lower value for the tuning of c in the proposed constrained loop.

Notice that (4.57) can also include constraints on the rate of change of the manipulated variable, its magnitude, and the output. Imposing restrictions on predictive control can lead to feasibility problems. That is, the optimiser may not find a solution that allows the system to be within the predefined conditions [96]. A common approach from an engineering perspective is to soften the output constraints since they are often desired rather than required in contrast to the hard input constraints associated with physical limitations of the system, such as actuator ranges and slew rates [35]. Therefore, to deal with infeasibility, the cost index (4.42) of the modified predictive controller can be reformulated as (4.62), where the last two terms are included to penalise with the weight ε_1 the slack variable ξ_1 that quantifies the violation of the output constraint, and through the weight ε_2 the slack variable ξ_2 associated to the equality constraint [103].

$$J_M = \sum_{i=1}^{p} \|y_{r,i|k} - y_{f,i|k}\|_\gamma^2 + \sum_{i=0}^{c-1} \|\Delta u_{0,i|k}\|_\lambda^2 + \sum_{i=1}^{p} \|\xi_{1,i|k}\|_{\varepsilon_1}^2 + \sum_{i=p+1}^{p+2} \|\xi_{2,i|k}\|_{\varepsilon_2}^2 \quad (4.62)$$

With the introduction of the slack variables plus the stability constraint, the optimisation problem (4.57) is transformed in (4.63), where $\mathbf{0}$ and $\mathbf{1}$ are all-zeros and all-ones matrices of proper dimensions, respectively. The above reformulation guarantees that the modified predictive controller computes a feasible control law for the modified plant, leading future outputs to stabilise at a computed reference.

$$\min_{\mathbf{\Delta u_0}, \xi} \left\{ \|\mathbf{y_r} - \mathbf{y_f}\|_\Gamma^2 + \|\mathbf{\Delta u_0}\|_\Lambda^2 + p\varepsilon_1\xi_1^2 + 2\varepsilon_2\xi_2^2 \right\}$$

$$\text{s.t.} \quad \begin{bmatrix} A_{\Delta u} & \mathbf{0} & 0 \\ A_u & \mathbf{0} & 0 \\ A_y & -\mathbf{1} & 0 \\ \mathbf{0} & -\mathbf{1} & 0 \\ \mathbf{0} & 0 & 1 \end{bmatrix} \begin{bmatrix} \mathbf{\Delta u_0} \\ \xi_1 \\ \xi_2 \end{bmatrix} \leq \begin{bmatrix} \mathbf{b_{\Delta u}} \\ \mathbf{b_u} \\ \mathbf{b_y} \\ 0 \\ \infty \end{bmatrix} \tag{4.63}$$

$$\begin{bmatrix} \widetilde{G} & \mathbf{0} & -\mathbf{1} \end{bmatrix} \begin{bmatrix} \mathbf{\Delta u_0} \\ \xi_1 \\ \xi_2 \end{bmatrix} = \tilde{\mathbf{y}}_\mathbf{r} - \tilde{\mathbf{y}}_\mathbf{f}$$

Finally, it is worth clarifying that the proposed control architecture can be implemented using the formulations (4.57) or (4.63) for the modified predictive controller. If (4.57) is the one selected, then the design relies on the proper selection of the tuning parameters to obtain a closed-loop stable response according to the desired performance, as is the standard approach in the classical MPC and ADRC implementations. On the contrary, the optimisation problem (4.63) addresses the stability and feasibility challenges, which let the designer test a broader range of combinations of the predictive controller parameters, given that the disturbance rejector adequately compensates for the total perturbation.

4.5 Validation examples for the Modified Active Disturbance Rejection Predictive Control

In this section, the control architecture of Figure 4.1, referred to hereafter as Modified Active Disturbance Rejection Predictive Control (MADRPC), is validated with different types of systems. The modified predictive controller operates under the formulation (4.63) in all cases. This is, the designs seek the desired performance while assuring feasibility and closed-loop stability.

Guide 4.5.1 lists general guidelines for selecting MADRPC parameters based on the practical experience reported in the literature on MPC tuning and discrete controllers implementation. This guideline proved adequate for the MADRPC loop design associated with the examples presented in this section.

Before addressing the validation examples, let the following be remarked.

The proposed control (Figure 4.1) combines the disturbance rejector mechanism of the ADRC with the receding horizon strategy of the MPC. This integration is done mainly by preserving the internal loop of the classical ADRC structure that includes the ESO together with the sum-gain configuration, through which the real dynamics is enforced to behave like the modified plant, and by redefining the optimisation problem constraints in the form of (4.50), (4.55), and (4.56) to directly incorporate the compensation term $u_{r,k}$. Consequently, the discrepancies between the real system and the assumed plant and the external disturbances are actively compensated in the loop relaxing the predictive controller modelling requirement to a second-order general integral system. Also, the inclusion of the compensation term in the constraints definition aims at maintaining the controlled and manipulated variables, and rate of change of manipulated variable within the real constraints bands. The name MADRPC is motivated by these characteristics.

From a practical application perspective, the MADRPC offers advantages in the control of systems with no identified model because the only modelling required information is the approximation of the control gain b_0 and the desired apparent time constant T. As a result, the future outputs (4.44) are obtained with a fixed second-order state-space prediction model, and the size of the optimisation problem (4.57) (or (4.63)) is only dependent on the horizon lengths. Additionally, the constraints on the controlled variable, the manipulated variable, and the rate of change of the manipulated variable can be included, and the closed-loop stability can be imposed through constraint (4.61).

The MADRPC design requires selecting the classical parameters involved in the MPC design (prediction horizon, control horizon, cost function weightings) besides the ESO bandwidth ω_0 and the modified plant parameters (b_0, T). These parameters should be appropriately selected for the trade-off among the performance requirements.

Guide 4.5.1: Guide for the implementation of the Modified Active Disturbance Rejection Predictive Control (MADRPC).

① *For the system.*

   a) Identify the process constraints on the manipulated and controlled variables, and decide on the desired closed-loop performance coherently with the constraints imposed.

   b) Select the sampling time, t_s.

From open-loop step response [104]	Shannon-Nyquist theorem	From closed-loop desired bandwidth [105]
$\dfrac{t_{95\%}}{15} \leq t_s \leq \dfrac{t_{95\%}}{4}$	$t_s \approx \dfrac{\pi}{\omega_{\max}}$	$\dfrac{1}{40 f_B} \leq t_s \leq \dfrac{1}{20 f_B}$

② *For the disturbance rejector* (4.32)-(4.39).

   c) Select the observer bandwidth ω_o according to the sampling frequency $\omega_s = \dfrac{2\pi}{t_s}$ [106].

$$\frac{\omega_s}{10} \leq \omega_o \leq \frac{\omega_s}{5}$$

   d) Determine the modified plant apparent time constant T and the nominal value of the critical gain b_0, for example, using the suggestions from Guide 2.5.1.

③ *For the modified predictive controller* (4.57) *or* (4.63)* *and* (4.50), (4.55)-(4.56).

   e) Select the control horizon c and prediction horizon p [107]. The latter may be computed considering t_0 as the open-loop (for self-regulatory plants) or desired closed-loop settling time.

Control horizon	Prediction horizon
$1\ (2^*) \leq c \leq p$	$p \approx \dfrac{t_o}{t_s}$

   f) Select the weighting factors γ, λ. For example, for a fixed γ, small values for λ lead to faster responses but with possible overshoot. Conversely, if λ increases, smoother inputs are achieved at the cost of a slower disturbance rejection response.

The parameters computed following the above steps should be considered as starting values and retuned iteratively according to the expected performance.

4.5.1 A classical problem of motion control

It is desired to control the shaft angle of a direct-current motor modelled as
(4.64) [108] with parametric uncertainty for the static gain $\underline{K} = 2.5 - 20\,\%$,
and for the apparent time constant $\overline{T} = 0.9 + 20\,\%$ s.

$$G_M(s) = \frac{2.5}{s\,(0.9s + 1)} \tag{4.64}$$

Regarding Figure 4.1 and following Guide 4.5.1, consider.

① *For the system.*

  a) The goal is to produce shaft movements of about 15° with no overshoot
     in approximately two seconds by manipulating the input voltage in the
     range $|u| \leq 24\,\text{V}$ and allowing input changes of $|\Delta u| \leq 5\,\text{V}$.

  b) A sampling time of $t_s = 0.05\,\text{s}$ is chosen.

② *For the disturbance rejector.*

  c) As the loop sampling frequency is $\omega_s = 2\pi/t_s = 40\pi$ rad/s, the ESO
     bandwidth $\omega_o = 20\,\text{rad/s}$ is selected.

  d) From (4.64) the nominal static gain is $K = 2.5$ and the nominal apparent
     time constant is $T = 0.9$. Therefore, $b_0 \approx K/T \approx 2.8$.

③ *For the modified predictive controller.*

  e) The control horizon is set as $c = 9$ and the prediction horizon is selected
     as $p = 40$.

  f) The error weighting and the input rate weighting are set as $\gamma = 1$ and
     $\lambda = 0.1$, respectively. The slack variables weights are set to $\varepsilon_1 = \varepsilon_2 = 10^5$.

As shown in Figure 4.2, the MADRPC drives the shaft angle to the desired
setpoints satisfying the performance requirements and constraints. Further-
more, in the presence of model uncertainty $(\underline{K}, \overline{T})$, the disturbance rejector
compensates for the total perturbation allowing the MADRPC to produce an
output response very similar to that of the nominal case (K, T). The same is
not valid if the system is controlled by a constrained OF-MPC designed with
the same parameters and full access to the states; the closed-loop response
deteriorates because an overshoot appears.
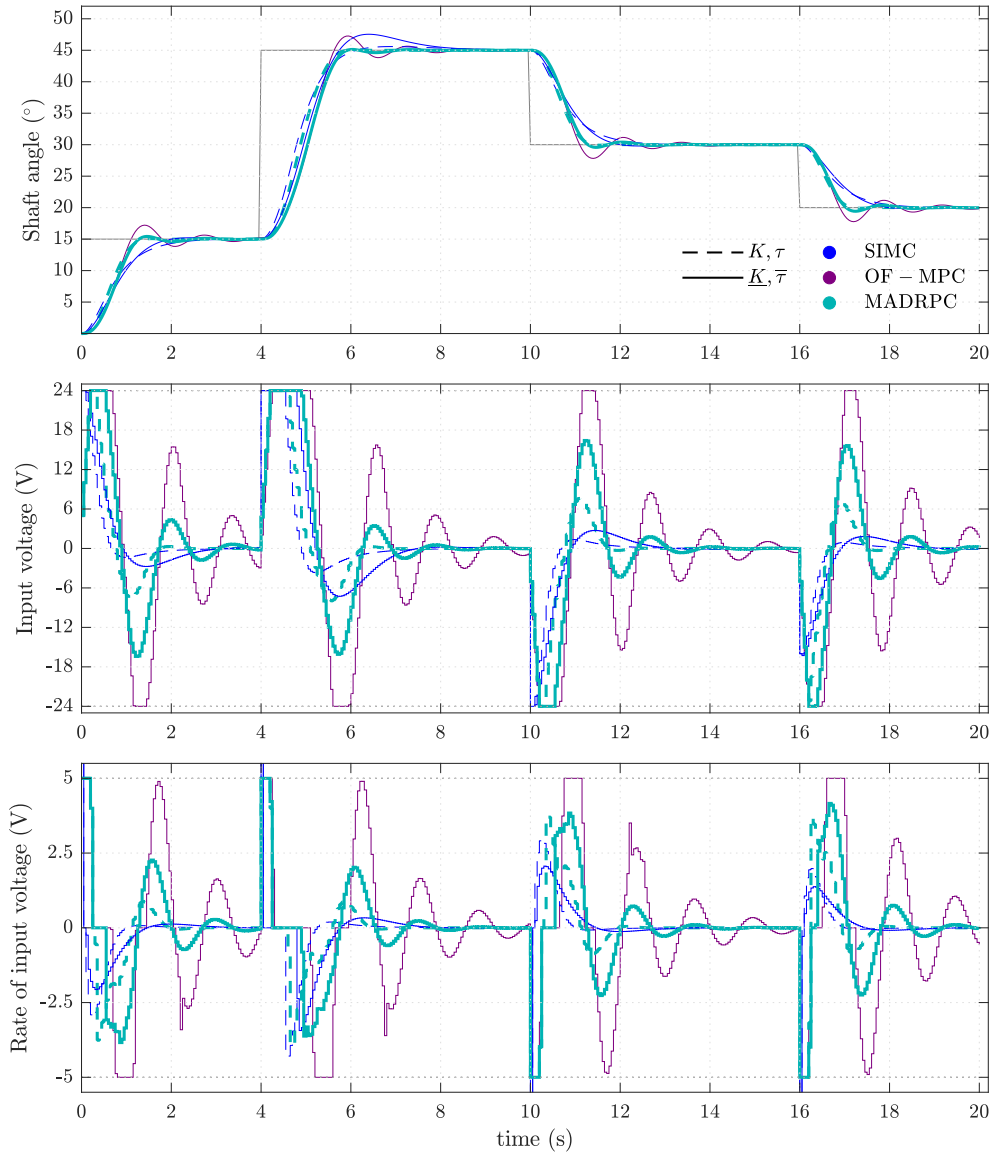
Figure 4.2: Closed-loop response of the DC motor subject to PID-control, OF-MPC and MADRPC for different reference steps. Nominal system: K, τ; System with uncertainty: $\underline{K}, \overline{\tau}$. System constraints: $|u| \leq 24\,\text{V}$, $|\Delta u| \leq 5\,\text{V}$, $y_{f,p+i|k} = y_{r,p|k}$, $i \in [1, 2]$.

A PID controller tuned with the SIMC rules [86] ($K_c = 1.6, T_i = 1, T_d = 0.9$) has been included in Figure 4.2 as an alternative comparative controller. The MADRPC outperforms the PID in the presence of uncertainty while keeping the changes in input within the desired limits.

The functioning of the disturbance rejector can be validated through the step response of the modified plant [25]. This is, an input step applied instead of the governing control input u_0 in Figure 4.1 should produce the open-loop response of the modified plant, which is expected to asymptotically change at a constant rate following the step response of the assumed first-order plus integrator system.

The above behaviour is presented in Figure 4.3 for different values of the ESO bandwidth. Notice that $\hat{x}_1$ and $\hat{x}_2$ are the estimations of the output and its rate of change for each instant. Consequently, $\hat{x}_1$ starts to follow a quadratic growth and then exhibits a linear tendency after approximately two times the time constant. This monotonic response drives $\hat{x}_2$ to a steady-state equal the desired static gain.

On the other hand, the disturbance rejector accuracy is dependent on the ESO bandwidth. For a low observer bandwidth, for example, $\omega_o = 5 \, \text{rad/s}$, there is a slight difference between the desired first-order plus integrator response and the modified plant output. However, as the bandwidth increases, the modified plant responses tend to be indistinguishable.
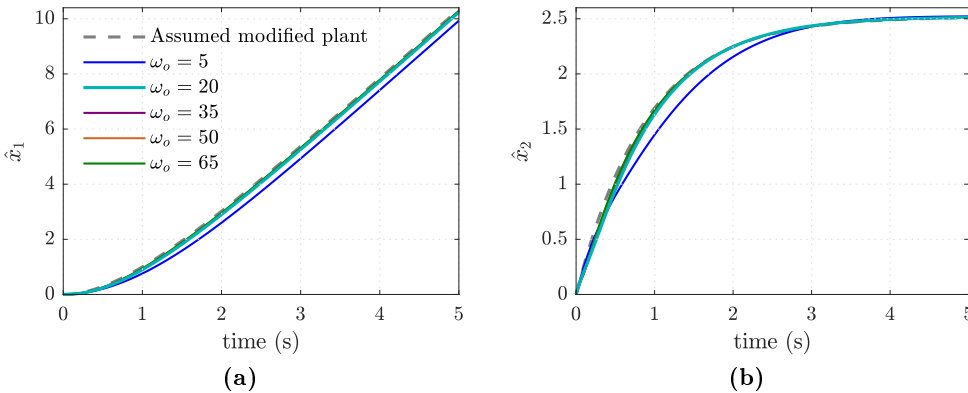
Figure 4.3: Open-loop response of the modified plant of DC motor with uncertainty $\underline{K}, \overline{\tau}$ under variations in the ESO bandwidth compared to the desired modified plant (first-order plus integrator). (a) Estimated output. (b) estimated rate of output.

With the selected ESO bandwidth $\omega_o = 20\,\mathrm{rad/s}$, the MADRPC actively compensates for the real system uncertainty and the closed-loop output satisfies the desired performance.

Finally, Figure 4.4 shows that the MADRPC satisfies the closed-loop stability constraint imposed while controlling the uncertain DC motor. Figure 4.4a plots the sequences of $p + n$ future outputs computed at three different instants in the time window $t \in [0, 4]$. The predicted outputs settle at the desired setpoint of 15 (°) at the end of the prediction horizon of $p = 40$ instants and remain unchanged for the imposed $n = 2$ consequent instants. Moreover, the cost function exhibits a monotonic convergence to zero along the said time window, as seen in Figure 4.4b.

(a)

(b)
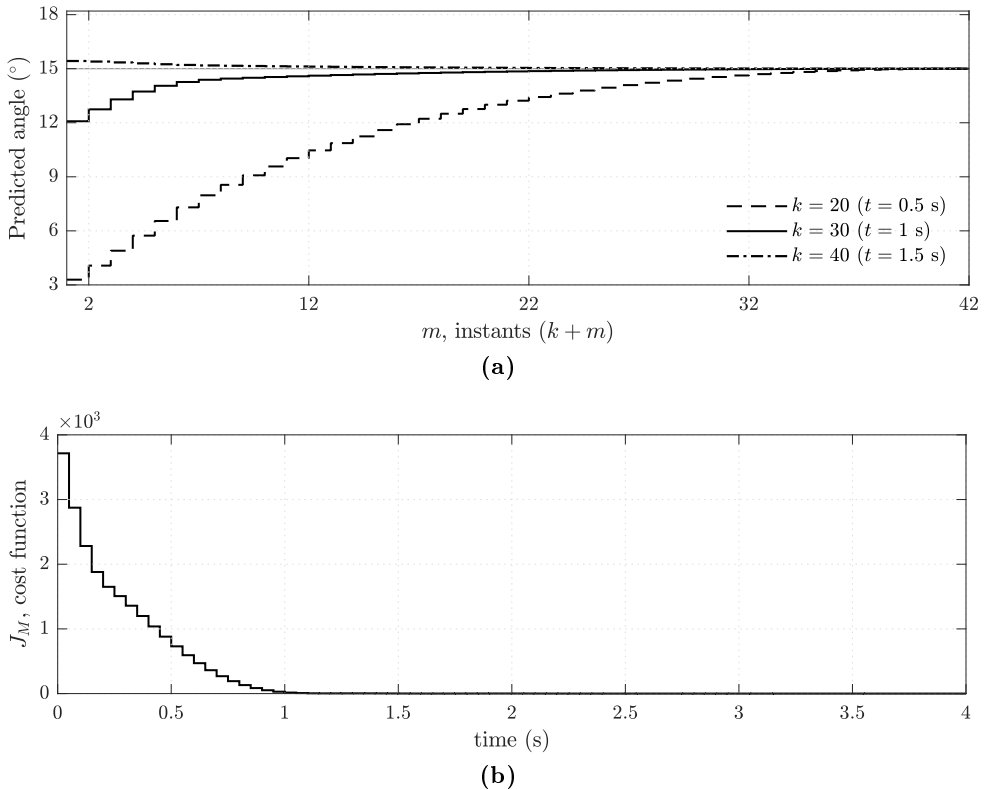
Figure 4.4: Closed-loop stability validation of the MADRPC when controlling the DC motor. (a). Equality constraint satisfaction $y_{f,p+i|k} = y_{r,p|k}$, $i \in [1,2]$. (b). Monotonic convergence of the cost function.

4.5.2   Linear benchmark systems: high-order systems

The proposed MADRPC is now validated through the control of two different linear examples resembling varied dynamics of common interest in literature, which are considered benchmark systems [109]. These are a fourth-order system with its pole spacing dependent on a parameter and a third-order plant with a right-hand plane zero or non-minimum phase behaviour. The case-study systems are listed in Table 4.1, together with the nominal values adopted here.

Table 4.1: Linear benchmark systems and its nominal values

Benchmark system	Parameters
$G_F(s) = \dfrac{K}{(s+1)\,(\beta s+1)\,(\beta^2 s+1)\,(\beta^3 s+1)}$	$K = 1 \; \beta = 0.5$
$G_R(s) = \dfrac{1 - \beta s}{(\tau s + 1)^3}$	$\beta = 1 \; \tau = 1$

The OF-MPC and the LADRC were also designed to control the aforementioned benchmark systems for comparison purposes. The OF-MPC, when no model mismatch exists, is considered a performance reference scheme because a complete, i.e. full-state model was used for its design. Therefore, the first validation objective was to test the MADRPC capability to emulate the OF-MPC performance with the advantage of a relaxation in the modelling requirement because of the disturbance rejector. On the other hand, it was expected that the MADRPC would outperform the conventional LADRC due to the modified prediction control law acting on the assumed modified plant.

As the MADRPC and LADRC algorithms uses their corresponding ESO configurations, a current-type Luenberger observer of complete order was used to estimate the OF-MPC model states required for output predictions. In order to assign the same observer bandwidth of the ESO from MADRPC, the OF-MPC observer poles s_i were designed by solving the characteristic equation (4.65), which is only dependent on the system order n and desired bandwidth ω_o, and then mapped as z_i to the unit circle through (4.66) with sampling time t_s. The remaining parameters of the OF-MPC and the tuning parameters of the MADRPC were selected as discussed in Guide 4.5.1.

$$\left(\frac{s}{\omega_o}\right)^{2n} = (-1)^{n+1} \tag{4.65}$$

$$z_i = \exp\left(s_i t_s\right) \tag{4.66}$$

In the case of the LADRC, Guide 3.5.1 was used to compute the main three design variables b_0, ω_c, and ω_o under the premise that the benchmark systems from Table 4.1 are adequately approximated by first-order plus dead time models, and thus, the parameters computed with the proposed rules offers a stable closed-loop response with a medium robustness specification. The approximation was performed following the method of moments reported in [83], according to which the parameters of the first-order plus delay model are given by

$$\begin{cases} K = G(0) \\[2mm] T_{ar} = -\dfrac{G'(0)}{G(0)} \\[2mm] T^2 = \dfrac{G''(0)}{G(0)} - T_{ar}^2 \\[2mm] l = T_{ar} - T \end{cases} \tag{4.67}$$

In (4.67), the first and second-order derivatives of the model transfer function $G(s)$ at $s = 0$ are used to compute the FOPDT approximation parameters. This methods gives similar results to those obtained, for example, using the half-rule [86].

Table 4.2 gathers the FOPDT approximations of the benchmark systems from Table 4.1 computed with (4.67).

Table 4.2: Linear benchmark systems and its approximated FOPDT model

Benchmark system	FOPDT model
$G_F(s) = \dfrac{1}{(s+1)\,(0.5s+1)\,(0.25s+1)\,(0.125s+1)}$	$\dfrac{1}{1.152s+1}e^{-0.723s}$
$G_R(s) = \dfrac{1-s}{(s+1)^3}$	$\dfrac{1}{1.414s+1}e^{-2.586s}$

The design parameters for the three control algorithms are reported in Table 4.3. It is worth clarifying that these control parameters were tuned considering that the main goal in servo operation, when possible, is to drive the system to the desired setpoint with an overshoot OS $\leq 2\,\%$ and a settling time $t_{98\%}$ lower than the natural pace of the system while constraints are satisfied. For this purpose, the control loops were designed with sampling time $t_s = 0.1\,\mathrm{s}$.

Table 4.3: Parameters for the control of the linear benchmark systems from Table 4.1. p, prediction horizon; c, control horizon; γ, weighting for error; λ, weighting for input rate; b_0, nominal critical gain; T, apparent time constant ω_o, ESO bandwidth; ω_c, controller bandwidth.

	$G_F(s)$			$G_R(s)$		
	LADRC	OF-MPC	MADRPC	LADRC	OF-MPC	MADRPC
p	-	50	50	-	85	85
c	-	10	5	-	20	20
γ	-	0.2	1	-	0.08	0.001
λ	-	1	0.1	-	1	5.5
b_0	25.68	-	2.4	10.37	-	4.5
T	-	-	1	-	-	1.62
ω_o	23.20	5	5	9.6	12	12
ω_c	2.32	-	-	0.96	-	-
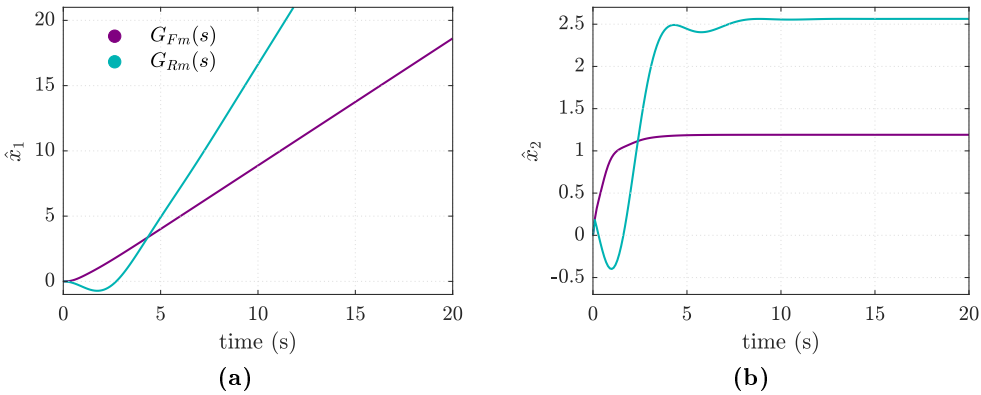
Figure 4.5: Open-loop response of the modified plants $G_{Fm}(s)$ and $G_{Rm}(s)$ of the nominal linear benchmark systems from Table 4.1. (a) Estimated output. (b) estimated rate of output.

As mentioned in subsection 4.5.1, the open-loop response of the modified plant is an indicator of the ESO convergence and the MADRPC disturbance rejector capability to enforce the real plant to behave like the assumed dynamics. Therefore, a unit step input was applied to the modified plants corresponding to the nominal linear benchmark systems from Table 4.1.

As can be seen in Figure 4.5a, the output of each modified plant resembles the desired dynamics of a first-order plus integrator model with the constant rate of change plotted in Figure 4.5b. The above shows that the disturbance rejector compensates for the ignored high-order dynamics; thus, the modified predictive controller can be designed to govern the assumed process.

Two scenarios were considered for validation. In the first one, the real plants to be controlled correspond to the nominal systems, and in the second one, the nominal parameters of each benchmark process were varied to test the designed control algorithms against uncertainty. Moreover, a step-type input disturbance was added to the manipulated variable in both scenarios at an instant when the output had reached the steady-state.

Quantification of performance was done through the indices reported in Table 4.4. The settling time $t_{98\%}$, percentage of overshoot OS (or absolute value of undershoot |US| in case of $G_R(s)$), and total variation of control action TV_s were computed for servo operation. In contrast, the percentage of maximum deviation MD, ITAE, and total variation TV_d were calculated in regulatory operation.

The closed-loop responses of system $G_F(s)$ when controlled by LADRC, OF-MPC, and MADRPC are presented in Figure 4.6. The MADRPC algorithm meets the required setpoint tracking performance and satisfy the constraints similarly to the OF-MPC. However, notice that in the first scenario, the OF-MPC has no model mismatch and complete state estimation. In contrast, the MADRPC manages to control the process assuming a fixed state-space realisation computed based on the values of the nominal critical gain and the apparent time constant. The MADRPC overcome the non-modelled dynamics and drives the output to the reference in a similar settling time to OF-MPC and with an overshoot within the desired band. Besides, the MADRPC reaches the setpoint in half of the time than the conventional LADRC.

During the second scenario, where the model mismatch is introduced, the OF-MPC holds the tracking performance at the cost of an increase in the total variation of the input, which is also reflected in the disturbance rejection response.

Table 4.4: Performance indexes for the control of the linear benchmark systems from Table 4.1. The uncertainties $\overline{a}(b\%)$ and $\underline{a}(b\%)$ indicate that the parameter a was increased or decreased by b % of its nominal value, respectively.

Uncertainty	Controller	$G_F(s)$					
		$t_{98\%}$ (s)	OS (%)	TV_s	MD (%)	ITAE	TV_d
none	LADRC	6.4	8.2	1.25	46.13	3.30	1.32
	OF-MPC	3.2	0	0.91	27.86	0.68	1.70
	MADRPC	2.9	0.8	1.04	26.64	0.68	2.82
$\underline{\beta}(20\,\%)$	LADRC	6.3	5.1	1.09	43.22	2.49	1.14
	OF-MPC	3.4	0.5	2.35	25.24	0.74	4.20
	MADRPC	2.9	1.2	0.90	24.02	0.49	2.11
Uncertainty	Controller	$G_R(s)$					
		$t_{98\%}$ (s)	|US|	TV_s	MD (%)	ITAE	TV_d
none	LADRC	12.6	0.03	0.92	74.03	28.49	1.22
	OF-MPC	5.3	0.16	2.08	48.54	3.61	6.25
	MADRPC	7.7	0.05	1.23	69.95	13.43	1.71
$\overline{\beta}(20\,\%)$ $\underline{\tau}(2\,\%)$	LADRC	12.1	0.05	0.92	78.89	28.58	1.30
	OF-MPC	5.7	0.35	8.93	95.18	3.78	30.16
	MADRPC	9.4	0.08	1.28	79.85	14.50	2.10

Although the maximum deviations from the desired reference produced by the MADRPC are comparable with those produced for the OF-MPC, about 25 %, the MADRPC returns the output to the steady state in less time and with a smoother variation in the control signal than the OF-MPC as reflected in the ITAE index. The disturbance rejection capability of the MADRPC also outperforms that of the LADRC.

On the other hand, Figure 4.7 shows the closed-loop responses of system $G_R(s)$. In this case, the non-minimum zero produces an inverse response in the output. The OF-MPC leads the controlled variable to the reference in a time that results lower than the open-loop settling time of the process, even when there is a model mismatch. The MADRPC satisfies the desired overshoot, but the output is about 2 s slower than the response produced by the OF-MPC, although the MADRPC loop settles 5 s faster than LADRC in the nominal case.
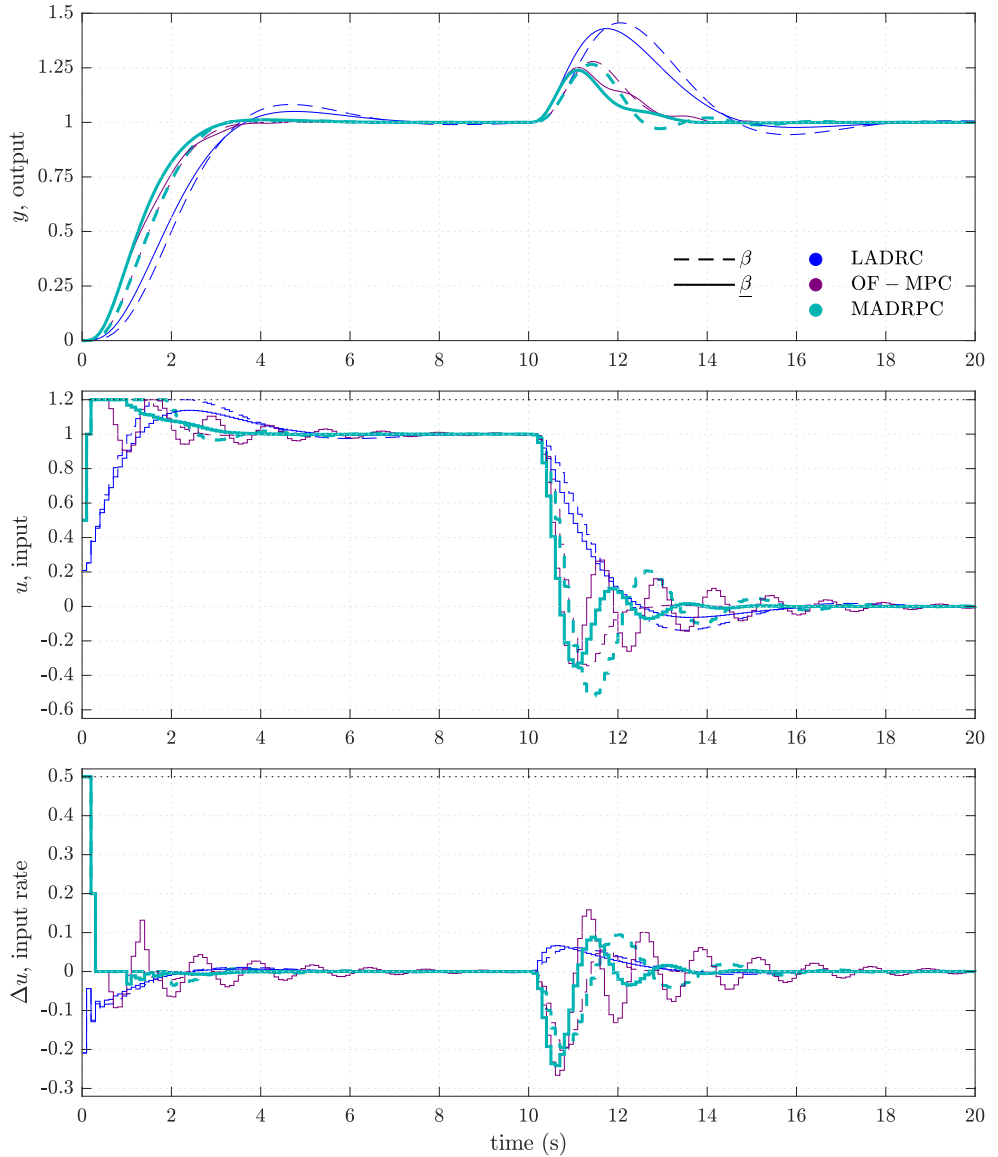
Figure 4.6: Closed-loop response of the linear benchmark system $G_F(s)$ subject to LADRC, OF-MPC, and MADRPC when the desired reference is set to one and a step-type input disturbance is applied to the system at steady-state. System constraints: $|u| \leq 1.2$; $|\Delta u| \leq 0.5$; $y \leq 1.5$, $y_{f,p+i|k} = y_{r,p|k}$, $i \in [1,n]$.
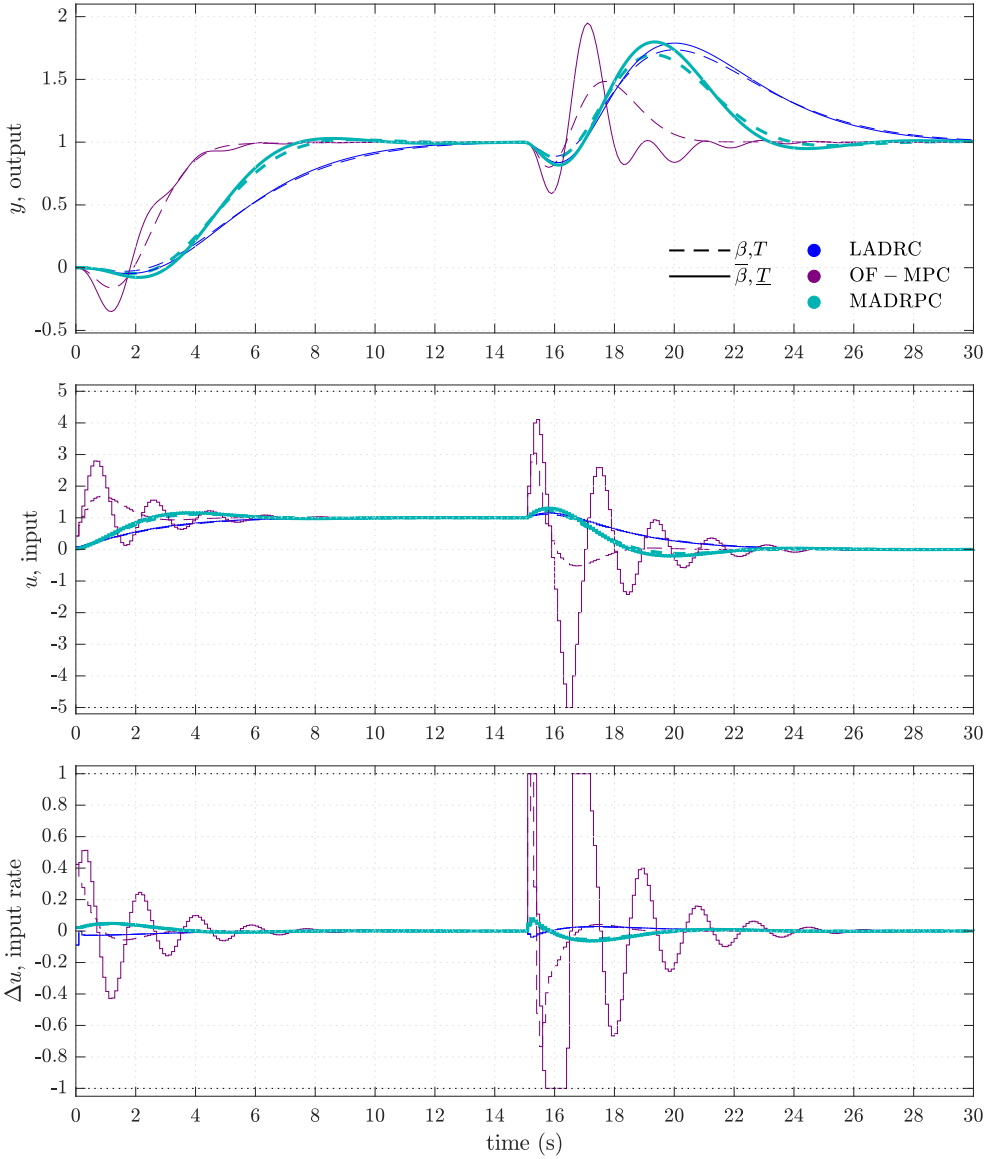
Figure 4.7: Closed-loop response of the linear benchmark system $G_R(s)$ subject to LADRC, OF-MPC, and MADRPC when the desired reference is set to one and a step-type input disturbance is applied to the system at steady-state. System constraints: $|u| \leq 5$; $|\Delta u| \leq 1$; $y \leq 2$, $y_{f,p+i|k} = y_{r,p|k}$, $i \in [1, n]$.

The complete model information used within the OF-MPC aids this algorithm in the disturbance rejection performance resulting in lower deviations and ITAE indexes than those produced by the MADRPC and LADRC schemes in the absence of uncertainty. However, the MADRPC and LADRC offer a higher level of robustness in contrast to OF-MPC, which, for the model mismatch introduced, produces oscillations in the manipulated variable that worsen the inverse response and deteriorate both the servo and regulatory operation. The MADRPC offers better setpoint following and disturbance rejection than conventional LADRC, with the advantage that all constraints are directly taken into account in the computation of the control law.

4.5.3 Control of a nonlinear benchmark system: The Continuous Stirred Tank Reactor

The functioning of the Continuous Stirred Tank Reactor (CSTR) was introduced in section 2.6. The CSTR is considered a benchmark system in process control because it constitutes a vital unit operation, particularly in the chemical industry [110], and, as it was explained previously, according to the formulation of the mass and energy balance equations, the concentration and temperature of the reactor can be controlled through the flow rates or the jacket temperature. In the following, these two scenarios are analysed to validate the proposed MADRPC algorithm. Additionally, the closed-loop performance is compared to OF-MPC and LADRC schemes.

Control of the reactor concentration

As first case, let the differential equations (2.65)-(2.67) be rewritten as (4.68)-(4.69) [111]. In this configuration, the controlled variable is the concentration of reactant A, C_a, and the manipulated variable is the coolant flow rate, F_j. The steady-state solution of the non-linear equations for a specific value of F_j leads to the operating points of the system. For example, with a coolant flow rate $F_j = 103 \, \text{L/min}$, the concentration and temperature of reactor are, correspondingly, $C_{as} = 0.09 \, \text{mol/L}$ and $T_{ss} = 438.77 \, \text{K}$, which indicates states of high conversion and high release of energy. Description of variables and their corresponding nominal values for this example are listed in Table 4.5.

$$\dot{C}_a = \frac{F}{V}\left(C_{a0} - C_a\right) - k_0 C_a \exp\left(-\frac{E}{RT_s}\right) \tag{4.68}$$

$$\dot{T}_s = \frac{F}{V}\left(T_0 - T_s\right) + \frac{\Delta H}{\rho c_p} k_0 C_a \exp\left(-\frac{E}{RT_s}\right)$$

$$+ F_j \frac{\rho_j c_j}{\rho c_p V}\left[1 - \exp\left(-\frac{UA}{F_j \rho c_p}\right)\right]\left(T_j - T_s\right) \tag{4.69}$$

Table 4.5: Parameters for the control of the CSTR concentration (subsection 4.5.3) [111], [112].

Variable	Value	Units	Description
V	100	L	Reactor volume
k_0	7.2×10^{10}	min^{-1}	Reaction rate constant
E/R	1×10^4	K	Activation energy term
ΔH	2×10^5	Cal/mol	Heat of reaction
UA	7×10^5	Cal/(min K)	Heat transfer term
ρ, ρ_j	1×10^3	g/L	Liquids densities
c_p, c_j	1	Cal/(g K)	Heat capacities
F	100	L/min	Inlet flow rate
C_{a0}	1	mol/L	Feed concentration
T_0	350	K	Feed temperature
T_j	350	K	Coolant temperature

Around the selected operating point, the system is open-loop stable, as shown in Figure 4.8. However, the non-linear dynamics become more evident as the coolant flow rate varies from its nominal value producing an under-damped-type response in the reactor concentration. Therefore, the control goal is to drive the system such that the reactant concentration C_a follows the desired setpoint with no overshoot, and it is required that the coolant flow rate operates in the range $80 \leq F_j \leq 115$ with changes $|\Delta F_j| \leq 1$.

The system was simulated with the three control algorithms: OF-MPC, the proposed MADRPC, and LADRC. For the OF-MPC design, (4.68)-(4.69) were linearised around the selected operating point and discretised with sampling time $t_s = 0.083\,\text{min}$. The corresponding state-space model is (4.70) with $\begin{bmatrix} x_1, x_2 \end{bmatrix}^\top = \begin{bmatrix} C_a, T \end{bmatrix}^\top$, $u = F_j$, and $y = C_a$.
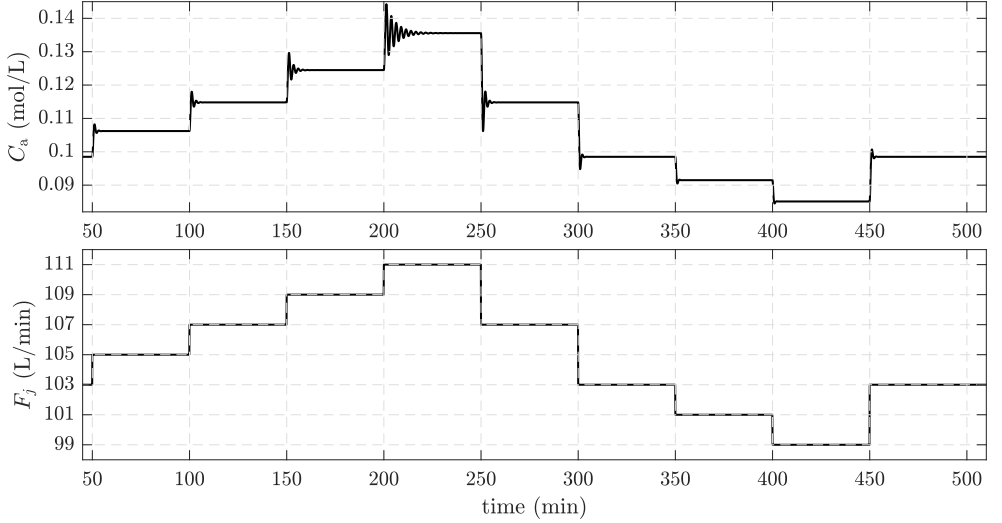
Figure 4.8: Open-loop evolution of concentration C_a when the coolant flow rate is varied from its nominal value $F_j = 103\,\text{L/min}$. The highly non-linear behaviour becomes more evident as the concentration reaches values far from the operating point $C_{as} = 0.09\,\text{mol/L}$.

$$\begin{bmatrix} x_{1,k+1} \\ x_{2,k+1} \end{bmatrix} = \begin{bmatrix} 0.2248 & -3.42 \times 10^{-3} \\ 133.3 & 1.501 \end{bmatrix} \begin{bmatrix} x_{1,k} \\ x_{2,k} \end{bmatrix} + \begin{bmatrix} 1.3071 \times 10^{-4} \\ -0.0926 \end{bmatrix} u_k$$

$$y_k = \begin{bmatrix} 1 & 0 \end{bmatrix} \begin{bmatrix} x_{1,k} \\ x_{2,k} \end{bmatrix}$$

$$(4.70)$$

As the sampling rate is $\omega_s = 75.7\,\text{rad/min}$, a current observer with bandwidth $\omega = 15\,\text{rad/min}$ was designed to estimate the states of (4.70). These estimated states are used within the OF-MPC algorithm to predict the output along a prediction horizon $p = 29$ with a control horizon $c = 10$ and weighting coefficients $\gamma = 2.22$ and $\lambda = 0.05$. As in the previous validation examples, the OF-MPC algorithm was implemented with the operating constraints, the equality constraint to assure stability and their corresponding slack variables with weights $\varepsilon_1 = \varepsilon_2 = 10^5$.

On the other hand, the disturbance rejector of the MADRPC was designed as follows: the values of the apparent time constant T and nominal critical gain b_0 were deduced from the open-loop response. As shown in Figure 4.8, for changes of $2\,\text{min/L}$ in the coolant flow rate, the reactant concentration varies approximately in $0.01\,\text{mol/L}$ with a mean settling time of $5\,\text{min}$.

Therefore, the modified plant parameters were set as $T = 1\,\mathrm{min}$ and $b_0 = 0.03\,\mathrm{mol/(min\,L)}$. The ESO bandwidth was chosen as $\omega_o = 15\,\mathrm{rad/min}$, and the modified predictive controller parameters were designed as $p = 29$, $c = 15$, $\gamma = 10$, $\lambda = 0.001$, and $\varepsilon_1 = \varepsilon_2 = 10^5$.

Finally, for the LADRC design, the same bandwidth $\omega_o = 15\,\mathrm{rad/min}$ was selected for the ESO, the controller bandwidth was set as $\omega_c = 10\,\mathrm{rad/min}$, and the nominal value of control gain had to be tuned to $b_0 = 3\,\mathrm{mol/(min\,L)}$ for the system to be closed-loop stable.

The closed-loop response of the CSTR is presented in Figure 4.9. A multi-step reference was applied to the system to test the dynamic behaviour when the concentration C_a is required to increase or decrease from its nominal value. What is more, uncertainty was included in the process at $t = 125\,\mathrm{min}$ reducing the feed concentration and increasing the reaction rate constant by $2\,\%$ of its corresponding nominal values, and at $t = 270\,\mathrm{min}$ when the coolant temperature was increased from $350\,\mathrm{K}$ to $352\,\mathrm{K}$.

According to the performance indices listed in Table 4.6, the MADRPC follows the desired setpoints with no overshoot and a settling time inferior to $3\,\mathrm{min}$ when the reference values are over the nominal concentration. The loop becomes slower for setpoints under C_{as}, but the MADRC algorithm is still the fastest.

Table 4.6: Performance indexes computed when the concentration of the CSTR from Table 4.5 is controlled with LADRC (L), OF-MPC (O) and the proposed MADRPC (M).

	Settling time (min)			Overshoot %			Total variation		
Setpoint	L	O	M	L	O	M	L	O	M
0.09 to 0.11	12.53	3.24	2.74	0	0	0	3.93	2.80	2.87
0.11 to 0.12	11.29	3.15	2.66	0	1.18	0	3.23	2.22	2.60
0.12 to 0.135	Osc.	13.20	2.57	Osc.	16.10	0	Osc.	5.41	4.08
0.135 to 0.125	12.45	5.81	2.66	0.53	11.62	0	2.86	2.14	3.23
0.125 to 0.11	11.45	3.07	2.74	0	0.13	0	4.71	3.11	4.48
0.11 to 0.08	16.27	3.90	3.07	0	0	0	11.92	8.84	8.97
0.08 to 0.05	25.23	5.98	3.65	0	0	0	16.70	13.75	13.75
Time (min)	Max. deviation %			ITAE			Total variation		
125 to 150	22.24	12.81	5.40	0.18	0.03	0.01	5.96	7.35	9.33
270 to 300	9.69	6.78	2.86	0.11	0.01	0.003	2.47	2.48	4.04
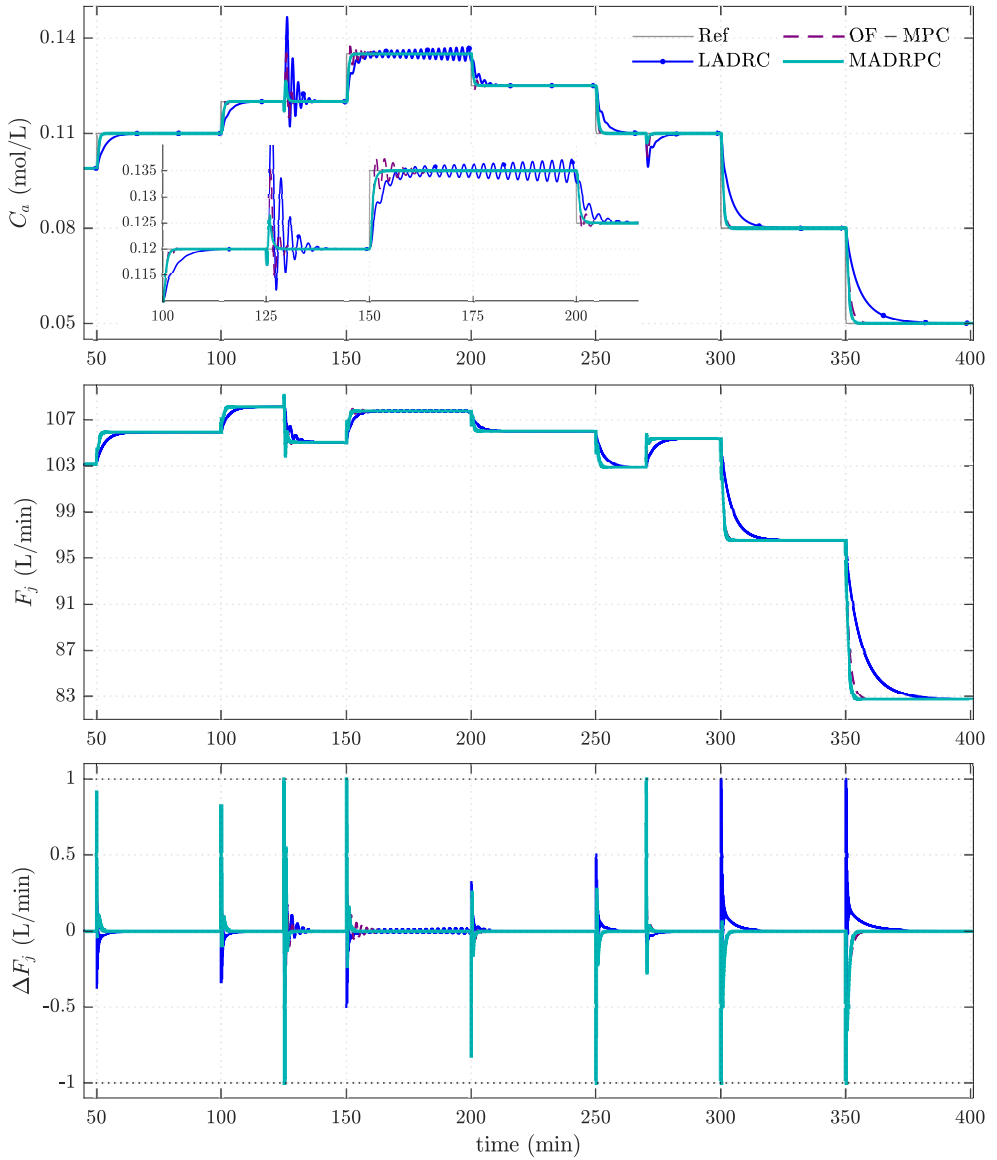
Figure 4.9: Closed-loop response of the CSTR from Table 4.5 subject to LADRC, OF-MPC, and MADRPC. System constraints: $80 \leq F_j \leq 115$, $|\Delta F_j| \leq 1$, $C_{Af,p+i|k} = C_{Ar,p|k}$, $i \in [1,2]$.

Notice that OF-MPC and LADRC produces an oscillating behaviour (referred to as Osc. in Table 4.6) when the concentration is increased from $0.12\,\mathrm{mol/L}$ to $0.135\,\mathrm{mol/L}$, as seen in the inset of the concentration from Figure 4.9. Although the OF-MPC manages to settle the output in the desired value, the detriment in the response is also present at the beginning of the next transient when C_A decreases to $0.125\,\mathrm{mol/L}$ causing that the system reaches the steady state with overshoot. The above exhibits the dependence of the OF-MPC on an accurate model, especially in the operating regions where the non-linear behaviour is more prominent, and the limitations of the LADRC to overcome such difficult dynamics.

With the selected tuning parameters, the MADRPC algorithm is also superior in terms of disturbance rejection. For example, the inset from Figure 4.9 also shows the response of the three algorithms to the first alteration in the operating conditions at $t = 125\,\mathrm{min}$. The MADRPC returns the concentration to the reference level producing the lowest deviation and the fastest response, as evidenced by the ITAE index. This rapid disturbance rejection increases the total variation of the coolant flow rate. However, the algorithm computes control actions that satisfy the given operation constraints.

Control of the reactor temperature

Consider now a CSTR in which it is desired to control the reactor temperature T_s by manipulating the coolant temperature T_j. The non-linear differential equations (4.71)-(4.72) [113] govern the process with the parameters and nominal values from Table 4.7. Under this operation, a coolant temperature $T_j = 311.1\,\mathrm{K}$ leads the system to the steady state $C_{as} = 9.341 \times 10^{-2}\,\mathrm{mol/L}$, $T_s = 385\,\mathrm{K}$.

$$\dot{C}_a = \frac{F}{V}\left(C_{a0} - C_a\right) - k_0 C_a \exp\left(-\frac{E}{RT_s}\right) \tag{4.71}$$

$$\dot{T}_s = \frac{F}{V}\left(T_0 - T_s\right) + \frac{\Delta H}{\rho c_p} k_0 C_a \exp\left(-\frac{E}{RT_s}\right) + \frac{UA}{\rho c_p V}\left(T_j - T_s\right) \tag{4.72}$$

In Figure 4.10, the open-loop response of the reactor temperature to changes in coolant temperature is presented. In this case, the critical zone for operation of the CSTR is reached when T_j is decreased by $5\,\mathrm{K}$, although the non-linear behaviour is also evident for positive changes in the manipulated variable.

Table 4.7: Parameters for the control of the CSTR temperature (subsection 4.5.3) [113].

Variable	Value	Units	Description
V	100	L	Reactor volume
k_0	7.2×10^{10}	min^{-1}	Reaction rate constant
E/R	8750	K	Activation energy term
ΔH	5×10^4	Cal/mol	Heat of reaction
UA	5×10^4	J/(min K)	Heat transfer term
ρ	1×10^3	g/L	Liquid density
c_p	0.239	J g/K	Heat capacity
F	100	L/min	Inlet flow rate
C_{a0}	1	mol/L	Feed concentration
T_0	350	K	Feed temperature
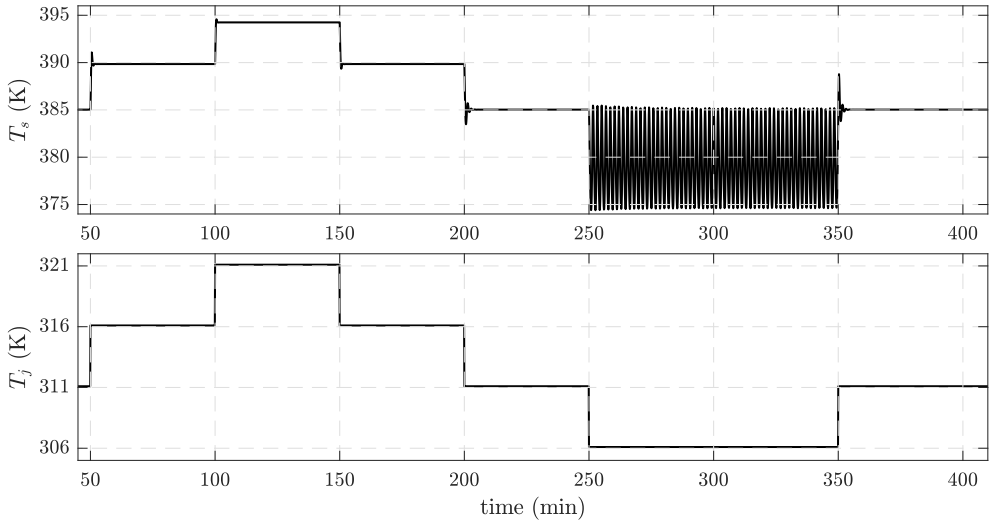
Figure 4.10: Open-loop evolution of the reactor temperature T_s when the coolant temperature is varied from its nominal value $T_j = 311.1$ K. The reactor experiences severe non-linear behaviour, particularly when the coolant temperature is decreased by 5 K.

The OF-MPC, MADRPC, and LADRC algorithms were designed similarly to the previous example, with the control purpose for the system to reach a desired reactor temperature with a settling time of less than 3 min and the minimum overshoot possible.

In addition, the input and rate of input constraints $291 \leq T_j \leq 331$, $|\Delta T_j| \leq 6$ were imposed, and process uncertainty was introduced at times $t = 125\,\mathrm{min}$ when the inlet flow rate is increased by $10\,\%$ of its nominal value, and at $t = 425\,\mathrm{min}$ with a reduction of the feed temperature from $350\,\mathrm{K}$ to $347\,\mathrm{K}$.

For the OF-MPC, the state-space model (4.73) was obtained by linearising (4.71)-(4.72) around the selected operating point and discretising the resultant continuous linear model with $T_s = 0.1\,\mathrm{min}$. The model states are defined as $\begin{bmatrix} x_1, x_2 \end{bmatrix}^\top = \begin{bmatrix} C_a, T \end{bmatrix}^\top$, the input is $u = T_j$, and the output $y = T$.

$$
\begin{bmatrix} x_{1,k+1} \\ x_{2,k+1} \end{bmatrix} = \begin{bmatrix} -0.0074 & -0.0045 \\ 172.331 & 1.589 \end{bmatrix} \begin{bmatrix} x_{1,k} \\ x_{2,k} \end{bmatrix} + \begin{bmatrix} -5.0512 \times 10^{-4} \\ 0.2786 \end{bmatrix} u_k
$$

$$
y(k) = \begin{bmatrix} 0 & 1 \end{bmatrix} \begin{bmatrix} x_{1,k} \\ x_{2,k} \end{bmatrix}
$$

(4.73)

A current-Luenberger observer was designed such that $\omega = 10\,\mathrm{rad/min}$ to estimate the states from (4.73) for future output predictions along an horizon $p = 10$ with control horizon $c = 5$ and weighting coefficients $\gamma = 1$, $\lambda = 0.03$, and $\varepsilon_1 = \varepsilon_2 = 10^5$.

From Figure 4.10, the apparent time constant for the modified plant of the proposed MADRPC was computed as $T = 0.15\,\mathrm{min}$, and the nominal value of critical gain was approximated by $b_0 \approx \Delta T_s / T \approx 25\,\mathrm{K/min}$. Likewise, the ESO bandwidth was set to $\omega_o = 10\,\mathrm{rad/min}$ and the modified predictive control parameters to $p = 10$, $c = 5$, $\gamma = 1$, and $\lambda = 0.3$. To maintain the same state estimation rate, the observer bandwidth of the LADRC was also adjusted to ω_o. The remaining LADRC parameters were tuned as $b_0 = 25$ and $\omega_c = 3\,\mathrm{rad/min}$.

Under the control designs mentioned above, the CSTR closed-loop response is as shown in Figure 4.11 with the performance indices from Table 4.8. In this case, the OF-MPC algorithm offers the fastest transition between reference values when the setpoints are in the range $T_{ss} + 10\,\mathrm{K}$. However, an overshoot superior to $2\,\%$ is produced along the whole operation, worsening in the critical zone where the controlled variable is required to settle in the range $T_{ss} - 10\,\mathrm{K}$, as seen in the inset from the temperature. The above is due to the highly non-linear dynamics that the CSTR exhibits in this region (see Figure 4.10).
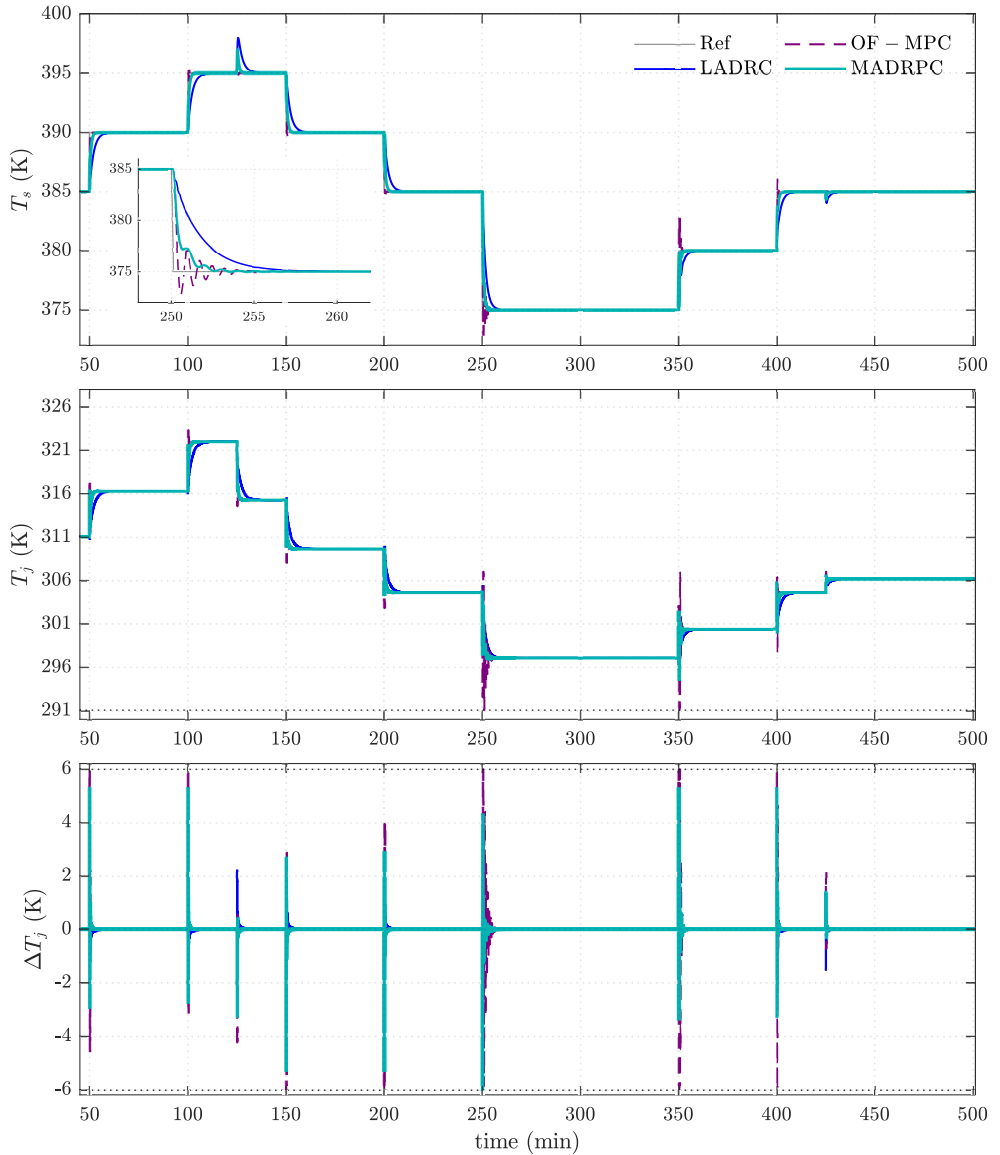
Figure 4.11: Closed-loop response of the CSTR from Table 4.7 subject to LADRC, OF-MPC, and MADRPC. System constraints: $291 \leq T_j \leq 331$, $|\Delta T_j| \leq 6$, $C_{Tjf,p+i|k} = C_{Tjr,p|k}$, $i \in [1,2]$.

Table 4.8: Performance indexes computed when the temperature of the CSTR from Table 4.7 is controlled with LADRC (L), OF-MPC (O), and MADRPC (M).

Setpoint	Settling time (min)			Overshoot %			Total variation		
	L	O	M	L	O	M	L	O	M
385 to 390	7.90	0.90	2.50	0	2.98	0	9.74	9.15	8.08
390 to 395	8.30	1	2.50	0	5.65	0	10.59	7.33	6.90
395 to 390	8.10	1	2.60	0	6.11	0	12.79	11.57	11.50
390 to 385	7.60	0.70	2.60	0	3.98	0	11.70	13.91	12.47
385 to 375	6.50	3.70	3.10	0	21.86	0	20.57	84.43	22.93
375 to 380	6.70	2.90	2.80	0	63.98	0	8.50	82.77	19.57
380 to 385	7.30	1	2.50	0	21.59	0	8.90	20.13	10.77
Time (min)	Max. deviation K			ITAE			Total variation		
125 to 150	2.99	1.53	1.98	20.70	0.17	1.48	10.49	9.19	7.52
425 to 300	0.98	0.47	0.68	4.03	0.03	0.29	4.16	4.30	3.04

On the other hand, both LADRC and MADRPC algorithms can fulfil the control task and avoid overshoot, although MADRPC is the one driving the system to the desired points in the required time. What is more, the MADRPC tends to maintain a mean settling time of approximately $2.6\,\mathrm{s}$ throughout the complete operation satisfying the imposed constraints.

Finally, in terms of disturbance rejection, the increase in the inlet flow rate and decrease in its temperature bring challenges to the system, which are appropriately handled by the three control schemes. The MADRPC improves the disturbance rejection compared to LADRC, producing lower deviations from the setpoint and computed ITAE indices. Through additional simulations, it was verified that a reducing the weight of the input changes from the MADRPC could produce a better disturbance rejection response at the cost of increasing the total variation of the control action. In contrast, a variation in the OF-MPC parameters in an attempt to reduce the overshoot only deteriorates the oscillations in the zone $T_{ss} - 10\,\mathrm{K}$.

Chapter 5

Conclusions and future research directions

This chapter closes the dissertation. The first section draws conclusions that answer the research questions stated in chapter 1. The second section discusses future research directions.

5.1 Conclusions

This thesis presented new strategies to design control loops under the Active Disturbance Rejection Control (ADRC) framework. In this sense, three contributions are given: a guide for the design and application of conventional linear active disturbance rejection controllers (LADRC), a set of rules for the tuning of LADRC applicable to the implementation of control loops where the process to be controlled is approximated to a first-order plus dead time (FOPDT) system, and a control architecture that merges the receding horizon strategy of the state-space MPC with the disturbance estimation and rejection capability of the LADRC intended for the control of constrained linear or non-linear processes with no identified nominal model.

In the conventional ADRC formulation, a precise model of the process, whether linear or non-linear, is not required to control it. To formulate the control problem under the disturbance rejection framework, once the manipulated and controlled variables have been identified, the dominant dynamics order and the nominal value of the critical gain must be selected.

It is a common practice to implement first-order or second-order ADRC formulations under the premise that these approximations appropriately describe the dominant dynamics. On the one hand, if a mathematical representation of the process behaviour is available, it results useful if it is defined in the form of an input-output model due to all neglected dynamics and unknown terms are regarded as the total perturbation, and the critical gain can be approximated from the model. On the other hand, the relative or dominant order and the nominal value of the critical gain can be deduced from the input-output signals analysis by measuring the apparent time constant and the apparent static gain from an open-loop response.

The ADRC order and critical gain definitions lead to the selection of the canonical form, which is the assumed behaviour of the modified plant. For the conventional ADRC, the above corresponds to an integrator chain. This way, the disturbance rejector of the ADRC loop enforces the actual process to behave like a modified cascaded integrator governed by the state-feedback control law. The designer chooses to incorporate the available process information in the canonical form. However, the main feature of the ADRC technology is that the control design can be performed even when the available information is minimal.

Regarding the LADRC design, the LESO and linear control law gains must be computed. The bandwidth parameterization has simplified this task by defining all the loop gains in terms of the observer and controller bandwidths. Nevertheless, selecting these two parameters for the conventional LADRC formulation could turn into a challenging tuning process, even though the desired performance offers good starting points.

The LADRC design under the conventional framework, which is the first contribution of this dissertation, is consolidated in Guide 2.5.1, supported by Tables 2.1 and 2.2. With this guide, the control practitioner interested in the ADRC subject can explore the control of systems using this technology and relate the ADRC theoretical knowledge to the practical application.

Each year, many scientific articles are published in the ADRC research area. In the range of successful applications, two non-linear examples, one single-input single-output and one multiple-input multiple-output, were chosen to validate the ADRC algorithm and to illustrate the use of Guide 2.5.1. For both examples, the necessary process information was deducted from the open-loop time response and the gains tuning was done according to the desired closed-loop performance. Consequently, it was verified that the ADRC could be used to control highly non-linear processes in unstable or stable operating points. Depending on the gains tuning, an improvement in the disturbance rejection can be expected compared to the classical PID controller.

The examples addressed following Guide 2.5.1 were simulated in Matlab®, and the corresponding files were uploaded to the open-access platform Matlab Central [63]. Likewise, the guide for design and application of active disturbance rejection controllers was published as the tutorial article [61].

One of the controversial discussions about the LADRC design is related to what are the parameters that certainly should be tuned for implementation. The bandwidth parameterization focused on the controller and observer bandwidths assumes that the nominal value of the critical gain can be approximated from the process knowledge. This is somewhat true as shown in chapter 2. However, when the controlled process presents lag-dominant or delay-dominant dynamics, the critical gain parameters may need to be retuned to a higher value from its initial approximation. Indeed, some literature suggests that this is the only parameter that should be adjusted because the closed-loop desired performance is used to compute the controller bandwidth, which is then scaled to obtain the observer bandwidth.

For First-order plus dead time (FOPDT) systems, the computation of the three main LADRC parameters becomes challenging because the closed-loop stability region expands as the nominal value of the critical gain is allowed to increase. Besides, the shape of this region is such that if a high observer bandwidth is desired, a low controller bandwidth must be selected to remain within the stability bounds. The contrary holds that if the controller bandwidth is expected to increase, the maximum allowed observer bandwidth tends to decrease.

Into a broader stability region, better disturbance rejection performance can be obtained. Notably, lower ITSE values are computed from the response to a step-type input disturbance at the cost of less robust loops, which evidences the conflicting nature of these design objectives. Therefore, by performing a Multi-objective Optimisation Design (MOOD) procedure under the Generate-First Choose-Later (GFCL) context, a set of solutions can be obtained with different trade-offs between the ITSE and robustness. Moreover, the MOOD procedure performed for controlling different FOPDT nominal plants provides an array of solutions whose analysis leads to the derivation of functions for the computation of the LADRC triads.

The Multi-objective Evolutionary Algorithms (MOEA) are valuable tools for searching for the approximations of the optimal solutions (Pareto Set) and their corresponding objective values (Pareto Front). The definition of the optimisation problem used by the MOEA and the MOEA itself influences the results obtained from the optimisation process. In this thesis, the $\wp^{\nearrow}-$MOGA was used to simultaneously minimise the loop robustness and the ITSE from the disturbance rejection response produced by the LADRC tuned with candidates parameters selected from a search space inside a stability region such that the design objectives were within desired ranges covering the possible performance indices produced by other reference controllers.

The optimisation problem was formulated using bandwidth parameterization to reduce the decision variables to the nominal value of the critical gain and the controller bandwidth. The observer bandwidth was set as ten times the controller bandwidth selected. With the above, a clear tendency in the array of solutions was recognised, i.e. each of the Pareto Sets approximations was located in an identified region of the search space, and the solution sets were moving, keeping their distribution throughout the space, as the normalised delay increased.

144

Multi-criteria Decision Making (MCDM) is the last step in the MOOD procedure. This step was performed to derive a set of tuning rules for the LADRC design, considering that it would be helpful for the designer to have a few controller options to evaluate but without the need for tuning any extra parameter. Consequently, three solutions from each Pareto approximation were selected according to three levels of robustness quality.

Following the graphical distribution of the chosen solutions, the data were fitted to three formulae for each tuning parameter. Furthermore, The rules were deduced separately for two groups comprising, on the one hand, the FOPDT general systems with normalised delay less or equal to 0.5 and, on the other hand, the FOPDT general plants whose normalised delay is greater than 0.5. For example, the nominal value of the critical gain decays exponentially as the normalised delay increases for the first of the groups and follows a quadratic behaviour for the second one.

The second contribution of this dissertation is summarised in Guide 3.5.1. The three main LADRC parameters: the nominal value of critical gain, the controller bandwidth, and the observer bandwidth, can be computed by selecting a desired quality of robustness (low, medium, or high) and substituting the parameters from the approximation of the actual plant behaviour to a FOPDT model into the given rules. Besides, a range of values can be obtained for each LADRC parameter whose limits are defined by the achievable loop robustness.

The proposed rules were validated with control of lag-dominated and delay-dominated systems, as well as the control of temperature on the cold face of a thermoelectric module, showing that these rules offer satisfactory performance for load disturbance rejection and setpoint following. Compared to the performance produced on the same systems for PID controllers and the LADRC configuration tuned with the dominant rules from the literature, the LADRC designed with the proposed tuning guide potentially improves the step-type input disturbance rejection.

The rules from Guide 3.5.1 were derived considering only two indices for the simultaneous minimisation, one related to the disturbance rejection of LADRC capability. The above is because the hypothesis at the beginning of the research was that through a GFCL multi-objective optimisation approach is possible to obtain solutions with a trade-off between the design objectives, reflected in the deduced rules. Moreover, it was desired to compare the performance achieved with the LADRC tuned with the resulting formulae to that obtained with the dominant LADRC rules from [32], which were developed using the same design objectives but with the AOF approach.

The rules from [32] offer an additional tuning parameter, as is the case with the widely accepted PID rules for FOPDT plants. In this dissertation, a comparison in the decision space was made among the Pareto alternatives obtained with the performed MOOD procedure and the alternatives computed with the other PID and LADRC rules by setting their corresponding additional tuning parameters to the values suggested by the authors. Usually, a designer interested in a set of rules seeks orientation about adjusting any additional variables; commonly, the proposals include the nominal value for them because that value produces proper performance.

From another point of view, a comparison among the Pareto Fronts approximations (design concepts) computed with the different controllers would have been possible. In this case, Pareto Fronts approximations are obtained by varying the unique tuning parameter of each of the reference sets of rules. Plotting these on the same objective space as the approximated Fronts obtained from the MOOD gives an insight into the design concepts performance, representing an alternative approach for the data visualisation required for the MCDM stage.

The work developed for formulating the LADRC tuning rules from Guide 3.5.1 was published as the research article [61]. An interactive tuning software was also developed as complementary material during its preparation. This tool is available at Matlab central [64] and allows the user to adjust the LADRC parameters by varying the robustness specification. On the other hand, the designer can modify the LADRC parameters within closed intervals to evaluate the overall loop performance.

The ADRC is nowadays considered an established control technology that proposes a reformulation of the control problems under the disturbance estimation and rejection framework. Many researchers view it as a strategy outside the model-based control methods because it can be implemented with a minimum knowledge of the controlled process. The core of the ADRC is its disturbance rejector, which makes it possible that an assumed disturbance-free modified plant is enforced on the controlled system. Therefore, the controller is designed to govern that desired plant instead of the uncertain one.

The active rejection of the total perturbation results in an attractive characteristic that raises interest in integrating the ADRC topology with the model-based techniques, for example, with the Model-Predictive Control (MPC). One of the directions to perform the above integration results from implementing the state-space MPC using a discretised LESO to estimate the system states and the total perturbation to make predictions of the disturbance vector. This

approach resembles the MPC with a state estimation configuration in which a detailed mathematical model is still needed, and the LESO aids in estimating the slight deviations from that prediction model.

Alternatively, this thesis proposes the Modified Active Disturbance Rejection Predictive Control (MADRPC) that maintains the disturbance rejector of the ADRC loop to enforce the actual process to behave like a first-order plus integrator plant, which includes the integral effect commonly present in industrial processes and approximate other types of dominant dynamics through a term with a time constant to enhance the estimation capability of the current-type LESO. As a result, a predictive control law to govern the modified plant is computed based on a second-order state-space realisation with only two model parameters: the apparent time constant and the nominal value of the control gain.

One significant advantage of the MADRPC is that the modelling requirement is relaxed because the prediction problem is solved based on a fixed discrete state-space model, despite the nature of the real system. Thus, the size of the optimisation problem is exclusively dependent on the horizon lengths, and the need for detailed identification of the real system is eliminated.

When the disturbance rejector of the ADRC is used to enforce a system to behave like an assumed plant, the manipulated variable is the sum of two contributions. One is computed by a controller governing the modified plant, and the other is a factor of the total perturbation. Supposing that the MPC is used as a controller, the handling of constraints is challenging because the predictive control law is further compensated in the loop, and there is a possibility that the constraint imposed to solve the optimisation problem may be violated due to the compensation. In the MADRPC, the constraints of the optimisation problem are reformulated to include the compensation term. In this way, the constraints of the manipulated and controlled variables are directly considered.

The MADRPC is the third contribution of this dissertation. Its control loop architecture is shown in Figure 4.1, and general guidelines for its implementation are given in Guide 4.5.1. The disturbance rejector uses the disturbance compensation term to transform the controlled system into a general integral plant which constitutes the prediction model of the modified predictive controller. The optimisation problem is defined such that the tracking error and the predictive control law rate are penalised subject to inequality constraints that include the compensation term computed from the estimation of the total perturbation and an equality constraint that forces the predictions to converge to a defined reference to assure the future output stability. Moreover, the opti-

misation problem feasibility is addressed by softening some of the constraints with the introduction of slack variables. Consequently, the MADRPC integrates the receding horizon strategy of state-space MPC with the disturbance estimation and rejection mechanism of ADRC suitable for controlling systems with no detailed model.

When combining ADRC with the state-space MPC, the challenge of meeting performance requirements arises because of the relaxation made in modelling. The MADRPC was validated in the control of linear and non-linear benchmark systems. The disturbance rejector of the MADRPC actively compensates for the total perturbation, which includes parameter uncertainty and external disturbances. Therefore, with the proposed control scheme is possible to achieve similar performance to that obtained with the MPC that uses a known linearised model of complete-order, a correction term, and constant state disturbance predictions to provide offset-free control. Moreover, the MADRPC was more robust than OF-MPC and conventional LADRC when it operated a CSTR unit in regions of prominent non-linear dynamics offering proper servo-regulatory performance while satisfying constraints.

The MADRPC requires tuning the classical MPC parameters besides the ESO bandwidth and the modified plant parameters. The above should be appropriately selected for the trade-off among the performance requirements. Guide 4.5.1 gives information to compute starting values for the parameters, but its iterative tuning may be needed.

The MADRPC strategy was written in scientific article format for publication and is currently under review.

5.2   Future research directions

This thesis was developed considering the ADRC as the primary research topic. Chapter 2 was written to give the interested researcher a general framework for designing active disturbance rejection controllers. Because of that, the implemented block diagrams of the simulation examples and their associated Matlab codes were publicly shared. As the research progressed, it was found that there is a growing interest in developing software tools for custom solutions of ADRC, as is the case of the ADRC Toolbox [114]. In this sense, creating ADRC-based software solutions for the continuous and discrete-time implementations is considered a future research direction as complementary material that aids in the theoretical and practical understanding of ADRC technology.

148

Chapter 2 also reviewed the canonical forms adopted in the literature for the ADRC modified plant. As they are concerned with incorporating process knowledge to enhance the ESO estimation, the proposal of new identification algorithms that provide the required information in the ADRC disturbance estimation and rejection framework would be a valuable contribution.

In chapter 3, an overall analysis of the conflicting objectives regarding the tuning of the LADRC was done. From that, it is identified as future research the possibility of expanding the objective space to include other performance criteria, for example, the total variation of the control signal. The parameterization (3.13) for the observer bandwidth oriented the optimisation process to a particular area of the stability region, and as a result, smooth manipulated signals were obtained. It would be of interest to analyse the trade-offs among other design objectives.

In the MCDM stage from the MOOD procedure performed in chapter 3, three alternatives were chosen from the Pareto Fronts approximations according to a specified robustness level, leading to three formulae for each LADRC tuning parameter depending on the normalised delay. For future work, the research could focus on going through the entire Fronts approximation and how doing this would be linked to selecting the alternatives in the Sets approximations. It is important to emphasise that the methodological approach in chapter 3 is ultimately expected to provide a set of parameters (solutions) distributed following some sort of tendency dependent on the normalised delay to fit their computation to formulae. Therefore, it would be challenging to find a way to go through the Sets approximations and subsequently fit the data to functions, especially if more than two design objectives are considered.

Chapter 3 showed how the proposed tuning rules were used to design the Cascaded-ESO (CESO) for its implementation as part of the LADRC loop used to control the thermoelectric module. This example opens up research questions related to optimising the LADRC with CESO. Following the same methodological approach from chapter 3, it would be interesting to study the possibility of deriving tuning rules for the LADRC with CESO based on MOOD procedures suitable for the FOPDT approximations. The introduction of new parameters related to the CESO as the number of its levels makes this a challenging research idea.

The MADRPC parameters selection (modified plant parameters, horizons and weighting coefficients) was oriented in chapter 4 through Guide 4.5.1. These guidelines were sufficient for the tuning of the reported case studies. Still, future work can be directed towards the MADRPC parameter tuning, considering the trade-off between different performance objectives for which the GFCL multi-objective approach would be helpful. The design objectives can be related to design requirements of interest, such as settling time, overshoot and total variation of control action.

Another research direction goes with the extension of the MADRPC to MIMO systems. In this case, each manipulated channel could be treated as a modified plant of the first-order plus integrator. With this approach, each controlled variable would be assumed to have fixed dynamics, and the coupling and external disturbances would be lumped in the total perturbation related to each channel. Moreover, the state-space formulation of the MADRPC would allow the control of a plant with no identified model as a fixed order system of $2n_y$ states, with n_y as the number of controlled outputs. The challenge here would be linked to selecting the dominant input-output pairs under the DDC framework or managing the static coupling and formulation for non-squared systems.

Bibliography

[1] J. Han, "From PID to active disturbance rejection control", *IEEE Transactions on Industrial Electronics*, vol. 56, no. 3, pp. 900–906, 2009 (cit. on pp. 2, 17, 23).

[2] W.-H. Chen, J. Yang, L. Guo, and S. Li, "Disturbance-observer-based control and related methods—an overview", *IEEE Transactions on Industrial Electronics*, vol. 63, no. 2, pp. 1083–1095, 2016, (In Chinese) (cit. on pp. 2, 22).

[3] Z. Gao, "On the centrality of disturbance rejection in automatic control", *ISA Transactions*, vol. 53, no. 4, pp. 850–857, 2014 (cit. on pp. 2, 24).

[4] S. Skogestad and I. Postlethwaite, *Classical Feedback Control*. John Wiley and Sons, 2001 (cit. on pp. 2, 55).

[5] J. Li, Y. Xia, X. Qi, and Z. Gao, "On the necessity, scheme, and basis of the linear–nonlinear switching in active disturbance rejection control", *IEEE Transactions on Industrial Electronics*, vol. 64, no. 2, pp. 1425–1435, 2017 (cit. on p. 4).

[6] B.-Z. Guo and Z.-L. Zhao, *Active Disturbance Rejection Control for Nonlinear Systems*. John Wiley & Sons Singapore Pte. Ltd, 2016 (cit. on p. 4).

[7]   Q. Zheng, L. Q. Gaol, and Z. Gao, "On stability analysis of active distur-bance rejection control for nonlinear time-varying plants with unknown dynamics", in *2007 46th IEEE Conference on Decision and Control*, IEEE, 2007 (cit. on pp. 4, 30).

[8]   Q. Zheng, L. Q. Gao, and Z. Gao, "On validation of extended state observer through analysis and experimentation", *Journal of Dynamic Systems, Measurement, and Control*, vol. 134, no. 2, 2012 (cit. on p. 5).

[9]   R. Sanz, P. Garcia, and P. Albertos, "Active disturbance rejection by state feedback: Experimental validation in a 3-dof quadrotor platform", in *2015 54th Annual Conference of the Society of Instrument and Con-trol Engineers of Japan (SICE)*, 2015, pp. 794–799 (cit. on p. 5).

[10]   S. Zhao and Z. Gao, "Active disturbance rejection control for non-minimum phase systems", in *Proceedings of the 29th Chinese Control Conference*, 2010, pp. 6066–6070 (cit. on p. 5).

[11]   W. Xue, Y. Huang, and Z. Gao, "On ADRC for non-minimum phase sys-tems: Canonical form selection and stability conditions", *Control Theory and Technology*, vol. 14, no. 3, pp. 199–208, 2016 (cit. on p. 5).

[12]   L. Sun, D. Li, Z. Gao, Z. Yang, and S. Zhao, "Combined feedforward and model-assisted active disturbance rejection control for non-minimum phase system", *ISA Transactions*, vol. 64, pp. 24–33, 2016 (cit. on pp. 5, 8, 24, 25, 27).

[13]   C. Fu and W. Tan, "Tuning of linear ADRC with known plant informa-tion", *ISA Transactions*, vol. 65, pp. 384–393, 2016 (cit. on pp. 5, 24, 26, 28).

[14]   S. Ahmad and A. Ali, "Active disturbance rejection control of DC–DC boost converter: A review with modifications for improved performance", *IET Power Electronics*, vol. 12, no. 8, pp. 2095–2107, 2019 (cit. on pp. 5, 24, 26, 28).

[15]   Q. Zheng and Z. Gao, "Active disturbance rejection control: Some recent experimental and industrial case studies", *Control Theory and Technol-ogy*, vol. 16, no. 4, pp. 301–313, 2018 (cit. on p. 5).

[16]   Z. Wu, Z. Gao, D. Li, Y. Chen, and Y. Liu, "On transitioning from PID to ADRC in thermal power plants", *Control Theory and Technology*, vol. 19, no. 1, pp. 3–18, 2021 (cit. on p. 5).

[17]   R. Fareh, S. Khadraoui, M. Y. Abdallah, M. Baziyad, and M. Bettayeb, "Active disturbance rejection control for robotic systems: A review", *Mechatronics*, vol. 80, Article 102671, 2021 (cit. on p. 5).

[18]   S. Talole, "Active disturbance rejection control: Applications in aerospace", *Control Theory and Technology*, vol. 16, no. 4, pp. 314–323, 2018 (cit. on p. 5).

[19]   Y. Huang and W. Xue, "Active disturbance rejection control: Methodology and theoretical analysis", *ISA Transactions*, vol. 53, no. 4, pp. 963–976, 2014 (cit. on pp. 5, 20).

[20]   H. Feng and B.-Z. Guo, "Active disturbance rejection control: Old and new results", *Annual Reviews in Control*, vol. 44, pp. 238–248, 2017 (cit. on p. 5).

[21]   Z.-H. Wu, H.-C. Zhou, B.-Z. Guo, and F. Deng, "Review and new theoretical perspectives on active disturbance rejection control for uncertain finite-dimensional and infinite-dimensional systems", *Nonlinear Dynamics*, vol. 101, no. 2, pp. 935–959, 2020 (cit. on p. 5).

[22]   G. Herbst, "A simulative study on active disturbance rejection control (ADRC) as a control tool for practitioners", *Electronics*, vol. 2, no. 4, pp. 246–279, 2013 (cit. on pp. 5, 31, 105, 109).

[23]   Z. Gao, "Scaling and bandwidth-parameterization based controller tuning", in *Proceedings of the 2003 American Control Conference, 2003*, 2003, pp. 4989–4996 (cit. on pp. 6, 25, 27, 29, 30, 51, 61).

[24]   C. Zhao and D. Li, "Control design for the SISO system with the unknown order and the unknown relative degree", *ISA Transactions*, vol. 53, no. 4, pp. 858–872, 2014 (cit. on pp. 6, 23).

[25]   L. Sun, Y. Zhang, D. Li, and K. Y. Lee, "Tuning of active disturbance rejection control with application to power plant furnace regulation",

Control Engineering Practice, vol. 92, Article 104122, 2019 (cit. on pp. 6, 122).

[26]   R. Zhou and W. Tan, "Analysis and tuning of general linear active disturbance rejection controllers", *IEEE Transactions on Industrial Electronics*, vol. 66, no. 7, pp. 5497–5507, 2019 (cit. on p. 6).

[27]   W. Tan and C. Fu, "Linear active disturbance-rejection control: Analysis and tuning via IMC", *IEEE Transactions on Industrial Electronics*, vol. 63, no. 4, pp. 2350–2359, 2016 (cit. on p. 6).

[28]   R. Madonski, A. Piosik, and P. Herman, "High-gain disturbance observer tuning seen as a multicriteria optimization problem", in *21st Mediterranean Conference on Control and Automation*, 2013, pp. 1411–1416 (cit. on p. 7).

[29]   R. Madonski, Z. Gao, and K. Lakomy, "Towards a turnkey solution of industrial control under the active disturbance rejection paradigm", in *2015 54th Annual Conference of the Society of Instrument and Control Engineers of Japan (SICE)*, 2015, pp. 616–621 (cit. on p. 7).

[30]   T. He, Z. Wu, D. Li, and J. Wang, "A tuning method of active disturbance rejection control for a class of high-order processes", *IEEE Transactions on Industrial Electronics*, vol. 67, no. 4, pp. 3191–3201, 2020 (cit. on pp. 7, 61, 69, 87, 90–92).

[31]   D. Li, X. Chen, J. Zhang, and Q. Jin, "On parameter stability region of LADRC for time-delay analysis with a coupled tank application", *Processes*, vol. 8, no. 2:223, 2020 (cit. on pp. 7, 61, 62).

[32]   B. Zhang, W. Tan, and J. Li, "Tuning of linear active disturbance rejection controller with robustness specification", *ISA Transactions*, vol. 85, pp. 237–246, 2019 (cit. on pp. 8, 57, 62, 69–73, 80, 81, 83, 84, 87, 90–95, 145, 146).

[33]   L. Sun, Q. Hua, J. Shen, Y. Xue, D. Li, and K. Y. Lee, "Multi-objective optimization for advanced superheater steam temperature control in a 300 MW power plant", *Applied Energy*, vol. 208, pp. 592–606, 2017 (cit. on p. 8).

[34] M. Srikanth and N. Yadaiah, "Optimal parameter tuning of modified active disturbance rejection control for unstable time-delay systems using an AHP combined multi-objective quasi-oppositional jaya algorithm", *Applied Soft Computing*, vol. 86:105881, 2020 (cit. on p. 8).

[35] M. Schwenzer, M. Ay, T. Bergs, and D. Abel, "Review on model predictive control: An engineering perspective", *The International Journal of Advanced Manufacturing Technology*, vol. 117, pp. 1327–1349, 2021 (cit. on pp. 10, 101, 116).

[36] T. Samad, M. Bauer, S. Bortoff, *et al.*, "Industry engagement with control research: Perspective and messages", *Annual Reviews in Control*, vol. 49, pp. 1–14, 2020 (cit. on p. 10).

[37] D. E. Quevedo, R. P. Aguilera, and T. Geyer, "Model predictive control for power electronics applications", in *Handbook of Model Predictive Control*, S. V. Raković and W. S. Levine, Eds. Cham: Springer International Publishing, 2019, pp. 551–580 (cit. on p. 10).

[38] P. Karamanakos, E. Liegmann, T. Geyer, and R. Kennel, "Model predictive control of power electronic systems: Methods, results, and challenges", *IEEE Open Journal of Industry Applications*, vol. 1, pp. 95–114, 2020 (cit. on p. 10).

[39] J. Drgoňa, J. Arroyo, I. C. Figueroa, *et al.*, "All you need to know about model predictive control for buildings", *Annual Reviews in Control*, vol. 50, pp. 190–232, 2020 (cit. on p. 10).

[40] S. Zhan and A. Chong, "Data requirements and performance evaluation of model predictive control in buildings: A modeling perspective", *Renewable and Sustainable Energy Reviews*, vol. 142, Article 110835, 2021 (cit. on p. 10).

[41] G.-P. Liu, "Predictive control of networked nonlinear multiagent systems with communication constraints", *IEEE Transactions on Systems, Man, and Cybernetics: Systems*, vol. 50, no. 11, pp. 4447–4457, 2020 (cit. on p. 10).

[42] Z. Pang, T. Du, C. Zheng, and C. Li, "Event-triggered cooperative predictive control for networked multi-agent systems with random delays

and packet dropouts", *Symmetry*, vol. 14, no. 3, Article 541, 2022 (cit. on p. 10).

[43]   P. D. Domański, "Performance assessment of predictive control—a survey", *Algorithms*, vol. 13, no. 4, Article 97, 2020 (cit. on p. 10).

[44]   S. Li, J. Yang, W.-H. Chen, and X. Chen, "Generalized extended state observer based control for systems with mismatched uncertainties", *IEEE Transactions on Industrial Electronics*, vol. 59, no. 12, pp. 4792–4802, 2012 (cit. on p. 10).

[45]   A. Castillo, P. García, R. Sanz, and P. Albertos, "Enhanced extended state observer-based control for systems with mismatched uncertainties and disturbances", *ISA Transactions*, vol. 73, pp. 1–10, 2018 (cit. on p. 10).

[46]   C. Liu, R. R. Negenborn, H. Zheng, and X. Chu, "A state-compensation extended state observer for model predictive control", *European Journal of Control*, vol. 36, pp. 1–9, 2017 (cit. on p. 10).

[47]   A. Castillo, T. L. Santos, P. Garcia, and J. E. Normey-Rico, "Predictive ESO-based control with guaranteed stability for uncertain MIMO constrained systems", *ISA Transactions*, vol. 112, pp. 161–167, 2021 (cit. on pp. 10, 115).

[48]   Y. Zhao, H. Liu, C. Ding, *et al.*, "Research on MPDPC with FADRC control strategy for three-phase rectifying converter", *Measurement and Control*, vol. 55, no. 7-8, pp. 757–766, 2022 (cit. on p. 10).

[49]   H. Zhang, Y. Li, Z. Li, *et al.*, "Extended-state-observer based model predictive control of a hybrid modular DC transformer", *IEEE Transactions on Industrial Electronics*, vol. 69, no. 2, pp. 1561–1572, 2022 (cit. on p. 10).

[50]   F. Liu, H. Li, L. Liu, R. Zou, and K. Liu, "A control method for IPMSM based on active disturbance rejection control and model predictive control", *Mathematics*, vol. 9, no. 7, p. 760, 2021 (cit. on p. 10).

[51] H. He, B. Liu, Q. Wang, F. Tan, H. Gui, and C. Zhang, "Active disturbance rejection control-based robust model predictive current control for induction motor", *Journal of Electrical Engineering & Technology*, no. 17, pp. 3413–3425, 2022 (cit. on p. 10).

[52] H. Liu, W. Lin, Z. Liu, C. Buccella, and C. Cecati, "Model predictive current control with model-aid extended state observer compensation for PMSM drive", *IEEE Transactions on Power Electronics*, vol. 38, no. 3, pp. 3152–3162, 2023 (cit. on p. 10).

[53] Z. Li, R. Li, and R. Bu, "Path following of under-actuated ships based on model predictive control with state observer", *Journal of Marine Science and Technology*, vol. 26, no. 2, pp. 408–418, 2020 (cit. on p. 10).

[54] J. Gao, X. Liang, Y. Chen, L. Zhang, and S. Jia, "Hierarchical image-based visual serving of underwater vehicle manipulator systems based on model predictive control and active disturbance rejection control", *Ocean Engineering*, vol. 229, p. 108 814, 2021 (cit. on p. 10).

[55] G. Li, R. Madonski, K. Lakomy, L. Sun, and K. Y. Lee, "Extended state observer-based model predictive temperature control of mechanically pumped two-phase loop: An experimental study", *Applied Thermal Engineering*, vol. 213, p. 118 663, 2022 (cit. on p. 10).

[56] J. Yang, H. Cui, S. Li, and A. Zolotas, "Optimized active disturbance rejection control for DC-DC buck converters with uncertainties using a reduced-order GPI observer", *IEEE Transactions on Circuits and Systems I: Regular Papers*, vol. 65, no. 2, pp. 832–841, 2018 (cit. on p. 10).

[57] H. Sira-Ramírez, "From flatness, GPI observers, GPI control and flat filters to observer-based ADRC", *Control Theory and Technology*, vol. 16, no. 4, pp. 249–260, 2018 (cit. on p. 11).

[58] S. A. Suhail, M. A. Bazaz, and S. Hussain, "MPC based active disturbance rejection control for automated steering control", *Proceedings of the Institution of Mechanical Engineers, Part D: Journal of Automobile Engineering*, vol. 235, no. 12, pp. 3199–3206, 2021 (cit. on p. 11).

[59]   Z. Chen, Y. Li, M. Sun, Q. Zhang, and Q. Sun, "ADRC-GPC control of quad-rotor unmmaned aerial vehicle", *Journal of Harbin Institute of Technology*, vol. 48, no. 9, pp. 176–180, 2016 (cit. on p. 11).

[60]   X. Wu, Y. Li, Z. Chen, and M. Sun, "On the design and realization of active disturbance rejection generalized predictive control", *Ima Journal Of Mathematical Control And Information*, vol. 36, no. 4, pp. 1275–1304, 2019 (cit. on p. 11).

[61]   B. V. Martínez, J. Sanchis, S. García-Nieto, and M. Martínez, "Active disturbance rejection control: A guide for design and application", *Revista Iberoamericana de Automática e Informática Industrial*, vol. 18, no. 3, pp. 201–217, 2021 (cit. on pp. 12, 143, 146).

[62]   B. V. Martínez, J. Sanchis, S. García-Nieto, and M. Martínez, "Tuning rules for active disturbance rejection controllers via multiobjective optimization—a guide for parameters computation based on robustness", *Mathematics*, vol. 9, no. 5, p. 517, 2021 (cit. on p. 12).

[63]   B. V. Martínez, *Active Disturbance Rejection Control-implementation examples. Version 1.0.0*, `https://www.mathworks.com/matlabcentral/fileexchange/78459`, Computer Software, 2020 (cit. on pp. 12, 33, 143).

[64]   B. V. Martínez, *LADRC automatic parameters computation based on robustness. Version 1.0.0*, `https://es.mathworks.com/matlabcentral/fileexchange/86403`, Computer Software, 2021 (cit. on pp. 12, 76, 146).

[65]   J. Li, X. H. Qi, H. Wan, and Y. Q. Xia, "Active disturbance rejection control: Theoretical results summary and future researches", *Kongzhi Lilun Yu Yingyong/Control Theory and Applications*, vol. 34, pp. 281–295, 3 2017 (cit. on p. 17).

[66]   S. Zhao and Z. Gao, "Modified active disturbance rejection control for time-delay systems", *ISA Transactions*, vol. 53, no. 4, pp. 882–888, 2014 (cit. on p. 18).

[67] Q. Zheng, Z. Chen, and Z. Gao, "A practical approach to disturbance de-coupling control", *Control Engineering Practice*, vol. 17, no. 9, pp. 1016–1025, 2009 (cit. on p. 20).

[68] Q. Zheng and Z. Gao, "On practical applications of active disturbance rejection control", in *Proceedings of the 29th Chinese Control Conference*, 2010, pp. 6095–6100 (cit. on p. 21).

[69] R. Parvathy and A. Daniel, "A survey on active disturbance rejection control", in *2013 International Mutli-Conference on Automation, Computing, Communication, Control and Compressed Sensing (iMac4s)*, 2013 (cit. on p. 21).

[70] M. Nowicki, R. Madonski, and K. Kozlowski, "First look at conditions on applicability of ADRC", in *2015 10th International Workshop on Robot Motion and Control (RoMoCo)*, 2015 (cit. on p. 22).

[71] P. Albertos, P. Garcia, Z. Gao, and T. Liu, "Disturbance rejection in process control", in *Proceeding of the 11th World Congress on Intelligent Control and Automation*, 2014 (cit. on p. 23).

[72] W. Xue and Y. Huang, "Performance analysis of active disturbance rejection tracking control for a class of uncertain LTI systems", *ISA Transactions*, vol. 58, pp. 133–154, 2015 (cit. on p. 23).

[73] S. Zhao, W. Xue, and Z. Gao, "Achieving minimum settling time subject to undershoot constraint in systems with one or two real right half plane zeros", *Journal of Dynamic Systems, Measurement, and Control*, vol. 135, no. 3, 2013 (cit. on p. 27).

[74] B. Ahi and M. Haeri, "Linear active disturbance rejection control from the practical aspects", *IEEE/ASME Transactions on Mechatronics*, vol. 23, no. 6, pp. 2909–2919, 2018 (cit. on p. 30).

[75] H. J. Goldsmid, *Introduction to Thermoelectricity*, 2nd ed. Berlin: Springer, 2016 (cit. on p. 33).

[76] V. Huilcapi, J. M. Herrero, X. Blasco, and M. Martínez-Iranzo, "Non-linear identification of a peltier cell model using evolutionary multi-

objective optimization", *IFAC-PapersOnLine*, vol. 50, no. 1, pp. 4448–4453, 2017 (cit. on pp. 34, 35).

[77] G. Reynoso-Meza, X. Blasco-Ferragud, J. Sanchis-Saez, and J. M. Herrero-Durá, "Background on multiobjective optimization for controller tuning", in *Controller Tuning with Evolutionary Multiobjective Optimization. Intelligent Systems, Control and Automation: Science and Engineering*, S. G. Tzafestas, Ed., vol. 85, Switzerland: Springer, 2017, pp. 23–58. DOI: `10.1007/978-3-319-41301-3` (cit. on pp. 37, 54).

[78] W. L. Luyben, *Process Modeling, Simulation, and Control for Chemical Engineers*. McGraw-Hill, 1990 (cit. on pp. 40, 45).

[79] T. Marlin, *Process Control: Designing Processes and Control Systems for Dynamic Performance*. McGraw-Hill, 2000 (cit. on p. 40).

[80] M. Pérez-Polo and P. Albertos, "Nonisothermal stirred-tank reactor with irreversible exothermic reaction a $\rightarrow$ b: 2. nonlinear phenomena", in *Selected Topics in Dynamics and Control of Chemical and Biological Processes*, Springer Berlin Heidelberg, 2007, pp. 243–279 (cit. on p. 40).

[81] A. Visioli, "Identification and model reduction techniques", in *Practical PID Control-Advances in Industrial Control*, M. J. Grimble and M. A. Johnson, Eds., United Kingdom: Springer-Verlag, 2006, pp. 165–207 (cit. on p. 52).

[82] W. Tan, J. Liu, T. Chen, and H. J. Marquez, "Comparison of some well-known PID tuning formulas", *Computers & Chemical Engineering*, vol. 30, no. 9, pp. 1416–1423, 2006 (cit. on p. 57).

[83] K. J. Åström and T. Hägglund, "Process models", in *Pid Controllers: Theory, Design and Tuning*, USA: Instrument Society of America, 1995, pp. 5–58 (cit. on pp. 60, 67, 125).

[84] O. Garpinger, T. Hägglund, and K. J. Åström, "Performance and robustness trade-offs in PID control", *Journal of Process Control*, vol. 24, no. 5, pp. 568–577, 2014 (cit. on p. 60).

[85]   Y. Lee, S. Park, M. Lee, and C. Brosilow, "PID controller tuning for de-
       sired closed-loop responses for SI/SO systems", *AIChE Journal*, vol. 44,
       no. 1, pp. 106–115, 1998 (cit. on pp. 62, 73).

[86]   S. Skogestad and C. Grimholt, "The SIMC method for smooth PID
       controller tuning", in *PID Control in the Third Millennium*, A. V. R.
       Vilanova, Ed., 2012, pp. 147–175 (cit. on pp. 62, 73, 122, 125).

[87]   K. Aström and T. Hägglund, "Revisiting the Ziegler–Nichols step re-
       sponse method for PID control", *Journal of Process Control*, vol. 14,
       no. 6, pp. 635–650, 2004 (cit. on pp. 62, 73).

[88]   D. Li, Z. Wang, W. Yu, Q. Li, and Q. Jin, "Application of LADRC
       with stability region for a hydrotreating back-flushing process", *Control
       Engineering Practice*, vol. 79, pp. 185–194, 2018 (cit. on p. 62).

[89]   L. Ou, W. Zhang, and D. Gu, "Nominal and robust stability regions of
       optimization-based PID controllers", *ISA Transactions*, vol. 45, no. 3,
       pp. 361–371, 2006 (cit. on p. 63).

[90]   G. Reynoso-Meza, J. Sanchis, X. Blasco, and J. M. Herrero, "Multiob-
       jective evolutionary algorithms for multivariable PI controller design",
       Expert Systems with Applications, vol. 39, no. 9, pp. 7895–7907, 2012
       (cit. on p. 64).

[91]   J. M. Herrero, M. Martínez, J. Sanchis, and X. Blasco, "Well-distributed
       pareto front by using the $\mathscr{E}$–MOGA evolutionary algorithm", in *Compu-
       tational and Ambient Intelligence*, F. Sandoval, A. Prieto, J. Cabestany,
       and M. Graña, Eds., Springer Berlin Heidelberg, 2007, pp. 292–299 (cit.
       on p. 64).

[92]   H. S. Sánchez, A. Visioli, and R. Vilanova, "Optimal nash tuning rules
       for robust PID controllers", *Journal of the Franklin Institute*, vol. 354,
       no. 10, pp. 3945–3970, 2017 (cit. on pp. 67, 70, 72, 73).

[93]   G. Reynoso-Meza, X. Blasco-Ferragud, J. Sanchis-Saez, and J. M. Herrero-
       Durá, "Multiobjective optimization design procedure for controller tun-
       ing of a peltier cell process", in *Controller Tuning with Evolutionary
       Multiobjective Optimization. Intelligent Systems, Control and Automa-*

tion: Science and Engineering, S. G. Tzafestas, Ed., vol. 85, Switzerland: Springer, 2017, pp. 187–199 (cit. on p. 93).

[94] K. Łakomy and R. Madonski, "Cascade extended state observer for active disturbance rejection control applications under measurement noise", *ISA Transactions*, vol. 109, pp. 1–10, 2021 (cit. on p. 97).

[95] P. Tatjewski, "Disturbance modeling and state estimation for offset-free predictive control with state-space process models", *International Journal of Applied Mathematics and Computer Science*, vol. 24, no. 2, pp. 313–323, 2014 (cit. on p. 103).

[96] J. M. Maciejowski, *Predictive control with constraints*, 1st ed. Boston: Addison-Wesley Educational, 2001 (cit. on pp. 103, 116).

[97] R. Miklosovic, A. Radke, and Z. Gao, "Discrete implementation and generalization of the extended state observer", in *2006 American Control Conference*, Minneapolis, MN, USA: IEEE, 2006, pp. 2209–22 014 (cit. on p. 104).

[98] R. Madoński and P. Herman, "Survey on methods of increasing the efficiency of extended state disturbance observers", *ISA Transactions*, vol. 56, pp. 18–27, 2015 (cit. on p. 108).

[99] J. F. Guerrero-Castellanos and L. L.González-Romeo, "Position control system via active disturbance rejection for laser optical systems", *Revista Iberoamericana de Automática e Informática Industrial*, vol. 19, no. 1, pp. 61–73, 2022 (cit. on p. 114).

[100] D. Mayne, J. Rawlings, C. Rao, and P. Scokaert, "Constrained model predictive control: Stability and optimality", *Automatica*, vol. 36, no. 6, pp. 789–814, 2000 (cit. on p. 115).

[101] D. Clarke, *Advances in model-based predictive control*. London, England: Oxford University Press, 1994, ISBN: 9780198562924 (cit. on p. 116).

[102] T.-W. Yoon and D. W. Clarke, "A reformulation of receding-horizon predictive control", *International Journal of Systems Science*, vol. 26, no. 7, pp. 1383–1400, 1995 (cit. on p. 116).

[103]   E. C. Kerrigan and J. M. Maciejowski, "Soft constraints and exact penalty functions in model predictive control", in *Proceedings of the UKACC International Conference (Control 2000)*, 2000, pp. 1–6 (cit. on p. 116).

[104]   R Isermann, *Digital control systems*, en. Berlin, Germany: Springer, Jun. 1981 (cit. on p. 119).

[105]   G. F. Franklin, J. D. Powell, and M. L. Workman, *Digital control of dynamic systems*, en, 3rd ed. Upper Saddle River, NJ: Pearson, Dec. 1997 (cit. on p. 119).

[106]   S. Zhao and Z. Gao, "Modified active disturbance rejection control for time-delay systems", *ISA Transactions*, vol. 53, no. 4, pp. 882–888, 2014 (cit. on p. 119).

[107]   M. Alhajeri and M. Soroush, "Tuning guidelines for model-predictive control", *Industrial & Engineering Chemistry Research*, vol. 59, no. 10, pp. 4177–4191, 2020 (cit. on p. 119).

[108]   E. Camacho and C. Bordons, *Model Predictive Control*, 1st ed. London: Springer, 2007 (cit. on p. 120).

[109]   K. Åström and T. Hägglund, "Benchmark systems for PID control", *IFAC Proceedings Volumes*, vol. 33, no. 4, pp. 165–166, 2000 (cit. on p. 124).

[110]   B. W. Bequette, *Process dynamics*. Philadelphia, PA, USA: Prentice Hall, 1998 (cit. on p. 131).

[111]   M. A. Henson and D. E. Seborg, "Input-output linearization of general nonlinear processes", *AIChE Journal*, vol. 36, no. 11, pp. 1753–1757, 1990 (cit. on pp. 131, 132).

[112]   S. Bhadra, A. Panda, P. Bhowmick, S. Goswami, and R. C. Panda, "Design and application of nonlinear model-based tracking control schemes employing DEKF estimation", *Optimal Control Applications and Methods*, vol. 40, no. 5, pp. 938–960, 2019 (cit. on p. 132).

[113] M. A. Henson and D. E. Seborg, "Theoretical analysis of unconstrained nonlinear model predictive control", *International Journal of Control*, vol. 58, no. 5, pp. 1053–1080, 1993 (cit. on pp. 136, 137).

[114] K. Lakomy, W. Giernacki, J. Michalski, and R. Madonski, "Active disturbance rejection control (adrc) toolbox for matlab/simulink", *arXiv*, 2021 (cit. on p. 148).